MECHANICAL ASSESSMENT OF VETERINARY ORTHOPEDIC IMPLANT TECHNOLOGIES: COMPARATIVE STUDIES OF CANINE FRACTURE FIXATION AND EQUINE ARTHRODESIS DEVICES AND TECHNIQUES

A Thesis

by

SEAN TRAVIS BAKER

Submitted to the Office of Graduate Studies of
Texas A&M University
in partial fulfillment of the requirements for the degree of

MASTER OF SCIENCE

Approved by:

Chair of Committee,	Michael Moreno
Committee Members,	Brian Saunders
	Harry Hogan
Head of Department,	Gerard Cote

May 2013

Major Subject: Biomedical Engineering

Copyright 2013 Sean Travis Baker

ABSTRACT

The Clamp-Rod Internal Fixator (CRIF) is a fracture fixation implant with growing popularity among veterinarian's for its versatility and ease of use. Although the CRIF is currently in clinical use, relatively few reports exist describing the biomechanical properties and clinical results of this system. The objective of this study was to determine the in vitro biomechanical properties of a 5mm CRIF/rod construct to a 3.5mm Limited Contact-Dynamic Compression Plate (LC-DCP/rod) construct using a canine femoral gap model.

Paired canine femora were treated with 40mm mid-diaphyseal ostectomies and randomly assigned to CRIF/rod or LC-DCP/rod. Five pairs of constructs were tested in bending and five pairs were evaluated in torsion. Single ramp to failure tests were conducted to evaluate construct stiffness, yield load, and failure mode.

While CRIF/rod and LC-DCP/rod were not significantly different when evaluated in bending, LC-DCP/rod constructs are significantly more rigid than CRIF/rod constructs at higher torsional loads. Below 10degrees of twist, or 4.92Nm torque, the LC-DCP/rod and CRIF/rod were not statistically different in torsion.

Catastrophic injuries of the metacarpophalangeal joint resulting in the disruption of the suspensory apparatus are the most common fatal injuries in thoroughbred racehorses. Fetlock arthrodesis is a procedure designed to mitigate suffering from injury as well as degenerative diseases affecting articulation. The objective of this study is to assess the in vitro biomechanical behavior of techniques for fetlock arthrodesis.

Twelve forelimb pairs were collected from adult horses euthanized for reasons unrelated to disease of the metacarpophalangeal joint (MCP). A 14-16-hole broad 4.5mm Locking Compression Plate (LCP) was compared to a 14-16 hole broad Dynamic Compression Plate (DCP). Both constructs used a two “figure-eight” 1.25mm stainless steel wire tension band. Fatigue tests and to failure tests were conducted.

There were no significant differences in stiffness between groups for fatigue tests. Stiffness increased after the first fatigue cycle for the LCP/wire (80.56+/-52.22%) and DCP/wire (56.58+/-14.85%). Above 3.5mm of axial deformation there was a statistical difference between the stiffness of the LCP/wire (3824.12+/-751.84 N/mm) and the DCP/wire (3009.65+/-718.25 N/mm) (P=0.038).

The LCP/wire showed increased stiffness above 3.5mm compression compared to the DCP/wire. Under fatigue testing conditions the constructs are not statistically different.

DEDICATION

This thesis is dedicated to:

My fiancée, Rita, for all of her love and support in all my endeavors. I hope that my hard work now will pay off for us in the future. That I may acquire a fulfilling job to support you in all your ventures. That our kids (Bazooka and Thor) (actual names pending) will have a home to grow up in, college paid for, and plenty of toys and junk food.

To my brother, Evan, may you and I both learn from my many mistakes and successes. I am going to let you make plenty of mistakes on your own, you need to learn something on your own (plus its funny for me), but if there are lessons to be learned I will share them the best I can. I will share my wisdom with you whenever I feel it is necessary.

My mother and father, Jana and Quentin, who have raised me to seek the best in myself, contribute all I can to the world, and for paying for all this education!

ACKNOWLEDGEMENTS

First, I must thank Dr. Moreno for the opportunity to work under him in the Biomechanical Environments Lab. Without Dr. Moreno's wisdom and guidance I would not have grown into the individual I am now. I must also thank all the current and past members of the Dr. Moreno Lab Group who have aided me in my projects, allowed me to participate in their projects, and in general made my time at TAMU a great one.

Thanks are also due to our project collaborators; Dr. Saunders and Dr. Bonin on the canine project, and Dr. McCormick and Dr. Jeffery Watkins on the equine project. The assistance in providing specimens, answering questions, and providing insight from the veterinarian perspective was vital in generating this thesis.

Thanks to Caleb Davis and Aubrey Hildebrandt for all their help on both projects. Your contributions helped keep these projects on time, as much as they could be, and provided an invaluable service during my research.

NOMENCLATURE

CRIF	Clamp-Rod Internal Fixator
LC-DCP	Limited Contact Dynamic Compression Plate
DCP	Dynamic Compression Plate
LCP	Locking Compression Plate
IMP	Intramedullary Pin
MCP	Metacarpophalangeal Joint

TABLE OF CONTENTS

LIST OF FIGURES

LIST OF TABLES

1. OVERVIEW

This thesis is composed of two biomechanical studies. The first project discussed is a biomechanical comparison study between the LC-DCP/rod and CRIF/rod for highly comminuted canine femur fractures. The second project discussed is a biomechanical comparison of two techniques for equine metacarpophalangeal joint arthrodesis using a DCP with stainless steel wire tension band and a LCP with stainless steel wire tension band.

The two studies in this thesis have several key differences and similarities. First, the major similarity is that both projects contain comparison studies between two different internal fixation and joint arthrodesis devices. The difference in species, differences between devices in each project, and intended use of the internal fixation systems provides a greater insight into orthopedic devices and a broadened understanding of the biomechanical properties of bone-plate systems. Second, the difference in joint arthrodesis and comminuted fracture fixation presents differences in the test protocols, the test setup, and analysis. This presents the challenge of developing physiologically relevant mechanical tests to provide useful insight into different internal orthopedic systems. Lastly, the biomechanical information obtained from this research partnered with an understanding of the clinical need, surgical procedures, and the biological impact of the systems allows for a well-rounded understanding from all perspectives.

The document is organized by project, starting with the canine and ending with the equine. The references sections and appendices are included after the equine project main body of material. The references list is a compiled list of both equine and canine literature, while the appendices are organized into canine and equine relevant material. The main body of each project contains;

- Introduction - that details the problem, history, and objectives.
- Methods – information related to device implant, testing protocols, test rigs, and the materials used for experimentation.
- Results – tables, charts, and figures for detailing the results of the study.
- Discussion – following the presentation of the results, a detailed discussion is necessary to explain the results for relevance and impact of the study.

2. CANINE INTRODUCTION

2.1 Problem

High energy fractures of the femur, especially the diaphysis, are common issues that orthopedic veterinarians encounter for canine injuries. Comminuted fractures of the shaft of the bone, or a diaphyseal comminuted fracture, require complex treatments to restore the structural support of the limb. Treating comminuted fractures can be accomplished by alignment and fixation of the multiple bone fragments via screws, pins, and cerclage wire. In the case that the bone is damaged beyond repair by reassembling the bone fragments, the orthopedic surgeon implant a bridge or buttress system to span the gap created between the remaining bone segments.

The Synthes® Clamp-Rod Internal Fixator (CRIF) was developed as a versatile and economical fracture fixation system for neutralization and bridge/buttress use for animals instead of adapting human fracture fixation devices to animal treatment. To date there are a limited number of reports detailing the biomechanical properties and clinical results of the CRIF device. A single report has described the biomechanical properties of the CRIF using a bone substitute model (1), but a biomechanical evaluation of the CRIF on a cadaveric bone setting in combination with an intramedullary rod has not been performed. This represents an important gap in our understanding and knowledge of the biomechanical properties of this fracture fixation system. While the structural properties of the CRIF are important, and provide insight into how the device may perform, this system must be evaluated in a manner that more closely resembles the clinical setting.

Construct rigidity, yield load, and mode of failure must be determined in order to improve our understanding of the CRIF's clinically relevant biomechanical properties.

2.2 Objectives

The overall goal of this research is to compare the biomechanical properties of a 5mm CRIF/rod to a 3.5mm LC-DCP/rod implanted in canine femur using a gap model. Therefore there is a need for the specific aims:

Aim 1. An in vitro comparison of the CRIF to the traditional LC-DCP using a canine femoral gap model.

Aim 2. Measure the mechanical properties of system rigidity, yield point, and mode of failure for torsional and bending scenarios.

Successful realization of these aims will represent a substantial advancement in our understanding of the biomechanical properties of both of these fixation systems. The impact that this research will provide to internal fixation device designers will be an improved understanding of how these devices behave as a system with the bone. The bone and device construct must be analyzed in order to understand how failures occur in an in vivo setting so that improvements may be made on the observed weaknesses. For orthopedic surgeons, this research will shed light on how each device behaves once implanted, what to look for when patients return with issues, and overall better patient recovery.

Based on loading direction and device geometry, it is expected that the plate will have a higher rigidity in torsion than the CRIF, and a lower rigidity in bending. One

issue is the presence of more part interfaces in the CRIF system, providing more paths for the system to fail than the LCDCP. It can be assumed that the CRIF rod may rotate inside of the clamps, as the only force keeping the two in place is static friction. An issue that may arise is the use of the IMR for bone alignment and reduction in plate strain in bending. The contribution of the IMR is suspected to reduce plate strain for both the CRIF and LC-DCP, but as the IMR serves as the neutral axis for torsion about the long axis of the bone its structural properties will likely be diminished in this loading regimen.

2.3 Hypothesis

The CRIF is expected to perform as a satisfactory fracture fixation device based on past research by Zahn, which showed the CRIF is an effective system across a large number of small animal patients with a variety of axial and appendicular fractures (2). This study will evaluate the mechanical performance of the CRIF in partnership with an IM pin, which has not previously been studied. In 2008, Zahn and colleagues evaluated the mechanical properties of 18 different bone plates and the CRIF system in vitro using a gap model and canevasit bone substitute (1). The 5 mm CRIF system, which accepts 3.5 mm clamps and bone screws, demonstrated increased bending rigidity (0.85 Nm/deg) as compared to 3.5 mm DCP (0.71 Nm/deg) or LC-DCP (0.57 Nm/deg) bone plates. However, when evaluated in torsion, the CRIF demonstrated decreased torsion rigidity (0.41 Nm/deg) when compared to 3.5 mm DCP (0.48 Nm/deg) or LC-DCP (0.42 Nm/deg) bone plates. This study will use cadaveric bone, an IM pin, and the CRIF

device. We expect to see increased rigidity and failure loads from the multicomponent system in bending and torsion. The CRIF/rod compared to the LC-DCP/rod, we expect to see increased bending rigidity from the CRIF system but lower levels of torsional rigidity. From a clinical standpoint, both constructs are expected to perform above compliant canine everyday working loads as established previously by Carter. (3)

2.4 Justification

Canine femur fracture fixation is a common occurrence for veterinarians. Comminuted femur fractures can be difficult to treat, and currently the CRIF device is being used with limited mechanical data to justify its use. Surgical procedures for implanting and treating comminuted femur fractures are well established for plates such as the DCP, LCP, and LC-DCP. Use of the IM pin is popular as it decreases the stress on the fracture fixation implant and serves as an alignment tool during fracture repair. A study is needed to bridge the knowledge gap between the use of the CRIF device partnered with an IM pin. The CRIF/rod construct will be compared with the LC-DCP/rod construct to provide valuable mechanical data to justify using a particular construct.

3. CANINE BACKGROUND

3.1 History of Canine Femur Fracture Fixation

Metal plates have been used for internal fracture fixation for more than 100 years. In 1895, Lane introduced the first metal plate for use as an internal fixation, but this implant had limited success due to issues of corrosion. (4) The problems with corrosion faded as knowledge of metal properties grew, and the predominant issue with implants changed focus from corrosion to implant strength. In 1949, Danis recognized that bone fragments and fracture healing benefited from compression at the fracture site. The suppressed interfragmentary motion and increased structural stability of the implant lead to a process now known as primary bone healing. This ground breaking concept paved the way for all subsequent plate designs, such as the DCP with specifically designed oval holes to provide interfragmentary compression during screw tightening. (5) The advantages of the DCP included: low incidence for malunion, stable fixation of limb, and no external immobilization necessary allowing for immediate movement and use of neighboring joints. The DCP required a large surgical incision and lengthy surgery, suffered from cortical bone loss underneath the plate, and the possibility of microscopic fracture gaps that could act as stress concentrators after plate removal. A main issue with clinicians was the limited ability to evaluate the healing process via radiograph as the disappearance of the fracture gap and development of an external bridging callus are key elements to assessing the fractures repair. Refracture upon removal of the plate was another issue with the DCP, where refracture occurred

regardless of the length of time the plate was left on the healing bone. The fracture most often occurred at sites of where the bone failed to bridge an existing gap. Bone plating with the DCP has been the long time go to device, but these plates can inhibit the vascular supply to the bone within the plate-bone contact region. This limited blood supply, large implant size relative to patient size, and material properties all contribute to stress protection or shielding. (6) The DCP's success suffered because it was developed and used during a time frame that used direct reduction as the primary technique for fracture repair. Direct reduction was a technique for reducing a fractured bone to its proper anatomical alignment by use of a large incision, manipulation of bone fragments, and use of multiple implants such as wires and screws to secure each bone fragment. The main failure with direct reduction of complicated fractures was the direct anatomical reduction was not possible. A surgeon cannot see every interface of every bone fragment, and thus despite a surgeons best efforts the likelihood of a fracture gap remaining is very high. With the complications of plates and direct reduction techniques there was a transition in surgical approach as well as advancement in plate technology. (7)

A theory for why refracture occurred presented by Perren was that porosis and refractures are due to cortical necrosis as a result of excessive bone to plate contact interfering with cortical perfusion. (8) The natural process of removal for dead or dying bone and its replacement by healthy cells was theorized to be the cause of transient porosis of the cortex. It was theorized that perfusion (the process of delivery of blood to a capillary bed in the biological tissue) was being interrupted by excessive bone to plate

contact leading to callus formation, and that a plate with significantly reduced bone-plate contact area would allow greater perfusion and lead to overall decrease in porosis. This theory lead to the development of the Limited Contact Dynamic Compression Plate (LC-DCP) with the goal of increasing cortical perfusion and decreasing cortical porosis. Studies argue as to whether the LC-DCP actually reduces contact with the surface of the bone, and its effectiveness at allowing cortical perfusion. While studies are still being conducted as to the ability of the LC-DCP to reduce bone contact and its effect on blood supply to the bone, the LC-DCP is a device currently in use as a fracture fixation device for comminuted diaphyseal canine femur fractures.

Issues with direct reduction of highly comminuted fractures such as refracture, infection, and delayed healing brought about a fundamental change in the approach to fracture fixation called biological osteosynthesis. Direct reduction or complete reconstruction of the boney column by manipulation required a large and strong implant. A large skin incision was required, resulting in damage to muscles and periostium. Two piece fractures are good candidates for direct reduction and this can be accomplished with compression plates. Traditional bone plates can be technically demanding require lengthy surgical procedures to reduce and stabilize multiple bone fragments. (9) Surgeons often encounter a region bone and soft tissue that does not favor anatomic reduction, and results in a small fracture gap that does not favor long bone healing. The lengthy surgical procedure, disruption of surrounding soft tissue, and limited reconstruction of the fragmented long bone shaft contribute to the failure of the fixation system. (10) Treatments that focus on biological osteosynthesis disregard stabilization of

all fragments to preserve soft tissue attachments. This allows the surgeon to restore spatial alignment of the bone while avoiding manipulation of bone fragments in the area of comminution. By circumventing the manipulation of bone fragments the vascular attachments to the fragments are preserved without sacrificing bone stability and potential for bone union. This surgical procedure leaves the implant plate at risk of acute failure or cyclical/fatigue failure, plastic deformation, and clinical failure in the postoperative period due to the increased load bearing requirements placed on the implant as a result of decreased load bearing of the bone. (9)

Complex femur fractures that result in a non-reconstructable fracture can be treated with bridging or buttress implant systems. These systems preserve the biological regenerative capacity while creating a stable limb by indirect reduction. Indirect reduction uses a bridging plate to anatomically preserve the length and orientation of the limb, but does not require manipulation of bone fragments in the area of comminution. The bone ends are re-aligned without the precise reconstruction of all fracture fragments to preserve blood supply to the bone via soft tissue attachments. The biological concept of surgical repair for veterinary surgery is to preserve the vascular integrity of the bone while maintaining alignment and the length of the bone during the healing phase. For canine femur fractures, two implant systems that accomplish the veterinary surgical concept with minimal manipulation of the fracture hematoma and bone fragments preserving the osteoinductive and vascularization properties are bone plates (DCP, LC-DCP) and the CRIF system. (10) (11) (12) Both implant systems bridge the fracture

fragments reducing the amount of manipulation to the bone fragments, while bearing the normal bending, torsion, and compressive forces as the bone heals. (13)

A recent treatment option for comminuted fractures is the use of Intramedullary Rods (IMR) in combination with a bridge plate. The addition of an IMR can reduce the implanted plate's applied stress and allow orthopedic surgeons to achieve high levels of bone alignment with original conditions. (9) (14) Use of the IM nails is a common fracture fixation method for humans, but the simpler IM pin requires combination with a plate for effectiveness of the implant. For situations in which the surgeon is unable to reconstruct the diaphyseal column anatomically, small fracture gaps can remain and contribute to implant failure. Small fracture gaps may lead to delayed union or nonunion as a result of motion caused by the weight bearing loads concentrated in the fracture gap. For the traditional direct reduction method this is particularly true. With a comminuted fracture and the direct reduction technique the potential for a fracture gap to exist is extremely high. This results from a surgeon attempting to anatomically align every bone fragment in an environment where all interfaces between bone fragments cannot be seen during reduction. Even if only one fracture gap remains the motion of one bone fragment will cause a cascade of instability between all other bone fragments and result in high levels of interfragmentary strain. The weight bearing loads lead to increased levels of interfragmentary strain, where strain is the change in gap width relative to the original gap width after loading. The level of interfragmentary strain is important because different connective tissues have different strain levels that are vital for proper function and tissue survival. Bone favors low levels of interfragmentary strain, and if the strain

levels are too high bone formation does not occur, and some studies have shown that high strain levels lead to bone resorption. (15) The DCP and LC-DCP are good implant candidates for direct reduction because they can function in the compression setting. Compression implants provide increased stability through direct reduction of a fracture.

The presence of the highly comminuted fracture can affect a veterinarian's choice in fracture fixation implant, as the large, non-reconstructable gap reduces the ability of the bone plate and remaining bone shaft to share physiological loads. This situation is most evident when fracture gaps are present in the transcortex, or cortex opposite the bone plate (cortex being the outer layer of the bone). A transcortex fracture gap decreases the load bearing cross sectional area of the construct, increases bending moment on bone plate by increasing moment arm, and decreases moment of inertia. The minimal or nonexistent ability of the bone to bear load places all of the weight bearing requirements on the implant. This requires increased fatigue resistance and strength of the fracture fixation device. The DCP, LC-DCP, and CRIF are all designed to function in a bridge setting. However, the increased demands placed on the plates in a bridge setting has increased the popularity of using a IM pin in combination with a plate. Hulse established that a IM pin that occupies 40% of the endosteal diameter can reduace plate strain by approximately 47% and increase strength by 40%. (14) A successful and popular treatment option now is to use the LC-DCP and IM pin in partnership. The IM pin helps surgoens establish proper anatomical alignment and length of the limb, as well as improves stability and reduces plate strain.

3.2 LC-DCP

The LC-DCP was designed around the notion of unimpaired native blood supply. (16) (10) LC-DCP plates are made from a prismatic piece of metal via cutting tools from either wrought, forged, or cast biocompatible stainless steel with evenly spaced plate holes that are symmetrical with two identical self-compressing inclined surfaces at each end. The faces of the plate are inclined to form a trapezoidal cross section with undercuts in the shape of arcs. The angled plate holes and arched undercuts contribute to the reduction in surface area, as well as allow for tilting of the screw within the plate hole by up to 40degrees along the long axis of the bone. (17) An image of one of this projects test specimens implanted with a LC-DCP/rod combination can be seen in Figure 1 and Figure 2.

Figure 1. Shown is one of the canine femur test specimens with a simulated comminuted diaphyseal fracture repaired using the LC-DCP and IM pin.

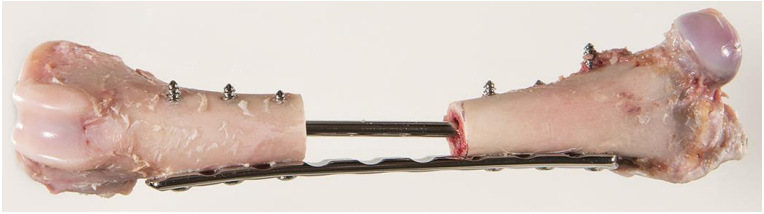

Figure 2. A side angle of the LC-DCP and IM pin implant construct on one of the canine femur test specimens with a simulated comminuted diaphyseal fracture.

The LC-DCP uses the approach where the surgeon considers the importance of preserving the soft tissue surrounding the bone as well as the viability of the bone itself. Today it is considered better to preserve biological tissue, and blood supply within the bone at the expense of implant stability.

The DCP and LC-DCP can function in the three basic fracture fixation setting of compression, neutralization, and bridge/buttress. How the DCP and LC-DCP function depends on the stability requirements for a particular fracture, and the surgical technique used to implant the device. Implanted constructs can serve as load sharing devices by acting as a neutralization or compression plate. A neutralization plate acts to neutralize bending, torsion, and axial forces at an already reduced fracture. Compression plates are used to reduce a fracture gap by direct reduction, applying compression at the fracture site for increased stability. Implanted devices can also serve as a bridge construct, where the implant is a load bearing device and not load sharing. Implants used as a bridge plate will usually span a fracture gap, use indirect reduction for anatomical alignment, and act to bear the majority or all the forces at would normally act at the fracture site. The DCP and LC-DCP can be used in all three settings of compression, neutralization, and bridge. The implantation of the devices differs how each construct performs, and the implantation technique is based on the fracture requirements for stability and healing.

3.3 CRIF

The CRIF was developed as a versatile and easy to use system capable of functioning in both neutralization and bridge/buttress mode. (18) (19) (2) Images of the CRIF/rod constructs can be seen in Figure 3 and Figure 4.

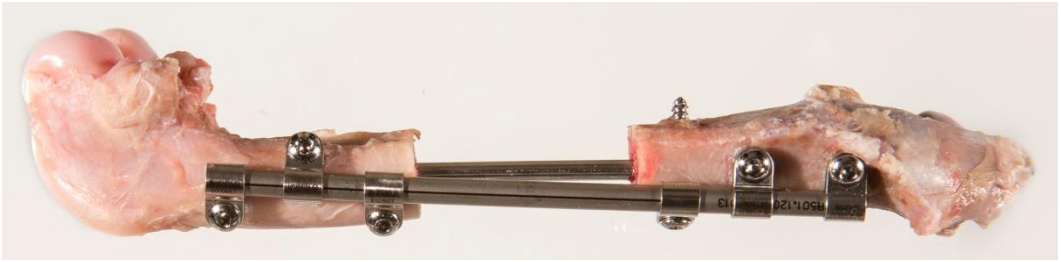

Figure 3. Shown is a lateral view of one of the canine femur test specimens with a simulated comminuted diaphyseal fracture repaired using the CRIF and IM pin.

Figure 4. A dorsal angle of the CRIF and IM pin implant construct on one of the canine femur test specimens with a simulated comminuted diaphyseal fracture.

Originally designed and marketed to a limited number of hospitals as the VetFix system, the CRIF consists of a cylindrical connecting rod of varying lengths, currently available in three diameters [mini (2mm), small (3mm), medium (5mm)]. Each rod is designed to accept a single sized clamp and cortical bone screw [mini (2.0mm), small (2.7mm), medium (3.5mm)]. The CRIF rod can be contoured in three dimensions using

custom bending irons and cut to length to accommodate individual patients bone lengths providing substantial versatility to the system. The CRIF allows for side specific clamps to slide along the rod, and for end clamps that are manufactured with a cap to capture each end of the CRIF rod. The structural properties of the end clamps provide construct stability by capturing the CRIF rod within two capped end clamps. Additional versatility is added by the ability to select both the number and position of fixation clamps along the CRIF rod. Both end and side clamps are designed to be positioned to accept bone screws either or cranial or caudal to the connecting rod which provides the third and final layer of versatility of the CRIF system.

The CRIF system like the DCP and LC-DCP can function in bridge and neutralization, however it cannot function in compression. The unique shape of the holes on the DCP and LC-DCP plates allow for the cortex head screws to adjust their position during tightening. While the CRIF uses the same cortex head screws, the use of a clamp-rod system does not permit axial motion of the bone underneath the plate via tightening of the cortex screws.

3.4 Past Mechanical Testing

Although the CRIF system is currently in clinical use only a small number of reports exist describing the biomechanical properties and clinical results of this system. In 2004, Zahn described the use of the CRIF for stabilization of a variety of appendicular and axial fractures in one hundred and twenty canine and feline patients (2). Of the ninety patients available for follow-up, eight-six (95%) patients underwent successful

fracture healing. This report demonstrated the effectiveness of the CRIF system in a large number of small animal patients with a variety of axial and appendicular fractures. In 2008, Zahn and colleagues evaluated the mechanical properties of 18 different bone plates and the CRIF system in vitro using a gap model and canevasit bone substitute (1). The 5 mm CRIF system (which accepts 3.5 mm clamps and bone screws) demonstrated increased bending rigidity (0.85 Nm/deg) as compared to 3.5 mm DCP (0.71 Nm/deg) or LC-DCP (0.57 Nm/deg) bone plates. However, when evaluated in torsion, the CRIF demonstrated decreased torsion rigidity (0.41 Nm/deg) when compared to 3.5 mm DCP (0.48 Nm/deg) or LC-DCP (0.42 Nm/deg) bone plates. It was hypothesized that perhaps certain structural properties of the CRIF system along with the method of application to the canevasit bone substitutes may have explained the decreased torsion rigidity. It was suggested that improving the CRIF design to increase friction between the clamps and rod and slightly contouring the rod in three-dimensions would improve torsion rigidity. Based on this recommendation, the surface of the current CRIF rod is roughened so as to increase the friction between the rod and clamps.

A previous report describes the clinical use of the CRIF system in combination with intramedullary (IM) pins and is referred to as CRIF/rod fixation (20). All seven patients treated with CRIF/rod fixation underwent successful fracture healing. While this small case series suggests that CRIF/rod fixation may be a suitable alterative to plate/rod fixation, biomechanical studies comparing the CRIF system to bone plates in combination with intramedullary pins are lacking. The objective of this study was to compare the in vitro biomechanical properties of a 5 mm CRIF/rod construct to a 3.5

mm LC-DCP/rod construct using a canine femoral gap model. Based on the structural properties and previous data available for the 5 mm CRIF and 3.5 mm LC-DCP, we hypothesized that when compared to a 3.5 mm LC-DCP/rod construct, the 5 mm CRIF/rod construct would demonstrate increased construct rigidity and load to failure when examined in bending and decreased construct rigidity and load to failure in torsion.

In previous studies the mechanical properties of different commercially available bone plates and the CRIF have been compared using an unstable fracture model. It was hypothesized that the CRIF would perform similarly to the corresponding DCP's in a gap model using rods of Canevasit (a bone equivalent material). From the comparison studies, none of the bone screws pulled free from the Canevasit material. All of the plates failed by plastic deformation between the two centermost screws to the gap. The smaller CRIF rods failed by plastic deformation, while the larger CRIF systems where believed to have failed by rotation of the CRIF rod inside the clamps. The CRIF clearly was inferior in torsional resistance, but showed high stiffness and yield load in bending. (1)

Past research on the addition of an IMR in reducing plate strain shows that the inclusion of an IMR and a plate is a valid method to treat comminuted fractures. An IMR that occupies 50% of the marrow cavity diameter reduces plate strain and extends fatigue life of the bone implant system. It is hypothesized that the IM pin will contribute to the bending stiffness in this study for both constructs, but will be negligible in the torsion results due to the test setup. Aligning the center of the IM pin with the neutral axis of the

test will mitigate the effects of the IM pin to the point where only the moment arm created from the IM pin to the implant will be a contributing factor.

4. CANINE METHODS

4.1 Overall Study Design

The overall objective of this study is to provide a biomechanical comparison between the LC-DCP/rod and CRIF/rod systems in the context of a clinically relevant fracture model. This information is necessary before orthopedic surgeons or veterinarians adopt the CRIF system. Previous studies have looked at the mechanical properties of the devices alone and on a bone substitute. An in vitro study will provide valuable information about failure mode of each system, the biomechanical properties, and potential remedies to design flaws with the CRIF device. (1)

4.2 Device Implant

Eleven pairs of canine femurs (22 total limbs) were harvested from healthy, skeletally mature large breed dogs (35-45 kilograms) euthanized for reasons unrelated to this project. Each femur was dissected free of surrounding soft tissues, wrapped in isotonic saline-soaked towels, double sealed in specimen bags, and stored at -20deg until the time of testing. Left and right femora from each dog were randomly assigned to either LC-DCP/rod or CRIF/rod treatment groups. Bone specimens were thawed overnight at room temperature and orthogonal view digital radiographs were obtained of each femur to screen for pre-existing trauma or other radiographic abnormalities. Femoral pairs with radiographic abnormalities were excluded from further analysis. A 10 cm radiographic calibration marker (10 cm marker, Biomedtrix, Boonton, NJ) was

positioned adjacent to each femur and equidistant from the radiographic detector to allow digital calibration and measurement of each specimen. Digital radiographic images were stored on a local and off-site picture archiving and communication system (PACS, Sound-Eklin, Carlsbad, California) and evaluated with commercially available software (eFilm version 3.3, Sound-Eklin, Carlsbad, California).

The mid-diaphysis of each femur was located using pre-implantation radiography and confirmed by direct measurement of each specimen. A 40 mm ostectomy was centered on the mid-diaphysis of each femur. Next, a 5/32 inch (3.175 mm) IM pin was placed in each femur in a retrograde fashion using a battery powered drive system (Small Battery Drive System, SynthesVet®, West Chester, PA). IM pin size was selected in order to ensure that 40% of the endosteal diameter of each bone was filled by the IM pin based on previously published work (14). While small variations in endosteal diameter existed between bone pairs, IM pin size remained constant across all specimens in order to maintain consistent implant size during biomechanical testing. IM pins were initially positioned along the caudomedial cortex of proximal bone segments and driven proximally so as to exit within the craniolateral aspect of the trochanteric fossa. A 40 mm spacer was utilized to maintain a 40 mm gap while IM pins were inserted into the distal bone segment. Pins were driven along the caudomedial aspect of the distal bone segments until seated into the cancellous bone of the medial femoral condyle. Gaps were measured again to confirm the 40 mm defect.

For femora assigned to the LC-DCP/rod group, a 9 hole, 3.5 mm stainless steel LC-DCP bone plate (plate length = 119 mm) (SynthesVet®, West Chester, PA) was

lightly contoured to the lateral aspect of the femur using a bending template and hand-held bending pliers. The LC-DCP plates were placed along the lateral aspect of each bone so that three plate holes were positioned over the proximal bone segment, three holes were positioned over the gap, and three holes were positioned over the distal bone segment Figure 5. Three 3.5 mm bicortical bone screws were used to secure the plate to each bone fragment using standard AO technique (21). Each screw hole was prepared by manual insertion of a 3.5 mm tap and screws were subsequently inserted manually to mimic screw insertion in the clinical setting. Femoral gaps were again measured to confirm a final 40 mm defect.

Figure 5. Shown are CRIF/rod and LC-DCP/rod constructs. The LC-DCP has been implanted along the lateral aspect of each bone and positioned so that three plate holes are positioned over the proximal bone segment. The CRIF was implanted with three clamps positioned along the proximal aspect of the rod, and three clamps positioned along the distal aspect of the rod. Both constructs use the same 3.5mm cortex screws. The ostectomy, length of the CRIF and LC-DCP implant, and overall anatomic length of the bone was maintained across contralateral pairs.

For femora assigned to the CRIF/rod group, a 5 mm diameter CRIF connecting rod (length = 120 mm) was lightly contoured to the lateral aspect of each femur using custom bending pliers specifically designed for the CRIF system. Six CRIF clamps were placed along each rod with three clamps positioned along the proximal aspect of the rod and three clamps positioned along the distal aspect of the rod. Four side clamps and two end clamps were used for each specimen. In order to ensure that the working length of both LC-DCP/rod and CRIF/rod constructs were equal, the side clamps adjacent to the gap were positioned 53 mm apart, the same distance as the two innermost LC-DCP bone screws. End clamps were secured to the end of each connecting rod 120 mm apart, a distance similar to the length of LC-DCP bone plates (119 mm). 3.5 mm bicortical bone screws were placed through each CRIF clamp in the same order for each specimen Figure 5; the number one screw (most proximal) was placed first, followed by the number six screw (most distal), then the third, fourth, second and fifth screws. Screw placement was performed in a manner identical to the LC-DCP/rod constructs. Once the CRIF was secured to each femur, the gap was again measured to confirm the 40 mm gap was maintained during CRIF placement. All implants were placed by a single investigator (redacted) experienced with both systems. Implant/bone constructs were radiographed to confirm proper implant placement Figure 6. Implant/bone constructs were individually wrapped in isotonic saline-soaked towels, double sealed in specimen bags, and stored at 4degC overnight in preparation for biomechanical testing.

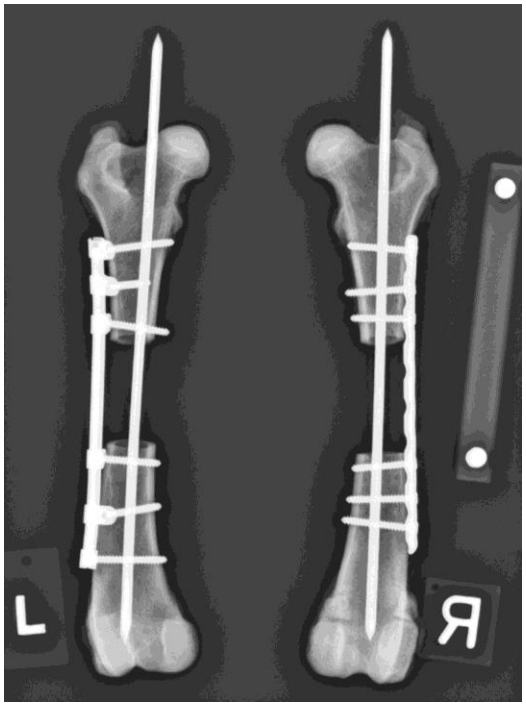

Figure 6. Shown are the CRIF/rod and LC-DCP/rod construct radiographs to compare contralateral pairs. Gap length, implant length, and overall bone length were measured to assure consistency between pairs.

4.3 Four Point Bending Testing

Five of the ten pairs of femora (ten implant/bone specimens) were evaluated under 4-point bend loading conditions. Prior to testing, the ends of each specimen were potted in an aluminum housing using West System Epoxy Resin 105 with Extra Slow Hardener 209 (West System Inc., Bay City, MI). A custom jig was designed to ensure the samples were potted such that the IM pin was aligned perpendicular to the direction of motion of the load frame crosshead. To ensure the working length of each construct was the same for all specimens, the bone-device constructs were potted such that the ends of the fracture fixation device were 1cm from the surface of the potting material. During the potting process, samples were maintained in saline soaked towels to prevent

moisture loss. Potted specimens and associated housings were then mounted to a TestResources 830-36 Dual Column Axial/Torsion Load Frame outfitted with a custom made four-point bending fixture. The constructs were oriented such that the fixation devices were on the tension side or outer radius of curvature when loaded. In conventional 4-point bend loading, the ends of the test specimen are free to translate toward each other as bending is induced and the ends of the specimen rotate about the inner bend points. A linear bearing and hinge combination was utilized to accommodate this tendency and facilitate free bending motion of the potted specimens. A custom jig was developed to ensure the samples were potted such that IM pin was aligned perpendicular to the direction of motion of the crosshead which can be seen in Figure 7.

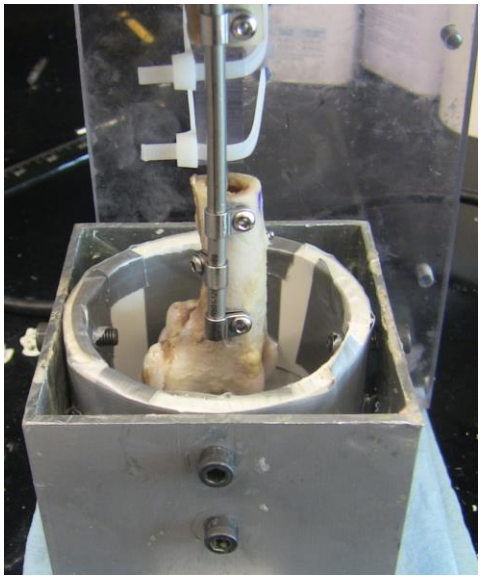

Figure 7. Shown is a CRIF/rod specimen mounted in the custom built alignment and potting rig. The custom rig holds each construct to via the IM pin and zip-ties to a Lexan plate. The aluminum and PVC housing are also secured to the Lexan plate to create a stable potting rig. Epoxy is poured inside the PVC to create a bond between the bone and epoxy, and set screws are used to hold the PVC to the aluminum housing.

To ensure the working length of each construct remained constant across specimens, bone ends were potted so that there was 1 cm of distance from the ends of the LC-DCP plate or CRIF and the surface of the potting material. During the potting process, exposed portions of the sample were maintained in saline soaked towels. Potting material was allowed to cure and specimens and associated housin were mounted to a TestResources 830-36 Dual Column Axial/Torsion Load Frame with a four-point bending fixture that secured each pot to a hinge and linear bearing system (Figure 8).

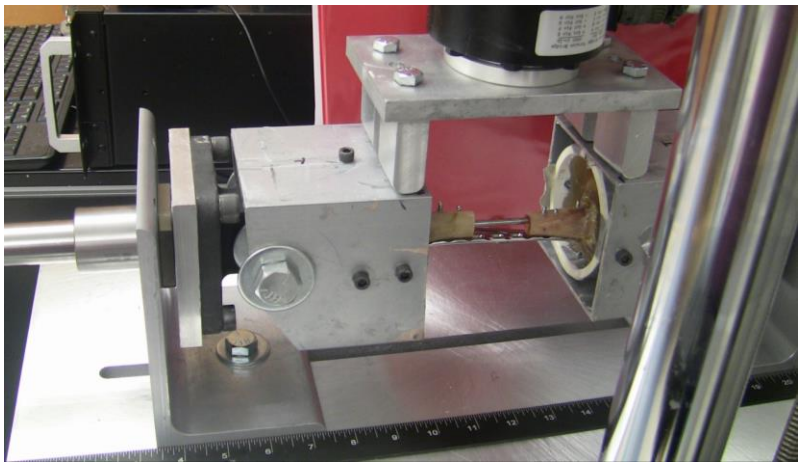

Figure 8. The test specimen is secured in epoxy inside of PVC, which is bolted to the aluminum housing. The aluminum housing is attached to a hinge and linear bearing mounted to an angle plate secured to the test platform.

The crosshead was lowered until the four aluminum prongs of the four-point bending fixture were in contact with the surface of the two aluminum pots (Figure 8). The hinges served as the outer bend points, while two aluminum prongs mounted to the crosshead of the load frame served as the inner bend points of the 4-point bend system. Once symmetrical alignment of the sample was ensured, a single load to failure four-

point bending protocol was initiated. A stroke control method was used wherein the crosshead was lowered at a rate of 0.167 millimeters per second. The load in Newtons (N) required to achieve the specified stroke position was recorded. Four-point bending was continued until construct failure occurred. Failure was defined as one of the following; a visual inspection during the experiment that indicated the system was deforming without increasing resistance to deformation, a visual or audible indication the bone had fractures, or by a sudden drop in load indicative of a yield point. The axial load was released and each construct was removed from the test machine for inspection and documentation of failure mode. Load data related to each integer crosshead position were analyzed in order to determine construct rigidity and load at failure. The load versus displacement data was converted to bending moment and angle of bending in degrees using the equations in Figure 9. This formula is a modified version of the formula used in a previous study. (1)

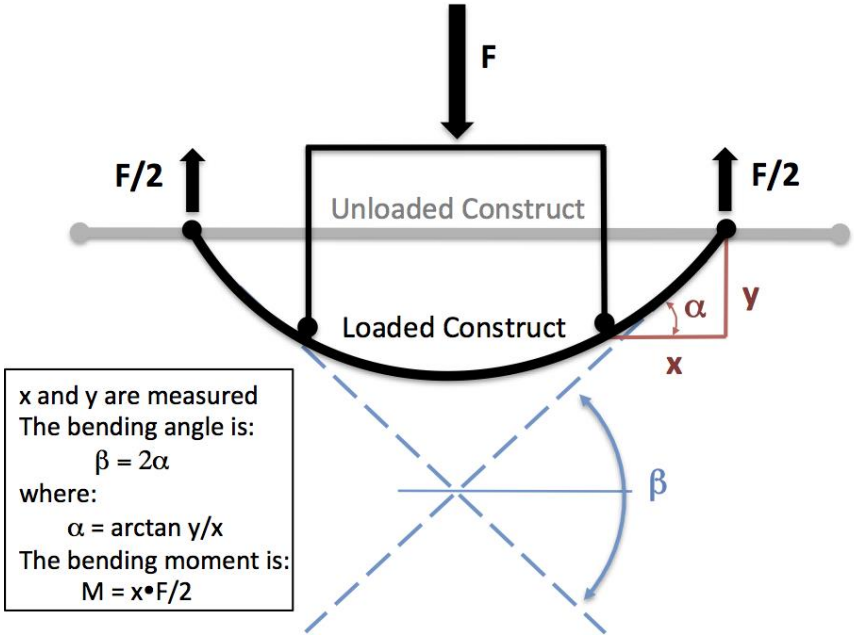

Figure 9. Geometry of the four point bending device and motion of the four points is described. The unloaded (straight) test specimen can be seen in gray, and the resulting arc induced by the test can be seen in black. The two inner points press downward in the vertical axis, and the outer points of contact move inward along linear bearings and hinges. Load F (N) and displacement y (mm) were recorded during testing. Permanent distance x, between the hinge and the applied load, was consistent across all test specimens (76.2mm). The bending moment M (Nm) and bending angle β (degrees) were found using $M=F/2*x$ and angle $\beta=2*\alpha$ where $\alpha=\tan^{-1}(y/x)$.

A mean and standard deviation for bending moment and bending angle was calculated for both devices from the load displacement data and the equations shown in Figure 9. The slope of bending moment versus bending angle was used for the device rigidity. Student's t-tests were utilized to determine if significant differences existed between treatment groups at each degree of bending and if differences existed in load to failure between each treatment group. Significance was set at $P \leq 0.05$.

4.4 Torsional Testing

Torsional testing was performed on six pairs of specimens. One implant/bone construct failed during initiation of torsional testing through propagation of a fissure fracture. The fissure fracture was generated during screw placement and was not apparent on post-implantation radiographs. This femoral pair was excluded from additional testing, resulting in the inclusion of five pair of femora in final torsional analysis. The proximal and distal end of each specimen was potted into custom-fabricated fixtures as seen in Figure 10, in a manner similar to bending tests.

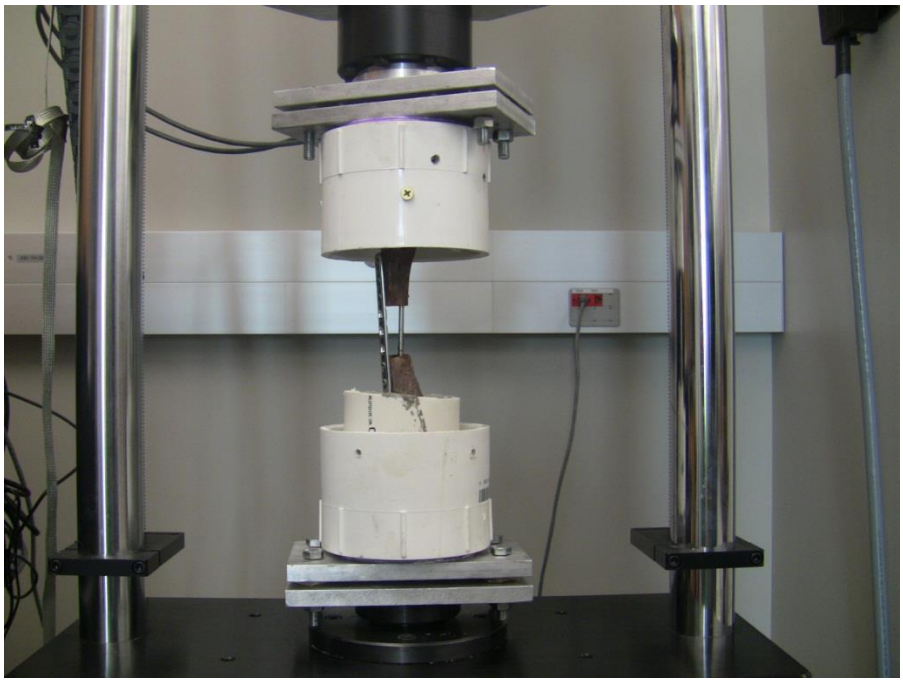

Figure 10. Image of a LC-DCP/rod specimen potted inside the PVC housings, attached to aluminum interface plates for mounting to the Test Resources machine.

A custom jig was again used to ensure each sample was potted such that the IM pin was aligned with the axis of torsional rotation. Potted samples were then mounted to

the TestResources 830-36 Dual Column Axial/Torsion Load Frame. Throughout torsion testing the axial component of the test machine was continuously adjusted such that a small, constant, (10N/2.24 pound), compressive load was maintained in the axial direction. The small constant axial load was included in the test protocol to mitigate the effects of increasing tension in a system that is rigidly deformed in torsion, thus creating a near pure torsion experiment. A pure torsion experiment is preferred compared to a torsion experiment in that the axial forces that are generated during a torsion experiment would be alleviated by the continuously adjusting axial crosshead. By compressing the bone by a small amount, the tension in the system was relieved throughout the test to assure that any failure that occurred was a result of torsional deformation not tension. A deformation control method was employed wherein the samples were twisted 30deg at 0.2deg/s (10mm/min) (1). Thirty degrees of rotation was selected as an endpoint for torsional testing as it would represent substantial clinical failure. The 30deg value is what clinical failure was defined by the veterinarian collaborators. This raised the question of permanent angular deformation versus implied angular deformation. Because veterinarians only see permanent angular deformation when a canine patient visits the clinic what angle was the construct deformed to in order to leave a permanent angular deformation of 30deg. In order to evaluate the recoil in both implant systems each construct the following protocol was used: twisted to 30deg, allowed to recoil to 0Nm, twisted to 40deg, allowed to recoil to 0Nm, twisted to 50deg, allowed to recoil to 0Nm, twisted to 60deg, and a final recoil to 0Nm. This testing protocol allows for each specimen's recoil and permanent angular deformation to be assessed to determine what

angular deformation is required to result in clinical failure of the device. Torque versus angle data was acquired at a rate of 100Hz. Axial and torsion loads were removed once 30deg of torsion was reached, and the implant/bone constructs were allowed to recoil freely. Residual rotation was identified by the MTS 810 machine and recorded as permanent angular deformation. Torque data (Nm) related to each integer of rotation (degree) were determined. The results were normalized by bone diameter, where the individual specimen torque values were divided by average bone diameter of the specimen. This created a normalized load vs. displacement for the specimens, removing the effect of bone size on the results. Mean and standard deviation torque deformation were determined for both LC-DCP/rod and CRIF/rod treatment groups at each integer degree of rotation. Torsional stiffness was determined for each treatment group by performing a linear curve fit of data plots displaying mean load deformation data at each integer degree of rotation. Rigidity and stiffness are used interchangeably in this report because stiffness is a measure of rigidity, where rigidity is defined as the resistance of a body to deformation. Stiffness measures the deflection of a material by a given load per unit area. Stiffness by definition is a material property, and the test specimen's in this report were comprised of bone, screws, plates, and some soft tissue making the use of the term stiffness inappropriate. With each specimen having multiple components that can each have individual stiffness's, the term rigidity is used is more appropriate to define the measured constructs resistance to deformation. However, due to the interchangeable nature of the terms stiffness and rigidity either is acceptable for this

study. The explanation is included in case publications for either project decide to use the term rigidity versus stiffness, and vice versa.

Failure was determined during the experiment as a fracture of the bone. After each experiment, the test specimen was removed and inspected for failure mode. If the test specimen survived the 30, 40, 50, and 60 degrees of twist, then the data was inspected to determine if there was a sharp drop in load indicating a yield point or specimen failure. Student's t-tests were utilized to determine if significant differences existed between treatment groups at each degree of rotation. Significance was set at $P \leq 0.05$.

One issue that needed to be addressed was the definition of clinical failure for a test specimen in torsion. From repeated discussions with collaborators Dr. Saunders and Dr. Bonin, it was expressed that 30deg of rotation when the patient was brought into the clinic was clinical failure of the implant. Within the elastic region of a material, upon removal of an applied load there is complete recovery of the strain experienced by the material. Within the plastic region of a material, upon removal of an applied load there is incomplete recovery of the strain experienced by the material producing a permanent deformation in the material. The same plastic deformation experienced by materials can be shown in systems of components, such as the LC-DCP/rod and CRIF/rod, but the application of terminology is not entirely correct as the deformation results for different reasons. As is expected in materials deformed within the plastic region but before yielding, there will be some amount of recoil or reduction in strain experienced by the test specimen. That is if the test specimen is rotated to an angular deformation of 30deg,

what is the permanent angular deformation and how much does the system recoil? The question of how much angular deformation is required to produce 30deg of permanent deformation when the patient enters the clinic developed during the design of the torsional experiments. In order to determine what load and angular deformation is required to produce a permanent 30deg of angular deformation the test protocol was expanded from 10mm/min up to 30deg to the following:

- Zero load on Test Resources 830 Biaxial Machine then attach test specimen and pots.
- After test specimen is secure, zero axial load and zero angle value.
- Stage 1 – Ramp from 0N to 10N axial load.
- Stage 2 – Ramp from 0deg to 30deg at a rate of 10mm/min.
- Stage 3 – Ramp down from 10N to 0N axial load and 0N torsion load allowing for test specimen recoil and attainment of near original shape.
- Stage 4 – Ramp from 0N to 10N axial load.
- Stage 5 – Ramp from current angle to 40deg at a rate of 10mm/min.

This process is repeated for rotations of 40deg, 50deg, and 60deg all at the same rate of 10mm/min, with the axial compressive load of 10N, and all allowing recoil to occur upon reaching the intended angle of rotation.

4.4 Statistical Methods

The four point bending data was considered as five contralateral pairs of constructs. Failure of specimen CRIF 4 was a result of bone pullout from the potting

epoxy. During the initial potting of the CRIF/rod construct, the bone is held vertically so that the proximal and distal ends are positioned vertically one above the other. Due to the gap model created, the tissue in the cancelous bone is allowed to flow or drain out of the bone segment. This bone in particular, along with its contralateral pair, had significantly more tissue exit the bone segment while the epoxy was curing. The saline soaked towel was able to capture some of the bone material, but the majority flowed down into the curing epoxy and mixed. It could not be determined after curing if the bone material and epoxy mix would be suitable for testing, and due to the fact that it was not possible to get the test specimen out of the epoxy without damaging the construct or bone it was decided to test the specimen. The bone material and epoxy mix was not suitable for testing, and the bone pulled away from the epoxy material after a small amount of bending was sustained. It cannot be determined whether or not the stiffness was a result of the rigidity of the construct or simply a geometry shift as the construct pulled away from the test rig. Failure of CRIF 1 was a result of improper test rig function. This specimen was not potted with the West Marine Epoxy, and as a result was used to determine the best potting material to use for the four point bending tests.

The four point bending tests gathered load and position data of the axial crosshead. To adjust this data to relevant physiologic values, the load and displacement values were converted to bending moment and bending angle. All constructs data was zeroed at the point of contact between the crosshead and the potted specimen. This was viewed as the transition from tensile to compressive force in the load data. Due to the sampling rate and amount of noise in the load system, this value was approximately -

0.25N and the closest load value to this for each specimen corresponded as the zero stroke value. Conversion from millimeters to meters, followed by the use of the equations in Figure 9 converted the load and displacement data to bending moment and bending angle. Moment versus angle was plotted for each specimen for inspection of the tests success, and comparison with contralateral and same device constructs. The ultimate strength of each device was defined as the bending moment at failure, determined as the highest point before a sharp decrease in bending moment. The bending angle at failure was determined to be the angle at ultimate strength. A 2-tailed paired students t-test was used to determine if the differences between the CRIF/rod and LC-DCP/rod constructs are significant. The mean and standard deviation was calculated for each construct group. Bending stiffness of the constructs is defined as the slope of the linear line of best fit for the moment versus angle curve from 0 to 30 degrees. The units of stiffness are Nm/degree. Thirty degrees was chosen as the cutoff because after thirty degrees specimens deviated from linearity and constructs failed shortly after 30 degrees of bending.

5. CANINE RESULTS

5.1 Torsion Results

Results of the torsion tests are summarized in Table 1. The CRIF/rod constructs exhibited a consistent bi-phasic behavior wherein two distinct phases of torsional rigidity were observed Figure 11. There was not a statistically significant difference in rigidity of LC-DCP/rod (0.553 +/- 0.684 Nm/deg) and CRIF/rod (0.543 +/- 1.682 Nm/deg) constructs from 0-4.9 Nm torque (P=0.819), however the LC-DCP/rod constructs were significantly more rigid (0.303 +/- 1.886 Nm/deg) when compared to CRIF/rod constructs (0.06 +/- 0.371 Nm/deg) at torsional loads above 4.9 Nm (P=0.003) observed in Figure 13. Torsional rigidity was normalized to account for variations in bone by dividing torque by individual bone diameter. While there was not a significant difference in normalized torsional rigidity of LC-DCP/rod (49.585 +/- 10.915 Nm/deg) and CRIF/rod (40.019 +/- 4.603 Nm/deg) constructs from 0-4.9 Nm torque (P=0.107), LC-DCP/rod constructs were significantly more rigid (26.716 +/- 4.116 Nm/deg.) when compared to CRIF/rod constructs (4.369 +/- 0.740 Nm/deg) at torsional loads above 4.9 Nm (P<0.001) observed in Figure 14. This represented a 46.12% and 89.1% decrease in torsional rigidity for LC-DCP/rod and CRIF/rod constructs, respectively. Lastly, CRIF/rod constructs experienced significantly higher permanent angular deformation (23deg +/- 0.89deg) when compared to LC-DCP/rod constructs (7.5deg +/- 2.08deg) (P<0.001), confirming important differences in the torsional properties of these two implant systems. Collectively, these data indicate that while LC-DCP/rod and CRIF/rod

constructs are not significantly different when evaluated under lower torsional loads, the LC-DCP/rod constructs may provide superior fracture stability at higher torsional loads.

In order to maintain a contralateral paired specimen analysis, due to the failure of LC-DCP/rod construct #5 as a result of damage to the bone during implantation of the plate, CRIF/rod and LC-DCP/rod specimens were removed from the data analysis. The individual device torque versus angular deformation plots for the CRIF/rod and LC-DCP/rod can be seen in Figure 11 and Figure 12, respectively. Using an Index Excel function angle and torque values were found that closely matched integer values from zero to thirty degrees. Based on the angle values for each specimen that most closely matched the integer value, an average torque value was generated for each construct at each integer point. The average torque was plotted with standard deviation, and can be seen in Figure 13. The torque data was normalized by the diameter of each bone at the gap. By dividing the torque by the diameter of each bone the moment arm created between the IM pin and the CRIF or LC-DCP was accounted for. The normalized average torque versus angular deformation for both constructs can be seen in Figure 14.

Table 1. The following table details the results of the torsion testing for LC-DCP/rod and CRIF/rod constructs. Torsional rigidity, permanent angular deformation under 30 degrees, and maximum strength were all compared using paired students t-tests for contralateral pairs. The permanent angular deformation after 30 degrees does not include contralateral pair evaluation due LC-DCP/rod constructs failing, decreasing the number of comparable pairs.

Torsion Results			
	LC-DCP	**CRIF**	**P-value**
Normalized Torsional Rigidity below 10 deg [Nm/deg]	49.585 +/- 10.915	40.019 +/- 4.603	0.107
Normalized Torsional Rigidity above 10 deg [Nm/deg]	26.716 +/- 4.116	4.369 +/- .740	<0.001*
Torsional Rigidity below 10 deg [Nm/deg]	0.553 +/- 1.684	0.543 +/- 1.682	0.003*
Torsional Rigidity above 10 deg [Nm/deg]	0.303 +/- 1.886	0.06 +/- 0.371	<0.001*
Permanent angular deformation after 30 degree torsion [deg]	7.47 deg +/- 2.08deg	23.1 +/- 0.89deg	<0.001*
Permanent angular deformation after 40 degree torsion [deg]	11.99 +/- 5.9	32.43 +/- 0.89	NA
Permanent angular deformation after 50 degree torsion [deg]	22.37 +/- 4.51	42.28 +/- 2.19	NA
Permanent angular deformation after 60 degree torsion [deg]	29.76 +/- 4.67	50.65 +/- 1.49	NA
Maximum Strength at 30 degrees [Nm]	11.546 +/- 2.79	6.078 +/-0.527	<0.012*

* - Statistically significant at the P=0.05 level

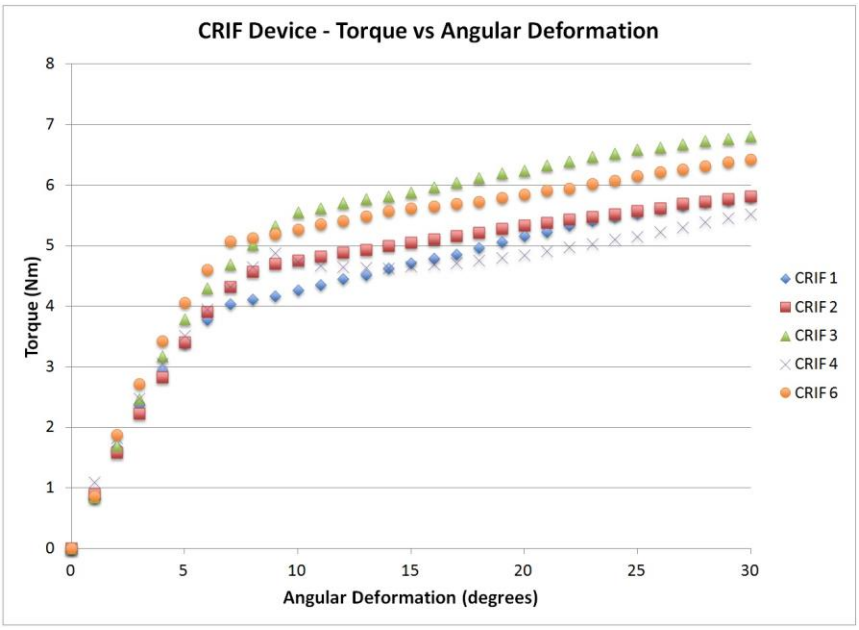

Figure 11. CRIF/rod torque versus angular deformation. CRIF #5 is excluded from this analysis due to complications with the bone during implantation. Torque and degrees were output by the Test Resources machine used for the experiments.

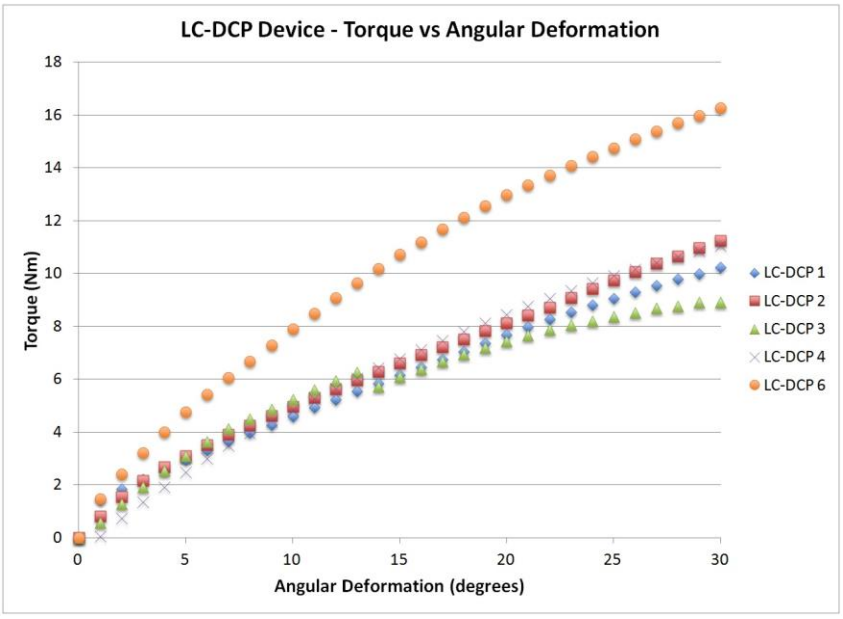

Figure 12. LC-DCP/ torque versus angular deformation. LC-DCP #5 is excluded from this analysis due to removal of the contralateral pair. Torque and degrees were output by the Test Resources machine used for the experiments. .

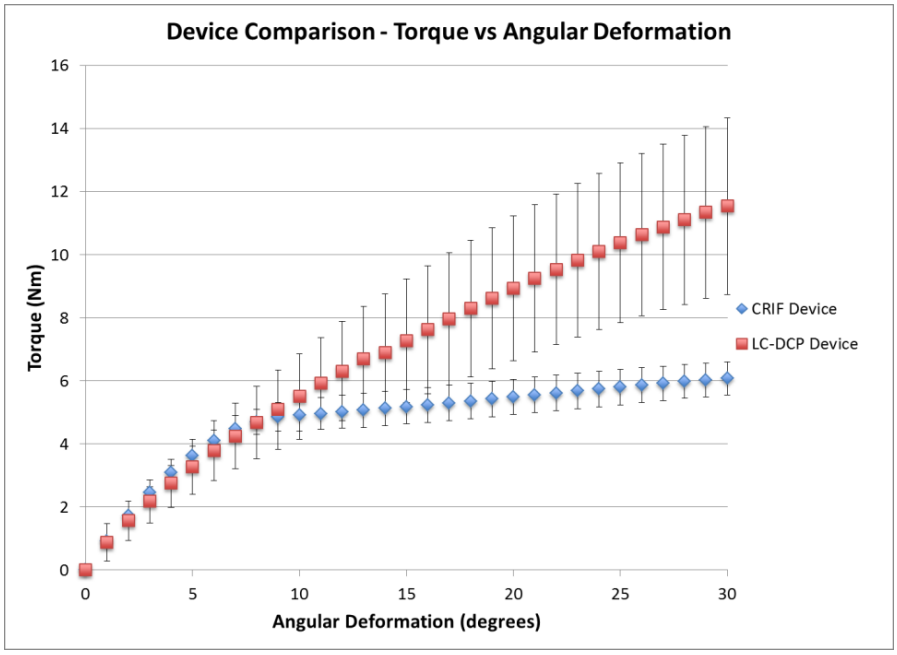

Figure 13. Device comparison between mean CRIF/rod and LC-DCP/rod torque versus angular deformation for contralateral pairs.

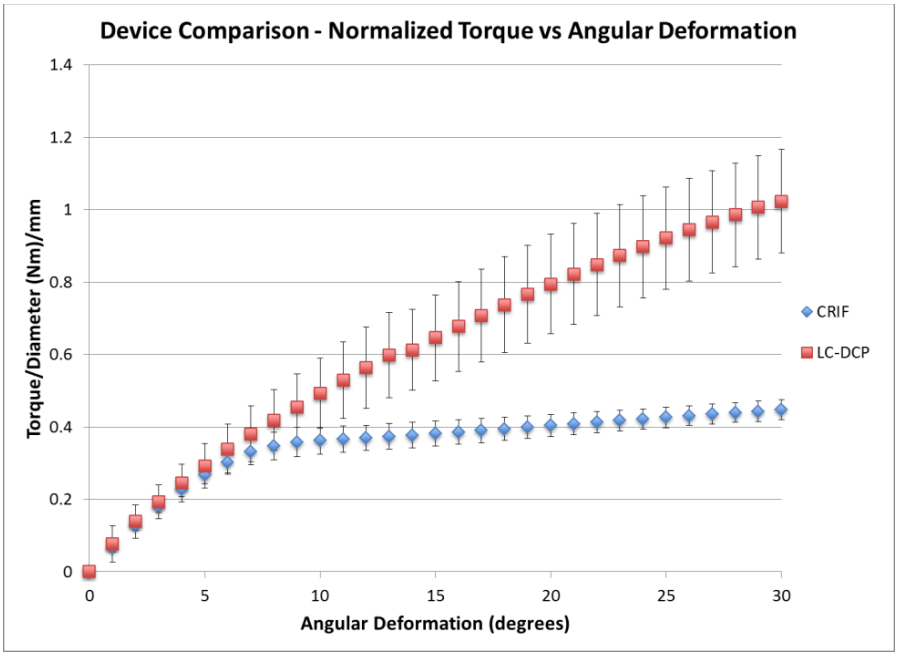

Figure 14. Device comparison between mean CRIF/rod and LC-DCP/rod torque versus angular deformation, where the comparison has been normalized by dividing the torque by the average diameter of each respective specimen.

The torsion experiments before 30 degrees revealed that there is a uniform failure load or angle of rotation that yields the CRIF/rod construct, but also that the measured recoil for both the LC-DCP/rod and CRIF/rod constructs was less than 30deg when deformation of 30deg was achieved. For angular deformation at 40deg, 50deg, and 60deg not all LC-DCP/rod test specimens survived, while all CRIF/rod test specimens survived up to 60deg of angular deformation. Table 2 summarizes each test specimen's angular deformation after release of the applied load at 30deg, 40deg, 50deg, and 60deg. All CRIF/rod constructs retained very similar angular deformations, while the LC-DCP/rod only had two test specimens survive up to 60deg. The results of paired contralateral LC-DCP/rod and CRIF/rod constructs can be seen in Figure 15. The CRIF/rod construct shows significantly more permanent angular deformation than the LC-DCP/rod construct at 30deg, 40deg, 50deg, and 60deg.

Table 2. The following table details the angular deformation after release of the applied torsion load at 30deg, 40deg, 50deg, and 60deg.

Permanent Angular Deformation				
	After 30deg	After 40deg	After 50deg	After 60deg
CRIF 1	23.39	32.72	45.73	51.02
CRIF 2	21.59	30.89	39.64	48
CRIF 3	23	32.45	41.83	51.49
CRIF 4	23.54	33.03	41.91	51.21
CRIF 6	23.9	33.06	42.31	51.52
Mean	23.084	32.43	42.284	50.648
StdevS	0.90	0.90	2.19	1.49
LCDCP 1	10.45	16.05	22.37	29.76
LCDCP 2	5.41	9.88	Failed at 47deg	Failed at 47deg
LCDCP 3	8.51	Failed at 38deg	Failed at 38deg	Failed at 38deg
LCDCP 4	7.27	Failed at 34deg	Failed at 34deg	Failed at 34deg
LCDCP 5	7.29	11.84	Failed at 50deg	Failed at 50deg
LCDCP 6	5.69	10.18	15.99	23.16
Mean	7.786	11.9875	22.37	29.76
StdevS	1.87	5.90	4.51	4.67

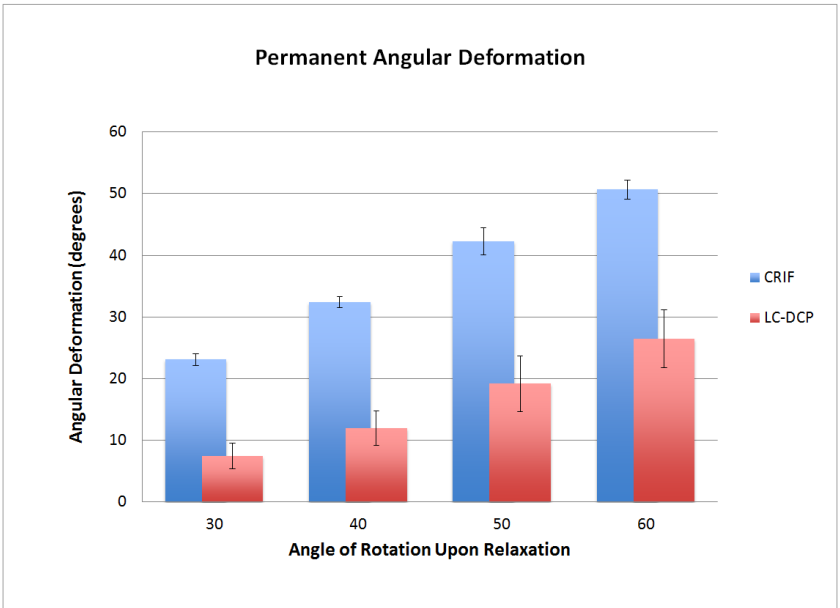

Figure 15. Permanent angular deformation for contralateral pairs including standard deviation for each construct.

5.3 Four Point Bending Data

Results of four-point bending tests are summarized in

Table 3. While there was a trend for the CRIF/rod constructs to exhibit greater mean bending stiffness (2.16 +/- 0.568 Nm/deg) compared to the LC-DCP/rod (2.05 +/- 0.637 Nm/deg), there was no statistically significant difference between construct bending stiffness (P=0.616). There was no significant difference in the mean bending strength for the LC-DCP/rod (133.53 +/- 70.29 Nm) and CRIF/rod (89.75 +/- 12.36 Nm) constructs (P=0.208). Lastly, there was no significant difference in mean bending angle at failure for LC-DCP/rod (39.4 +/- 3.36deg) and CRIF/rod (37.0 +/- 4.53deg) constructs (P=0.445). These data indicate that when evaluated in a canine femoral gap defect in combination with an IM pin, there is no significant difference in the bending properties

of LC-DCP/rod and CRIF/rod constructs. Plots of the CRIF/rod and LC-DCP/rod constructs individual specimen bending moment versus bending angle can be seen in Figure 16 and Figure 17, respectively. Figure 18 shows the mean and standard deviation for mean bending moment versus bending angle for both constructs.

Table 3. The following table details the results of the four point bending testing for LC-DCP/rod and CRIF/rod constructs. Mean bending rigidity, mean failure bending moment, and mean failure bending angle were calculated for contralateral pairs with significance evaluated by paired students t-test.

Four Point Bending Results			
	LC-DCP	CRIF	P-value
Mean Bending Rigidity +/- standard deviation [Nm/deg]	2.05 +/- 0.637	2.16 +/- 0.568	0.616
Mean Failure Bending Moment +/- standard deviation [Nm]	133.53 +/- 70.29	89.75 +/- 12.36	0.208
Mean Failure Bending Angle +/- Standard Deviation [deg]	39.4 +/- 3.36	37.0 +/- 4.53	0.445
Max Bending Moment [Nm/deg]	244.6	96.22	NA
Min Bending Moment [Nm/deg]	64.96	65.48	NA
Max Bending Angle [deg]	44.1	44	NA
Min Bending Angle [deg]	35.24	26.75	NA

* - Statistically significant at the P=0.05 level

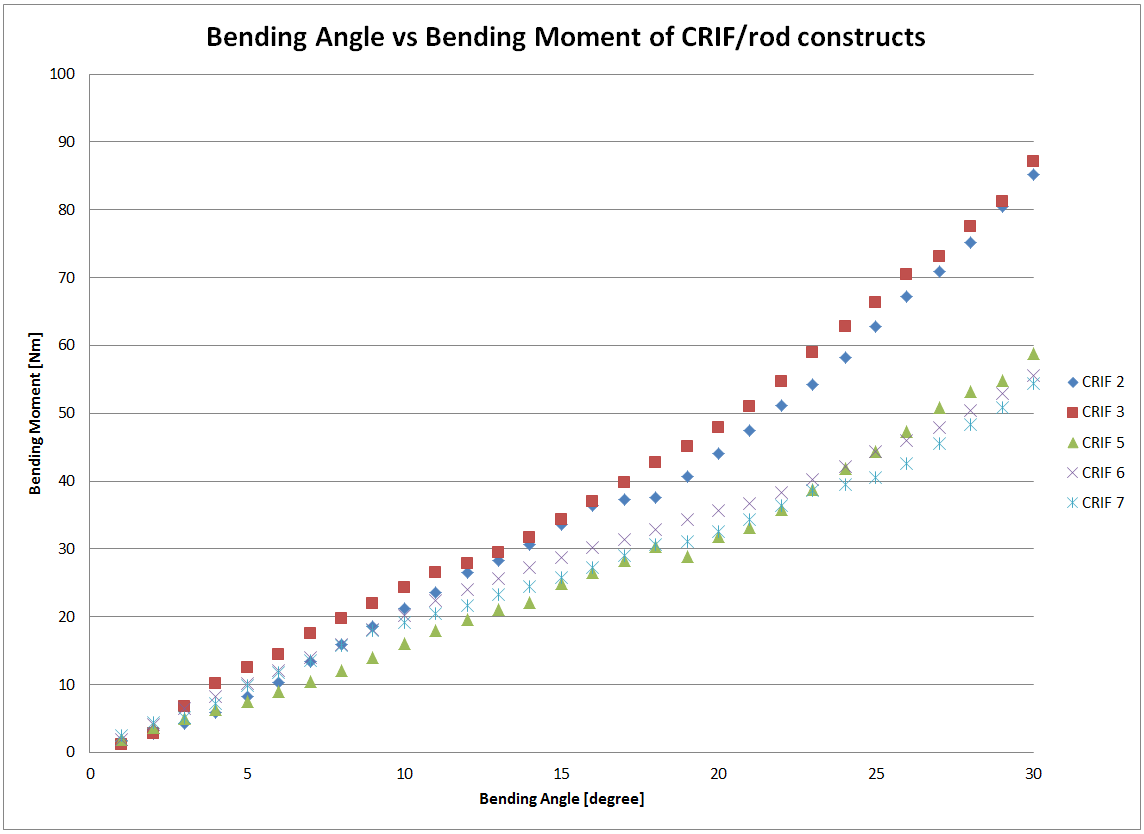

Figure 16. Bending moment versus bending angle for the CRIF/rod constructs.

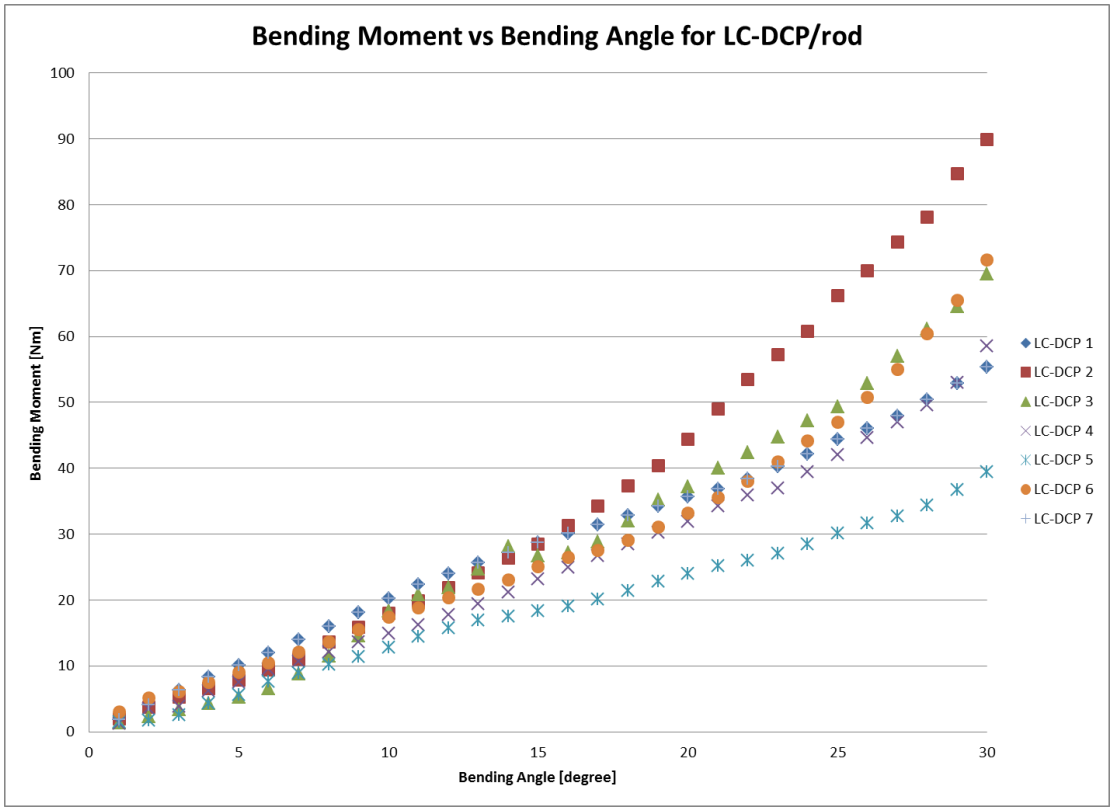

Figure 17. Bending moment versus bending angle for the LC-DCP/rod constructs.

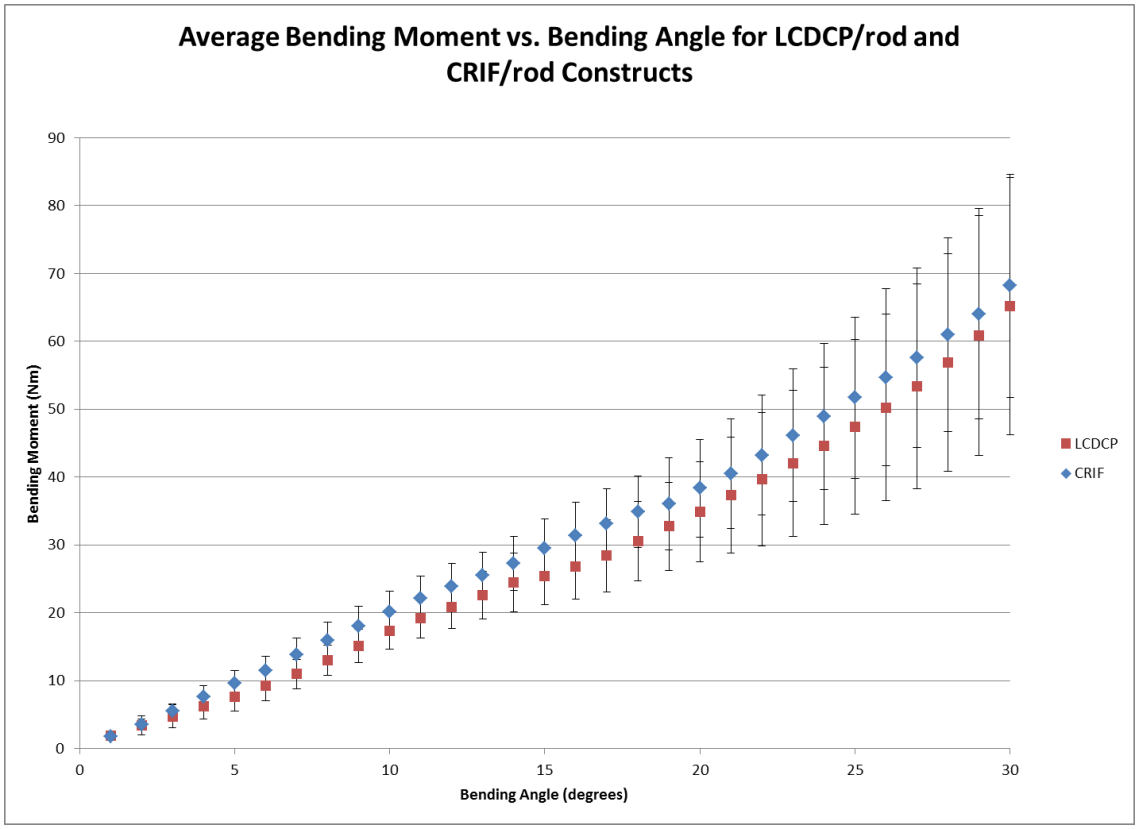

Figure 18. The average bending moment versus bending angle for the CRIF/rod and LC-DCP/rod constructs for contralateral pairs including standard deviation for each construct.

6. DISCUSSION AND SUMMARY

6.1 Torsion Discussion

The torsion results reported in this study are similar to those described by Zahn and colleagues, however the bending results show a different trend. While there were no significant differences in torsion rigidity of LC-DCP/rod and CRIF/rod constructs under lower torsion loads, LC-DCP/rod constructs were significantly more rigid at torsion loads of 4.92 Nm and higher. There was no statistical difference in the bending rigidity between the two constructs, and it is reasoned that the influence of the IM pin contributed to the nonexistent statistical difference between groups. Carter has established that a 36 kg dog experiences 0.56 Nm of torque at a controlled leash-walk and 2.5 Nm of bending moment (3). The significance of the bending moment at a walk can be seen in Figure 19. With both constructs failing beyond 60Nm and 30 degrees of bend, the walking bending moment of 2.5Nm is well within the bounds of both constructs capabilities. However, this is for a leash controlled canine at a walk. The loads and moments placed on an implant under a canine run or jump are unknown. It can be assumed that the running and jumping axial loads and bending moments will be higher at a run or jump, but the exact values are not provided in the literature and will not be assumed here. As approximation could be made based on human femur loading patterns, but the differences in anatomy and gait between dogs and humans could provide an inaccurate prediction. A similar prediction could be made about the established torque value of 0.56 Nm, but the significance of a higher torque placed on

these constructs at a run is of more significance than for a bending moment because of the CRIF/rod's bi-phasic stiffness behavior. While there is no statistical difference between the constructs in bending, the CRIF/rod's bi-phasic behavior at 4.92 Nm provides a cutoff point for comparable performance to the LC-DCP/rod. It can be predicted that the bending moments from a walk to a run the overall determination of which constructs is better in bending will not change. The torsion evaluation of which construct is superior does change above 4.92 Nm. Thus if the torsion experienced by a canine at any motion is higher than this bi-phasic behavior point then the superior construct is the LC-DCP/rod. The significance of the bi-phasic cutoff point and the torque applied during a walk can be seen in Figure 20. When evaluated in this context, both CRIF/rod and LC-DCP/rod implant systems are likely suitable for repair of comminuted femur fractures in canine patients provided the patients do not exceed the normal walking loads.

Statistical analysis of the torsion data for torque versus angular deformation with performed using a Student t-test against the mean LC-DCP/rod and CRIF/rod torque at each angle integer. This assessment was performed to determine what point if any was there a significant difference between the average torque values between the constructs. The average torque versus angular deformation plot shown in Figure 13 details that there is a point where the CRIF/rod construct shows a distinctly biphasic behavior. The paired Student t-test was used to determine this point. The CRIF/rod construct showed distinctly two different slopes at above and below approximately 4.92 Nm or 10 degrees of angular deformation from linear curve fit comparisons, and the t-test significance

confirms that below 10 degrees the average torque value between constructs was not significant (P=<0.05 for significance). At 10 degrees of angular deformation the statistical significance falls from P=0.819 at 9 degrees to P=0.003, and the significance stays below P=0.05 for the duration of the experiment. This result showed that there was a mean point where all CRIF/rod specimens exhibit a change in stiffness, and that the mean stiffness slope deviates from the original rigidity that is not statistically different from the LC-DCP/rod.

An attempt was made at normalizing the torsional and bending data in order to decrease the standard deviation and improve the overall accuracy of the data. For the torsion study, the torque data for a specimen was divided by the distance from the center of the IM pin to the center of either the CRIF or LC-DCP. These measurements were taken by software designed to interpret radiographs. The torque (Nm) was divided by the radius (m) to achieve the force (N) required to achieve a given bending angle. The radius between the IM pin and implant was between 9-15mm, thus dividing by a small value caused a large spike in the values for force. The information provided by this method of normalization was unrealistic, but because the study is a comparison study when looking at the relative change in the results the standard deviation for both construct groups did shrink. The overall comparison between constructs did not change. Several attempts at normalizing the bending data were made, but due to the unique nature of the test rig these assumptions could not be justified and were not included.

The failure mode for the CRIF/rod and LC-DCP/rod are key components to the story portrayed by the torque vs. angular deformation plots and table values. The CRIF

failed, consistently with each specimen, by the CRIF rod rotating inside of the clamps. This result occurs despite the alignment of the IM pin with the neutral axis during testing. It would be expected that the moment arm created by the distance from the IM pin to the CRIF would cause either the rod to deform inside of the clamps, or the clamps deform around the rod. The result however indicates that the amount of compressive force between the CRIF clamp and rod is the weakest link in this biomechanical system. At approximately 10 degrees of rotation or 4.9 Nm, the CRIF rod overcomes the static coefficient of friction holding it inside the clamps and transitions into the dynamic coefficient of friction explaining the biphasic behavior of the CRIF/rod construct. The CRIF rod only twisted only within one set of the three clamps. Either the rod rotated within the proximal or distal three clamps, not within both. This can be explained by the differences in static coefficients of friction between the two sets of clamps, which will vary by the angle of the contoured rod inside the clamps and the compressive force applied by the clamps. When the weaker of the two static coefficients is reached that set of clamps yields, or moves to dynamic friction and the opposing three clamps remain fixed to the CRIF rod. Figure 21 shows the simple method used to determine the failure mode of each CRIF/rod device. A black line was drawn along the CRIF rod and clamp interface on both the proximal and distal ends. The CRIF failure occurs at the interface of machine produced components, which contributes to the consistency of the failure mode as well as the lower standard deviation among the CRIF/rod samples when compared to the LC-DCP/rod constructs. The CRIF/rod construct compared to the LC-DCP/rod is rather uninfluenced by the bones mechanical properties when determining

torsion failure mode.

The LC-DCP/rod under 30 degrees of angular deformation did not have a test specimen fail by yield or fracture, but out to sixty degrees of deformation only two of the six specimens tested survived. The two specimens that did survive the highest angular deformation were also the largest bones by diameter. In all LC-DCP/rod specimens that did fail, the fracture was of the bone and not the LC-DCP or bone screws. Figure 22 shows a LC-DCP/rod fracture around the cortical bone screw holes, which acted as stress concentrators in the bone-implant system.

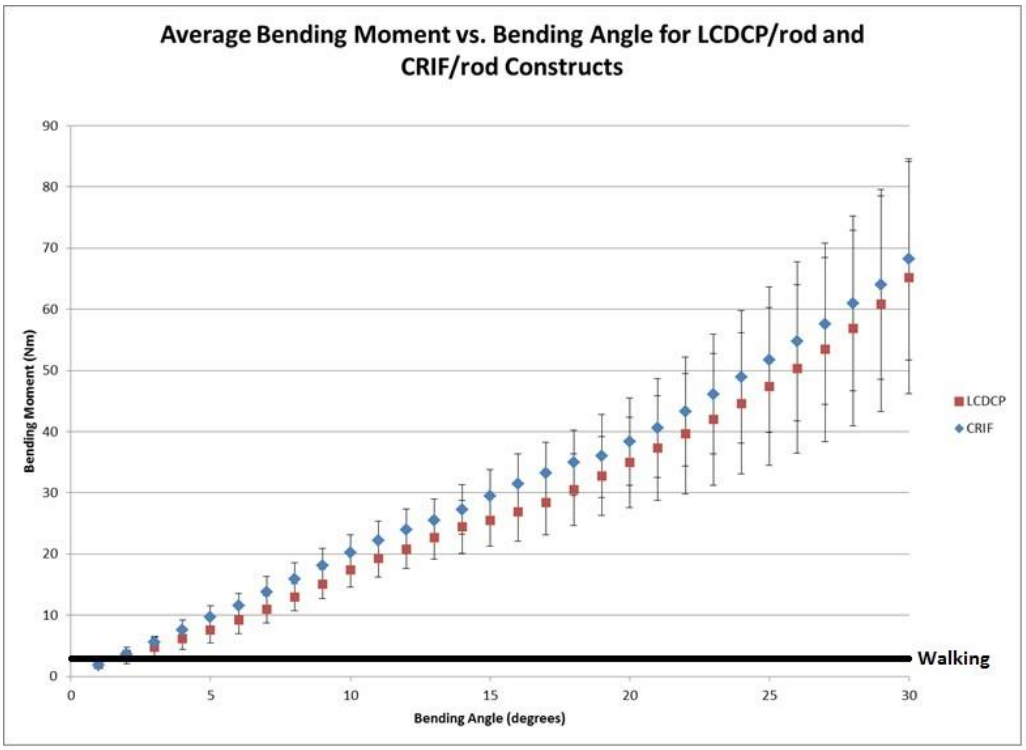

Figure 19. This image is a modified mean bending moment versus bending angle plot. The black line include in the plot shows the normal bending moment at a walk for a canine. Compared to the failure of the constructs beyond 60Nm and 30 degrees of bend, the walking bending moment is well within the bounds of both constructs.

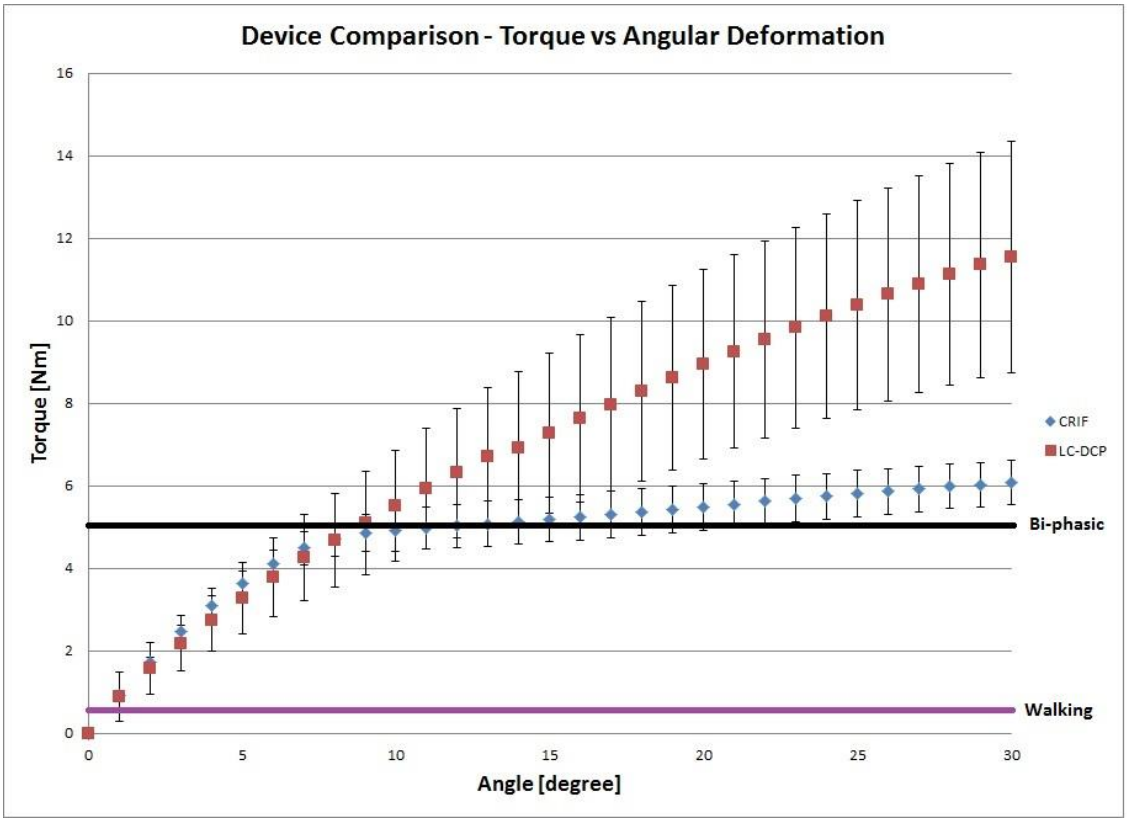

Figure 20. This image is a modified mean torque versus angle plot. The black line include in the plot shows the bi-phasic behavior point at a walk for a canine. The purple line represents the torque placed on a canine (36kg) femur at a walk. Running and jumping torsional values are unknown, but if these values exceed 4.92Nm the superior construct is the LC-DCP/rod.

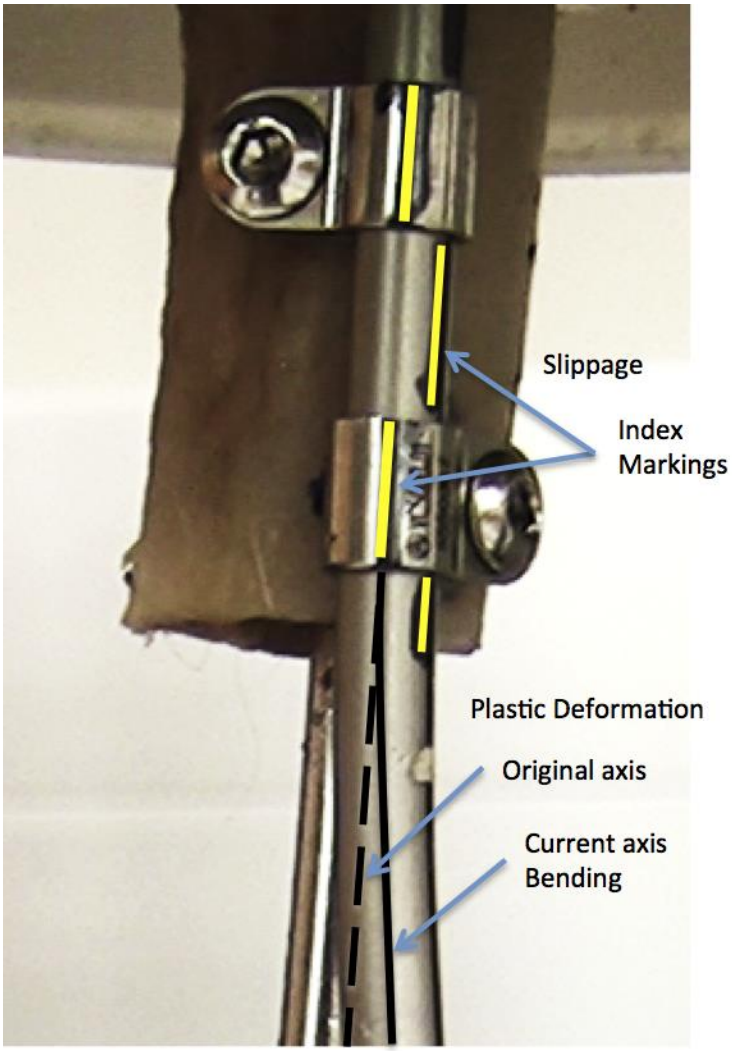

Figure 21. This image shows the sharpie lines that were created on the CRIF rod and clamps to determine if the rod was freely rotating inside of the clamps. As was the case with all CRIF/rod specimens, above 4.92Nm or 10 degrees of angular deformation there was a change in rigidity when the clamp-rod interface shifted from static to dynamic friction. The yellow lines indicate the difference between the rod and clamp after rotation has occurred. There is also a bending of the CRIF rod that results from the changing geometry position of the proximal clamps relative to the distal.

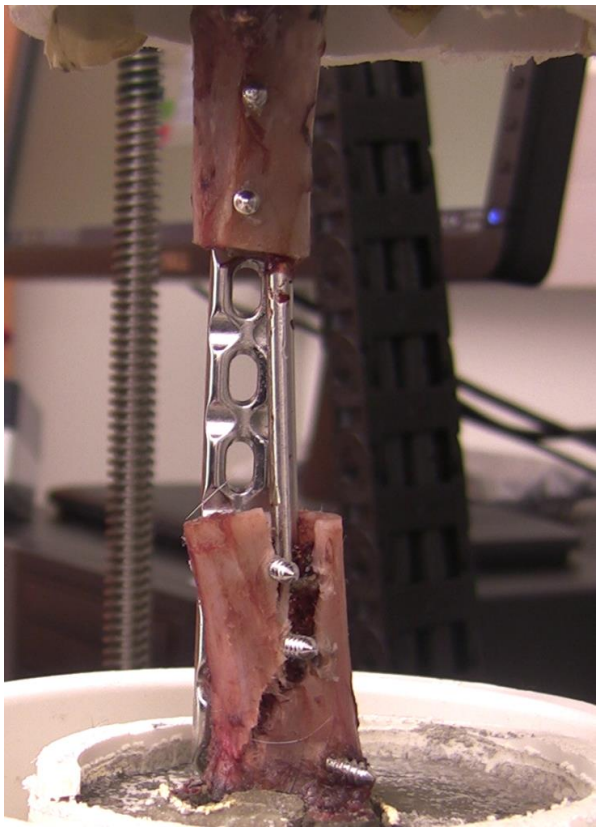

Figure 22. This image shows a LC-DCP/rod fracture of the bone. As was the case with most LC-DCP/rod specimens, the bone was the weakest component to the system and failed at the stress concentration around the cortical bone screw holes.

6.2 Four Point Bending Discussion

Originally, the decision was to test the CRIF/rod and LC-DCP/rod constructs in a buckling scenario as this was determined to be a more physiologic representation of the loading forces compared to four point bending. The rationale for pursuing a four point bending test versus a buckling test was multifold. First, a four point bend would allow for a one to one comparison between past experiments conducted by Hulse and Zahn. Second, past research for calculated strain measurements indicated that a canine femur at a stand exhibits a bending loading scenario when loading is primarily concentrated at the

hip joint reaction forces. (22) A test rig was constructed and several test specimens were used to analyze the buckling test rigs ability to provide physiologically relevant information. The main issue with the buckling test and the test specimens was that the IM pin was exposed at both the proximal and distal ends. The test rig was designed to allow the distal end of the test specimen to be potted, similar to the torsion tests in epoxy or cement, and the proximal end was to be left exposed allowing direct contact with the femoral head preserving the physiologic loading representative of a normal femur in vivo. As the test experiment was conducted, it was immediately apparent that the weakest interface for both the CRIF/rod and LC-DCP/rod constructs was between the bone and the IM pin. As load was applied to the constructs, the IM pin would translate inside the caudomedial cortex of the proximal bone segment and was driven proximally exiting the cranial aspect of the trochanteric fossa. For both the CRIF and LC-DCP the test would proceed and each construct would be subjected to a degree of bending, but the IM pin translated through the trochanteric fossa until it contacted the test rig. In more than one case the IM pin contacted the test rig and it could not be determined if the IM pin was bearing the applied load or the femoral head. Image of the IM rod after buckling testing can be seen in Figure 23. While the CRIF/rod and LC-DCP/rod constructs did resist the applied buckling loads it was readily apparent that the system was yielding at the IM pin to bone interface, and that the IM pin would be pressing into the femoral cup before either the CRIF or LC-DCP would yield. Based on these issues, it was determined that a four point bending loading scenario would be more beneficial because both the proximal and distal ends of the bone could be potted. Potting would mitigate the

translation of the IM pin inside of the bone and the four point bending scenario would allow comparison to past literature results by Zahn.

Figure 23. This image shows the IM pin pressing through the femoral neck region after a buckling experiment. This result is one of the main reasons for pursuing a four point bend test.

The bending results in this study are similar to those found by Hulse and Zahn. (14) (1) While the effect of the IM pin in the torsion tests was mitigated by aligning the IM pin with the neutral axis, despite alignment before testing the effect of the IM pin's on the test results could not be avoided. The two constructs showed no significant differences in bending stiffness, ultimate strength, or angle at failure. During the stance phase of a 350N (35.69kg) canine, the bending moments on the anterior (Mx) and lateral

(My) aspects of the bone were -2.5Nm and -1.4Nm respectively. These values were also among the highest recorded during that experiment. (3) This indicates that despite the fact that the CRIF/rod and LC-DCP/rod constructs are not significantly different in four point bending, during the everyday activities of a compliant canine the loads that the constructs will be subjected to will be low by comparison to what they devices are capable of before fracture. However, this is different from what may be clinically acceptable. Based on the information in this study it would require 1-3 degrees of bending angle in either construct to reach -2.5Nm. The influence of this 1-3 degrees of bending if based on how much strain is occurring at the fracture gap. Stiffness of the constructs in bending will directly influence the amount of strain, and different amounts of strain result in different modes of bone healing. Primary bone healing occurs in environments where strain is less than 2%. Secondary bone healing occurs when strain is between 2% and 10%, and bone will not form at strains above 10%. (23) The fracture model simulated in this study is representative of secondary bone healing where the healing process follows the classical model of injury healing (injury, hemorrhage inflammation, primary callus, cartilage is mineralized, bone remodels). Whether or not the 1-2 degrees of bending in the constructs results in 2-10% strain is something that future studies should investigate for in vitro or in vivo cases.

Failure mode for both the CRIF/rod and LC-DCP/rod constructs came by failure of the bone, and not of the implant for the four point bending tests. Both constructs fractured the bone, or caused a failure of the bone inside the potting material in all specimens. Images of the fractures for the four point bending experiments can be seen in

Appendix A, Figure 32 through Figure 60. Fracture most commonly occurred about the stress concentrations at the interface of the bone and cortical bone screws. In several instances the bone failed completely creating two separate bone segments from the original proximal or distal half. Unlike the torsion tests where the CRIF/rod constructs failure was unique compared to the LC-DCP/rod, the bending tests showed no distinct failure mode for either construct leading to the conclusion that these constructs are not statistically different in bending.

6.3 Effect of Intramedullary Rod

As expected, both bending and torsion rigidity values of the LC-DCP/rod and CRIF/rod constructs evaluated in this study were higher than the stiffness values previously reported for CRIF and LC-DCP implants. Two possible explanations exist for these findings. As detailed above, addition of an IM pin dramatically increases construct rigidity (9) (14). Second, because we utilized an implant/bone/IM pin construct, it is likely that the IM pin contacted the cadaveric bone and implant-associated bone screws, providing additional construct rigidity during bending and torsional analysis. The Zahn study reported that a 3.5mm LC-DCP had a mean bending stiffness of 0.57+/-0.01 Nm/deg and a torsion stiffness of 0.42+/-0.01 Nm/deg, while the 3.5mm CRIF had a mean bending stiffness of 0.85+/-0.01 Nm/deg and a torsional stiffness of 0.41+/-0.02 Nm/deg. The torsional stiffness between the two constructs in the Zahn study was not statistically different, but the bending stiffness was with the CRIF being approximately 30% stiffer. This study reported the torsional stiffness of the LC-DCP/rod

(0.553+/-0.134 Nm/deg) was not statistically different from the CRIF/rod (0.543+/-0.056 Nm/deg) below 4.92 Nm or 10 degrees. The increase in torsional stiffness for both constructs is likely a result of several factors including bone size and the frictional contribution of the IM pin inside the endosteal cavity. Also, with the small axial compression and displacement during the torsion tests, as well as the alternating placement of the CRIF clamps to either side of the CRIF rod the deformation in the clamps likely contributed to increased rigidity. The bending rigidity from this study for the LC-DCP/rod (2.05+/-0.637 Nm/deg) was not statistically different from the CRIF/rod (2.16+/-0.568 Nm/deg), however both were significantly more rigid than that described in the Zahn paper. The influence of the IM pin can be debated in the torsional experiment, but the contribution for the bending results is significant.

To the authors' knowledge, this is the first report comparing the biomechanical properties of LC-DCP/rod and CRIF/rod constructs using a canine femoral gap model. Zahn and colleagues previously reported that the 5 mm CRIF exhibited significantly higher bending stiffness and load to failure than the 3.5 mm LC-DCP (1). In that study, the LC-DCP and CRIF were used in a gap model with canevasit bone substitute and examined under bending and torsion in a single load to failure experimental design. We commonly utilize both the LC-DCP and CRIF systems in conjunction with IM pins to stabilize comminuted femur fractures. Therefore the objective of our study was to determine the biomechanical properties of these implant systems when combined with an IM pin using a canine cadaveric femoral gap model. We did not find a significant difference between LC-DCP and CRIF implants when examined in conjunction with an

IM pin for the four point bending experiments. This is not surprising given the fact that IM pin size remained constant throughout testing and that the contribution to reduced strain in plates by IM pins has been documented (14). Based on structural properties of the CRIF connecting rod as compared to a LC-DCP plate, the cylindrical CRIF is predicted to resist load more than a prismatic plate when evaluated in bending. We selected an IM pin that filled approximately 40% of the endosteal diameter based on previously published recommendations. When utilizing an IM pin of this size, previous work demonstrated a 40% increase in construct rigidity as compared to a construct lacking an IM pin (14). In our study, cadaveric femora were harvested from dogs weighing 35-45 kilograms. Endosteal diameter was evaluated radiographically and again during implant placement. While there were small variations in endosteal diameter between cadaver specimens, we utilized an IM pin with a diameter of 5/32 inches (3.175 mm), as this pin filled 40% of the endosteal diameter for the majority of our specimens. While it would have been possible to alter IM pin diameter based on individual cadaveric specimens, this would have introduced an additional level of variability within the two treatment groups. Furthermore, it would have shifted the focus of our study to the effect of IM pin diameter on construct rigidity rather than maintaining focus on the biomechanical properties of LC-DCP/rod and CRIF/rod constructs. As the effect of IM pin diameter on construct rigidity has been adequately described (14), we maintained a uniform IM pin size across all cadaver specimens.

6.5 Study Strengths and Limitations

There were several limitations of our study. Our experimental design utilized a single load to failure approach for both bending and torsional experiments. Cyclical loading was not performed, which would have provided additional clinically-relevant data regarding these two implants systems. However, it is based on our collaborators firsthand experience that these implant systems fail during running or jumping as opposed to fatigue failure by walking. The information provided by the testing the devices to failure can be applied to determining how these devices will fatigue, but a fatigue study would provide validation of any predictions made. Bending is the most important biomechanical force sustained by the femur during both walking and running in both dogs and humans (22). As such, it was important that we evaluate both the LC-DCP/rod and CRIF/rod constructs in this context. However, the previous study describing the biomechanical properties of the CRIF highlighted important differences between the 5 mm CRIF and 3.5 mm LC-DCP under torsional loads (Zahn et al., VCOT 2008). Based on this report, it was necessary to determine the biomechanical properties of the LC-DCP/rod and CRIF/rod constructs in torsion. Thus we examined the LC-DCP and CRIF in combination with an IM pin under bending and torsional loads. While our study represents an important advance in the understanding of CRIF/rod constructs, additional studies are necessary to evaluate the biomechanical properties of CRIF/rod fixation in response to cyclical loads.

We utilized digital radiography to evaluate cadaveric bones for pre-existing abnormalities. Ideally both digital radiography and Dual-energy X-ray Absorptiometry

(DEXA or DXA) scanning would have been used to evaluate cadaveric specimens prior to implantation. DEXA scanning is a validated and widely-accepted technique to detect small variations in bone quality (Wahner et al., Mayo Clinic Proceedings 1988), however, this equipment was not available at the institution of study. Lastly, as with any cadaveric study there was variation in the size of the bone specimens tested. As detailed above, all bones were from 35-45 kilogram dogs. The 5mm CRIF, 3.5 mm LC-DCP, and 5/32 inch (3.175 mm) IM pin were appropriately sized implants for all femora utilized in the study. In addition, implant/bone/IM pin construct working length was normalized across all specimens by controlling the distance from the surface of the potting material to the end of the CRIF or LC-DCP implants.

6.6 Potential Improvements

There are several improvements that can be made to the CRIF devices based on this study. The CRIF/rod and LC-DCP/rod constructs were not statistically different in bending, but were statistically different at high torsional loads. The failure mode of the CRIF during torsion was at the mechanical interface between the clamp and rod. As previously mentioned by Zahn, the cross sectional geometry of the CRIF rod being round and that the connection is held together by friction contributes to the CRIF failure at the clamp-rod interface (1). These findings were confirmed in this study, and the first improvement to the CRIF device would be to increase the surface coefficient of friction for the inside of the clamps and the outside of the rod. A second option would be to alter the geometry of the CRIF rod where the clamps attached, and use clamps designed to fit

a rectangular or triangular geometry. This would require plastic deformation of the CRIF rod using a crimping or cutting device, but the strength of the device would likely be increased to the point where a patient's bone would fail before the CRIF as was the case with the LC-DCP.

The overall design of this study would benefit from a fatigue test on the CRIF/rod and LC-DCP/rod in both bending and torsion. Using the established compliant canine loading values from Carter (3), a fatigue study would detail the biomechanical performance of each device over time. This would bridge the knowledge gap that currently exists for how these devices behave in an in vitro setting for a compliant canine. While the information presented in this study can be used to approximate how these devices will perform in a fatigue study, both an in vivo study as well as an in vitro fatigue study would benefit the veterinarian community.

7. EQUINE INTRODUCTION

7.1 Problem

Among the most common fatal injuries in thoroughbred racehorses are injuries to the metacarpophalangeal or fetlock joint resulting in disruption of the suspensory apparatus to the leg beneath the joint. (24) The suspensory apparatus is an essential component for proper limb function because it braces the fetlock joint for passive, non-muscle dependent support. (25) (26) Without this support, the limb cannot properly bear load and the horse cannot walk or support its own weight. Injuries to this joint are common, and currently there is not treatment to provide horses with an athletic future. (27) (28) Indications of damage to the joint include: anatomical breakdown encompassing loss of palmar or plantar support structures, fracture of the distal third metacarpal, fracture of the proximal phalanx, and functional loss due to infections and degenerative arthritis. (29) (30) (31) (32) (33) Currently, surgical stabilization of the fetlock joint by arthrodesis is the best option for mitigation of pain and promoting proper healing for return to pasture or breeding. (23)

Fetlock arthrodesis has historically used the DCP applied to the dorsal aspect of the limb. (34) The DCP shows stability during compression loads as a result of the compression force between the DCP and bone from the cortical screws. Transfer of the forces from the bone, through the screws, and into the plate provide the system with structural stability but also a zone of shear loads when the axial loads exceed the forces holding the plate to the bone. The weakest link of the DCP-bone system is the shear

stresses between the screw and bone generated by the screw moving independently of the plate. The DCP arthrodesis technique has proven successful in uncomplicated cases, but in situations that involve limb laminitis and infection the result can be implant failure or cast sores developing during recovery with a final outcome of unsuccessful arthrodesis. (29) (30) (31) (32) (33) A support limb with laminitis can cause the repaired limb to be subjected to increased loads as the horse attempts to shift weight from the laminitic foot to the repaired limb. Surgical site infection results in a poor healing environment, decreasing the likelihood of a successful arthrodesis. To increase the success rate for this procedure, a stronger, stiffer, more stable and fatigue resistant system is needed. This need led to the development of the locking compression plate as well as orthopedic cables. The LCP uses the combination of locking and compression holes to increase stability, strength, and fatigue life. (35) (36) The locking head screw creates a fixed angle between the screw and plate preventing motion of the plate-screw-bone system. This creates a single rigid system where all the screws and the plate are fixed and converts shear stresses into compressive stresses. The locking compression plate allows for locking head screws or cortical bone screws to be used. The flexibility of choice between the two screws allows the orthopedic surgeon to choose the screw best suited for that particular fracture configuration to achieve the most stable fixation. (37) The claims of the LCP performance for fetlock arthrodesis has not yet been reported.

Comparative information on fetlock arthrodesis techniques has been limited to a small number of retrospective studies and a model to test the biomechanical properties of the implants has not been reported.

7.2 Objectives

Catastrophic injuries of the metacarpophalangeal joint resulting in the disruption of the suspensory apparatus are the most common fatal injuries in thoroughbred racehorses. Fusion of the metacarpophalangeal joint or fetlock arthrodesis is a procedure designed to mitigate suffering from injury as well as degenerative diseases affecting articulation. The surgical procedure for treatment is well established, but a model designed to test the biomechanical properties of the bone-implant construct has not yet been reported. A comparative study is needed to assess the mechanical behavior of two techniques for fetlock arthrodesis: the DCP with stainless steel tensions band and the LCP with stainless steel wire tension band. The second technique, using the superior plate determined by the first stage of the project will compare a "figure-eight" tension band using two, 1.25-mm stainless steel wires and a single 1.7-mm stainless steel cable crimping sleeve system (Synthes). Thus there is a need for the specific aims:

Specific Aim 1 – An in vitro comparison of the DCP to the LCP with stainless steel wire tension band, and the superior plate construct with stainless steel wire tension band and stainless steel cable tension band.

Specific Aim 2 – Measure the mechanical properties of the systems such as stiffness, yield point, and mode of failure for cycling and ramp to failure loading scenarios.

The objectives of this study are to biomechanically compare two techniques for fetlock arthrodesis: the DCP with a stainless steel wire tension band and the LCP with a stainless steel tensions band, against the superior plate construct with a stainless steel tension band and a stainless steel cable tension band.

Realization of these specific aims will represent a substantial advancement in our understanding of the biomechanical properties of these fetlock arthrodesis techniques. The impact of the research will provide useful information regarding the use of LCP versus DCP and tension band thickness to both internal fixation device designers and orthopedic surgeons. By providing information based on an in vitro study to surgeons and device makers, this research can promote the best avenue for fetlock arthrodesis treatment based in sound mechanical results from this study. For device makers the results of this research will provide useful information about device and bone interactions, failure modes, construct stiffness, and other system properties. For orthopedic surgeons the information will detail which plate and tension band system result in certain mechanical properties, allowing the surgeon to select the best possible combination for a joint arthrodesis.

Based on the loading regimens for cycling and the single ramp to failure certain predictions can be made about each system. It is likely that both the LCP and DCP bone systems will survive the cycling regimen, but will differ in the amount of compression

allowed over the experiment and the system stiffness. During the single ramp to failure, it can be predicted that the DCP-bone system will have more motion amongst the system components, and thus remain structurally intact for longer despite needing a lower load to deform the system. The LCP-bone system uses a locking cortical screw, which will limit the motion of the plate relative to the bone resulting in increased stiffness. Whether or not this increased stiffness will result in a higher load to fail or lower axial compression distance is something to be determined from experimentation. Failure mode is a category that will require collaboration with surgeons because this is a system, and failure of the system in vivo is determined by a surgeon and may not be the results of structural failure of any component of the plate-bone system. If enough motion is allowed simply from interfragmentary motion to cause discomfort or pain to the horse, a surgeon may deem that system failure. As a result of this collaboration it is likely that a given axial compression value, or angle of bend in the device will be the main determinant of the system failure.

7.3 Hypothesis

We hypothesize that a LCP in combination with a stainless steel cable tension band will be superior in stiffness, yield load, and failure load compared to the DCP with stainless steel wire tension band for fetlock arthrodesis as well as more resistant to biomechanical degradation following cyclic loading. In addition we hypothesize that a stainless steel cable tension band will be superior in stiffness, yield load, failure load, and biomechanical degradation following cyclic loading when compared to stainless

steel wire tension band used with the superior plate determined from stage 1 of the study.

7.4 Justification

Fetlock arthrodesis is a procedure designed to salvage horses suffering from intractable pain associated with end stage degenerative disease of the articulation. It is also performed following traumatic disruption of the suspensory apparatus, a common career ending injury of race horses, which in many instances necessitates euthanasia (38) (33) (39) (40) (41). The surgical procedure is well-established; however there is a paucity of information on the biomechanical behavior of the bone-implant construct as currently employed. Recently, locking compression plates and orthopedic cables have become available and offer potential mechanical advantages over conventional implants (23) (42) (43). However, data on their mechanical behavior when employed for fetlock arthrodesis are non-existent.

Although currently employed methods of fetlock arthrodesis are adequate in uncomplicated cases, there are many instances that a construct which provides more stability and strength and has a greater fatigue life would be beneficial. The most common and serious complications following arthrodesis are support limb laminitis and infection at the surgical site. When support limb laminitis occurs, the repaired limb will be subjected to substantially greater loads as the patient attempts to shift weight off the laminitic foot onto the repaired limb. When surgical site infection occurs, healing will be negatively impacted. If healing is delayed, a construct with an extended fatigue life is

needed. In addition, unless absolute stability is maintained, bone healing in the presence of infection is unlikely. In these instances, a stronger, more stable and fatigue resistant construct would be likely to increase success of the procedure. Comparative information on fetlock arthrodesis is limited to a small number of clinical retrospective studies. A model designed to test the biomechanical properties of implants or tension band materials for fetlock arthrodesis has not been reported. The purpose of this study is to compare what we believe will be a stronger, more stable, and fatigue resistant construct to what is currently employed.

8. EQUINE BACKGROUND

8.1 History of Equine Arthrodesis

Internal fixation and arthrodesis techniques have advanced in the past decades as a direct result of improving expertise by practicing orthopedic surgeons, correct application of the implant, and improved implants based on proven mechanical principles. Although advancement in internal fixation has been fairly even across the board there are still limitations to bone repair found in horses due to infection, delayed union, and failure of the implant. For horses it is generally recognized that stability and the comfort level of the horse are directly related. The more stable an implant-bone construct the less likely it is to see excessive weight bearing in the contralateral limb, or delayed union of the arthrodesizing bones. The need for stability pushes orthopedic surgeons to favor aggressive open fracture repair to minimize the reduction in stability that may result from mechanical instability in less invasive surgical techniques.

8.2 LCP

The LCP is an implant that combines two established treatment methods into one device. The LCP system combines a compression plate and an internal fixator. The plate features a combination of locking and compression screw holes allowing the use of either cortical bone screws or a locking screw. The LCP uses 4.5 or 5.5 mm cortical bone screws and 4.0 or 5.0 locking screws. The use of both screws allows the device to be adapted by the surgeon for the optimum fracture configuration to achieve the most

stable implant. (36) (23) An image of the locking and compression screw holes can be seen in Figure 24. The locking screws have a larger core diameter than the cortical bone screws, and thus are several times stronger and can resist bending and shear forces better than the cortical screw. The locking screw inserts into the LCP plate creating a secure plate-screw interlock reducing the need for a large bone-screw interface to secure implant to the bone. The LCP has been evaluated as being stiffer than the LC-DCP making it favorable for fetlock arthrodesis. (34) (43) (23)

Figure 24. The top half of the image above shows a close up view of the LCP locking and compression screw holes. The smooth surface of the hole represents the cortical bone screw surface, where the threaded portion is used for the locking screws. The bottom half of the image shows a locking screw on the left and a cortical bone screw on the right. (23)

Previous studies have demonstrated the success of the LCP and stainless steel cable tension band in fetlock arthrodesis. Carpernter et al evaluated the LCP/cable for fetlock arthrodesis in six thoroughbred racehorses and found that four out of six horses with suspensory apparatus disruption were sound for breeding one year later. Another study reported 34 of 52 horses with fetlock arthrodesis went on to unrestricted exercise leading to an approximate success rate of 66% between the two studies. (23) (44) The prognosis for arthrodesis has better results when the treatment is used to treat degenerative disease versus disruption of the suspensory apparatus. (45) The LCP/cable has the advantage of not being needed to be contoured exactly to fit the bone because of its function as an internal fixator. The fixation strength is not dependent on the compressive force between the plate and the screw as with the DCP. The fixed angle generated by the locking screws allows the LCP to be applied to the bone with less compressive force, which is favorable to preserve the integrity of the periosteum. Preservation of the periosteum helps mitigate disturbances of the fracture site and or blood supply to the bone. (35) (46) A biomechanical test comparing the DCP, LCP, LC-DCP, and CRIF using a 20 degree oblique mid-diaphyseal fracture model with a bone substitute material with double plating in a four point bending scenario showed results that the LCP had increased yield strength, higher stiffness, and decreased movement at the fracture plane. (43) The LCP shows the disadvantage of being more expensive by using screws that cost roughly 3 times as much as the LC-DCP screws. This cost is mitigated by the ultimate goal of returning a damaged thoroughbred racehorse to breeding soundness, a cost that most horse owners are willing to incur. (23)

8.3 DCP

A well-established technique for MCP arthrodesis by Bramlage is one of the most commonly utilized and successful MCP arthrodesis techniques. (44) (39) (27) This procedure uses a 14-16 holes DCP on the dorsal face of the third metacarpal and proximal phalanx to maintain limb stability, and a tension band wire on the palmar surface to mitigate some of the cyclic loads. The limb is placed in 10 degrees of extension with a contoured bend in the DCP. This technique suffers from contralateral limb laminitis, infection, implant failure, and cast sores that develop during healing. (27) (44) (33) Despite successful implantations, 19 out of 43 horses were euthanatized due to implant complications. (44)

Surgeons often try to mitigate the effects of cyclic loading on the implant and reduce the risk of implant failure by changing the configuration of the DCP and MCP joint to closer to a linear arthrodesis with the negative result of a slightly longer limb. (27) (29) While horses can adapt to the longer limb length the result is often overloading of the contralateral limb, which can result in degenerative joint disease and pastern joint subluxation. (39) The tension band is used to mitigate the effects of cyclic loading, allowing surgeons to place the MCP joint at an angle that allows for better anatomical length with the contralateral limb, and prevent failure of the DCP. (35) (47)

8.4 Tension Band and Cable

Orthopedic wires or tension bands have many different uses and functions depending upon the need for repair. An orthopedic wire is simply a biocompatible

stainless steel wire, most often SS316L. Wires cannot resist bending loads, but perform to resist loads that are applied perpendicular to its cross sectional area. For wires, the weakest point of a wire is usually the knot associated with the fixation method. A tension band wire is commonly placed to oppose the pull of a muscle or a ligament on bone fragments. In this case the tension band is being utilized to mitigate the tension forces that would be experienced on the palmar aspect of the MCP joint. A medial to lateral hole is drilled in the MC3 and P1 bones and figure-8 loops of 316L stainless steel wire is placed through these holes across the palmar surface of the joint. As the joint flexes, the intention is that tension forces on the palmar surface are converted to compressive forces inside the P1 and MC3 holes by the tension band.

8.5 Biomechanics of Plates

The function of standard fixation constructs depends upon the stability requirement for an individual fracture, and can either function as a load sharing or load bearing device. Stability of the fracture being the ultimate goal has several concepts associated with fracture fixation. Stability ultimately affects the amount of strain that will be sustained at the fracture site, and strain in turn is determined by the type of healing occurring or that can occur at the fracture site. Primary bone healing results when strain is less than 2%; whereas secondary bone healing occurs when strain is in the range of 2-10%. Fracture gap strain levels determine the type of bone healing that can occur. Primary (endosteal) bone healing results under high stability or rigid fracture fixation. Compressive plating provides rigid fixation through minimization of fracture

gap motion. Compressive plating works best when the construct is placed on the tension side of the fracture. For equine arthrodesis, this is not possible due to the presence of vital tissues on the palmar aspect of the joint.

Secondary (endochondral) bone healing is characterized by callus formation, and results under relatively stable conditions provided by splints, casts, locked plates, and external fixators. Callus formation begins with the hematoma, then inflammation, and the formation of fibrous tissue. Mesenchymal stem cells differentiate into cartilage that will eventually ossify into bone. Strain affects tissue differentiation because tissues differentiate into more rigid materials such as cortical bone. During each phase of healing the motion at the fracture gap decreases; eventually resulting in an environment that is suitable to bone formation. (48)

Conventional plates such as the DCP are designed to provide the absolute stability required for primary bone healing. When the DCP is loaded axially the applied force is converted to a shear stress at the bone-plate interface. The applied axial force is resisted by frictional forces at the bone-plate interface generated by the compressive force generated by the screws. The screws function independently, and as a result the screw contributing most to the compressive force is also bearing the most load. Once the compressive force between the bone-plate has been exceeded by the axial load the strength of the construct falls to the axial stiffness of the screw located farthest from the fracture site (in either direction) depending on where the load is propagating from. The DCP lacks axial screw control, which places the demand for axial stability on the bone cortex nearest the plate. The strength of the construct falls to the strength of the cortical

bone nearest the plate, which under high shear stresses can result in bone failure, absorption, or screw loosening. These unfavorable results can increase the strain at the fracture gap and lead to malunion or nonunion of the healing bone. (23)

Bending loads for conventional plates have varying effects on the bone and construct, depending on the nature of the fracture repair. The resistance of a plate-screw construct to bending forces falls to the resistance of the bone within the threads of a single screw to the applied shear stress when the plate is placed on the tension side of the bone. The highest shear stresses experienced by a DCP construct are located at the furthest screw from the applied load on the tension side. When the DCP is located on the compression side the screws closest to the fracture site bear the greatest shear stress. In either case, the resistance of the construct falls to the strength of the bone within the screw threads. The DCP relies on the bone within the screw threads because its design renders it unable to prevent the screw from orienting to the direction of the applied load. The weakest link in the DCP-bone construct is the shear interface between the bone and screw. (23)

The DCP requires a compressive force between the plate and bone to resist plate motion, but the compressive force prevents periosteal perfusion and can lead to compartment syndrome. Compartment syndrome occurs at the bone under the plate as a result in periosteum and bone necrosis at and adjacent to the plate. (49) Localized bone resportion around the screws can lead to loosening of the plate, although studies have shown that plates can maintain compressive forces between the plate and bone for up to 3 months in vivo. (50) (8) The issues with periosteum interference by conventional plates led to the development of the LC-DCP, which mitigates plate to bone contact

through a unique plate surface design. (36) (51) (52) The LC-DCP may reduce contact with the bone by ~50% the construct still relies on the plate to bone interface for stability. (23)

Conventional plates and screws have the following disadvantages:

- Lead to necrosis, which can result in infection
- Lead to stress shielding, which results in a weakened bone and a higher potential for refracture of the bone upon device removal
- Result in delayed union or non-union at the fracture gap due to lack of stability

The disadvantages created by the DCP at the plate to screw interface are mitigated by newer locking plates that control the axial orientation of the screw relative to the plate. This creates a single beam structure where there is no motion between connected components. The benefit of a single beam construct is that it is four times stronger than simple load sharing beam constructs where motion can occur between components. Locked plates such as the LCP are single beam constructs by design. A locked plate creates a fixed angle between the plate and bone. The benefit of having a fixed angle device is that fracture fixation healing can be improved in scenarios where fracture reduction does not provide sufficient bone to achieve the compression necessary for a DCP construct. The application of shear stress to a fixed angle device results in the conversion of forces from shear to compressive stress at the bone to screw interface. Bone has a much higher resistance to compressive versus shear stress resulting in an improved fracture fixation device. Locking plates rely on the strength of the sum of all screw-bone interfaces for fixation compared to unlocked plates using a single screws

axial stiffness or bone-screw pullout resistance. Strain at the fracture site for locking plates is ideal for secondary bone healing. (53) Locking plates act as internal fixators and do not rely on the frictional force between plate and bone as non-locking plates require. This allows for less contact between the locking plate and the surface of the bone improving the local blood supply provide by the periosteum. (23)

Locking and compression plates utilize different mechanical loading schemes to achieve fracture fixation and in doing so create different environments for bone healing. Compression plates such as the DCP and LC-DCP create an environment that promotes primary bone healing through absolute stability by anatomic reduction at the fracture gap to strains less than 2%. Locking plates provide a wider fracture gap, less stability, and increased strain amounts up to 10% creating an environment conducive to secondary bone healing. Locking plates are ideal for indirect fracture reduction, diaphyseal/metaphyseal fracture in osteoporotic bone, bridging highly comminuted fractures, plating scenarios that require the plate to be placed on the compression side of the fracture. Non-locking plates will continue to be useful for fracture fixation in scenarios that require absolute stability and anatomic reduction, where reduction is necessary to preserve motion, and where increased stability can lead to bone union.

9. EQUINE METHODS

9.1 Overall Study Design

Stage 1: In vitro biomechanical testing of six paired cadaver equine forelimbs following arthrodesis by 1 of 2 plating techniques (DCP vs LCP). Stage 2: In vitro biomechanical testing of six paired cadaver equine forelimbs following arthrodesis by 1 of 2 tension band techniques (stainless steel wire vs stainless steel cable).

9.2 Construct Design

Twelve forelimb pairs will be collected from adult horses euthanized for reasons unrelated to disease of the metacarpophalangeal joint (MCP). Forelimbs will be wrapped in 0.9% saline soaked lap sponges, double bagged and stored at -20^{o}C. Each forelimb pair will be randomly assigned to 1 of 2 arthrodesis techniques and the contralateral limb will be assigned to the other group by default. The first technique, using a 14-16-hole broad 4.5-mm LCP in combination with two "figure-eight" tension bands using 1.25-mm stainless steel wires will be compared to a 14-16 hole broad DCP in combination with two "figure-eight" tension bands using 1.25-mm stainless steel wire, which is the technique currently employed by most equine surgeons. The second technique, using the superior plate determined by the first stage of the project will compare a "figure-eight" tension band using two, 1.25-mm stainless steel wires and a single 1.7-mm stainless steel cable crimping sleeve system (Synthes).

Before arthrodesis limbs will be thawed at room temperature (20^{o}-22^{o}C). A linear incision will be made through the skin and common digital extensor tendon. The metacarpophalangeal joint capsule will be incised parallel to the joint surface to expose the dorsal aspect of the articular surface. The lateral collateral and lateral metacarposesamoidean ligaments will be transected and the metacarpophalangeal joint manually disarticulated. The articular cartilage will be removed by a bone curette. Cartilage removal is normally performed clinically to maximize friction and therefore stability across the joint surface which improves patient comfort and the progression of the arthrodesis. Osteostixis will be performed on the articular surface of the 3rd metacarpal (MC3) and proximal phalanx (P1) using a 2.5mm drill bit. Ostectomy of the dorsal aspect of the sagittal ridge will be performed as needed to improve contact area and reduce plate contouring. A 14-16 hole 4.5-mm broad LCP or 4.5-mm broad DCP will be contoured with a 10-12^{o} bend centered over the metacarpophalangeal joint, oriented with 4 holes distal to the articular margin of P1. Once aligned the plate will held in place with a Push-Pull Reduction Device 9Synthes) inserted at the 6th hole from the proximal end of the plate. The plate will be fixed to the dorsal surface of MC3 and P1 with the placement of 5.5mm cortical screws and 5.0-mm locking screws. In DCP constructs all holes will be filled with 5.5-mm cortical bones screws of appropriate length. In LCP constructs holes 1,3-7,9,11, and 13 will be filled with 5.0-mm locking screws of appropriate length. Once the tension band is created a tention device is applied at the most proximal hole and is used to pull the plate proximal further tightening the palmar tension band. All screws engaged both the cis- and trans- cortices of MC3 and

P1. Two additional 5.5-mm cortical bone screws will be placed transarticular dorsoproximal P1 to distopalmar MC3 to achieve additional compression across the joint. During all drilling, heat was minimized by saline dripped over the drill bit to avoid thermal necrosis. Fluoroscopy will be utilized as appropriate to guide screw placement.

Two 1.25-mm stainless steel wires or one 1.7mm stainless steel cable will be used to create a "figure-eight" tension band on the palmar aspect of the metacarpophalangeal joint. A 3.2-mm drill will be used to create 2 holes in the frontal plane, parallel to the joint surface; 1 hole placed half way between the dorsal and palmar cortex of P1, 6 cm distal and the 2^{nd} hole placed 6 cm proximal to the articular surface of MC3. A curved wire-passer will be used to ensure the tension bands are placed against the bone and soft tissues are not interposed. The wire tension band will be applied and manually tightened with the joint flexed 15^{o}, before the plate is affixed to the metacarpus to ensure appropriate tension across the palmar aspect of the joint. The cable tension band will be placed and tightened to 10 kg, the plate then affixed to the metacarpus followed by final tensioning of the cable to 50 kg.

Mechanical behavior during axial compression, including construct stiffness, cyclic fatigue, and single cycle to failure, of each construct will be elucidated by appropriate loading regimens using a materials test system. Clinical computed tomography (CT) imaging will be employed for measurement of 3-D bone mineral density to validate equal bone density of the third metacarpus and first phalanx to ensure

limb pairs are comparable (54). CT scans will also be performed after failure to document mode of failure in each specimen.

9.3 Mechanical Testing

In vivo forces exerted in a longitudinal direction along the radius and metacarpus places the majority of load in axial compression limiting the importance of testing constructs in torsion or bending. All constructs will be tested in axial compression to include non-destructive cyclic loading followed by failure testing. Soft tissues and proximal sesamoid bones will be removed and the limb will be disarticulated at the carpometacarpal joint and proximal interphalangeal joint and fixed on a pedestal to facilitate mounting in the materials test system. Construct stiffness will be defined as the slope of load versus displacement curve, with displacement measured by optical strain measurements and an extensiometer spanning the metacarprophalangeal joint on its palmar aspect. Mechanical integrity of the constructs will be compared using non-destructive loading followed by testing to failure. In the single cycle to failure test, loading rates for axial compression, are chosen to represent the largest compressive forces in the distal forelimb occurring during recovery (20.6kN for a weight range of 450-550kg) (55). In cyclic fatigue testing, under axial compression, the loading rates are chosen to represent loads on MC3 during walking (7.52kN for a weight range of 450-550kg) (56). When both walking and shifting of weight are included the activity of the forelimb in a 24-hour period is 190$\pm$184steps/h.

Axial Compression- single non-destructive load. Construct stiffness will be determined by using single non-destructive loading ramp (axial compression) to a pre-determined load of 7.5kN, with baseline valued determined prior to cyclic loading and repeated after each of the four cyclic loading sessions. The maximum load of 7.5kN is 50% of the yield load of the 4.5 broad limited-contact DCP-MC3 construct in a previous study and within the elastic region of the load deformation curve (57).

Axial Compression- cyclic fatigue testing. Four cycles of loading at 2 Hz will be performed for 5000 cycles using a pseudo-load control protocol previously described by Zoppa et al. After each cyclic loading interval, construct stiffness and MCP gap formation will be determined using a single non-destructive loading ramp. Data will be collected at 60 Hz (58).

Axial Compression- single cycle to failure. After 25,000 cycles each construct will be loaded to failure at a displacement rate of 0.2mm/s. Failure will be defined as a sharp, observable decrease in the monotonically increasing force profile (58). Data will be acquired at 0.02s intervals throughout the test by analog conversion. CT data will provide descriptive information to identify failure modes specific for each construct.

For all testing, load-deformation curves for each construct will be plotted with load on the y-axis and displacement on the x-axis.

9.4 Statistical Methods

The experiment is designed in randomized blocks with repeated measures. 2-way repeated measures ANOVA will be used to detect differences in construct stiffness,

yield and ultimate failure loads for each time point. P-value <0.05 will be considered significant.

The fatigue test data was considered as five contralateral pairs of constructs. Failure of the TestResources machine for DCP#2 resulted in abnormal loading conditions that were determined to be unfavorable to include in this study. The fatigue tests gathered load and position data of the axial crosshead. Matlab was used to process the large amount of information gathered from each fatigue test to extract load and position for the individual ramp and cycling stages. Load versus displacement was plotted for each ramp section for each specimen, and the slope of these displacements was fit with a linear curve line to represent stiffness. The average and standard deviation of each ramp stage for stiffness was tabulated for both constructs, as well as the displacement during each fatigue cycle. Paired student's t-tests were used to evaluate the statistical significance of the contralateral pairs between construct groups for stiffness and displacement.

The single ramp to failure test data was considered as four contralateral pairs of constructs. During testing of LCP #5 the MTS component that interfaced with the custom fabricated aluminum housings failed. This component interface with the MTS machine via a pin attachment, and the aluminum housing with a threaded extension. The difference in diameters between the pin and threaded extension was significant, and due to the off axis loading created by the unique geometry of the test specimen a large moment was created that deformed the MTS attachment at the threaded extension. The results of the test could not be verified to be the result of deformation in the test

specimen versus deformation of the MTS attachment. Thus LCP/wire and DCP/wire specimens #5, and DCP/wire and LCP/wire specimen #2 had to be removed from the single ramp to failure data in order to maintain a contralateral comparison. The single ramp to failure results contained less data points, and were processed in Excel instead of Matlab. The load versus displacement data gathered by the MTS 810 machine was plotted. Each specimen contained different slopes during the test due to interfragmentary motion and decreasing stiffness under increased load. The first test specimen to fail occurred at 5mm of axial compression, and the tabulated values only consider 5mm and under data in order to maintain contralateral pair comparison.

10. EQUINE RESULTS

10.1 Fatigue Results

The results of the fatigue tests are summarized in Table 4 and Figure 25. There was no significant difference in the mean stiffness at the initial ramp, or each preceding ramp stage between the LCP/wire and DCP/wire constructs. There was a trend for both devices to have a lower initial stiffness during the first ramp stage than all preceding ramp stages. This difference is likely a result of interfragementary motion and components of the LCP/wire and DCP/wire constructs moving and adjusting under the repeated cyclic loading. There was no LCP/wire or DCP/wire construct that failed during the fatigue tests. After a fatigue test the test specimen was removed from the Labstone potting material via hydraulic press, and then visually inspected to confirm that the construct was intact. Inspection was to confirm that the tension band wire, plate, and screws, were still functional and that no failure had occurred and not registered on the load readout. The percent change in stiffness varied widely from specimen to specimen, and construct to construct. The trend among both specimens is an increase in stiffness from the first ramp to the second as seen in the percent changes in stiffness from the initial ramp stage in Table 5. The average change in stiffness for the LCP/wire (80.56+/-52.22%) and the DCP/band (56.68+/-14.85%) from the initial to second ramp stage was not statistically significant, nor was the change in stiffness in any ramp stage from the initial. The most significant jump in stiffness occurred for both constructs after the first fatigue cycle, where all changes in stiffness for ramps 2 thru 5 averaged a percent

change of less than 4.05%. The percent change in stiffness between ramp stages for both constructs and all specimens can be seen in Table 6. While the trend among both constructs was to increase stiffness after the initial ramp stage, there was no statistical difference between the LCP/wire and DCP/wire constructs for percent change in stiffness during the fatigue test. Table 7 shows the change in displacement during each fatigue cycle for each specimen, as well as the average, standard deviation, and statistical significance of a paired students t-test for construct groups. The only stage that shows any statistical difference is stage three, but stages 1-2 and 4-5 show no statistical difference. Table 8 shows the percent change in each test specimen's maximum displacement from the initial ramp stage's maximum displacement. This table shows how much each specimen changed from the initial ramps maximum axial compression length, as well as mean, standard deviation, and statistical significance for each construct group. Fatigue cycle 2 and 3 show a statistical difference in the percent change from initial displacement, but fatigue cycles 1, 4, and 5 do not show a statistical difference.

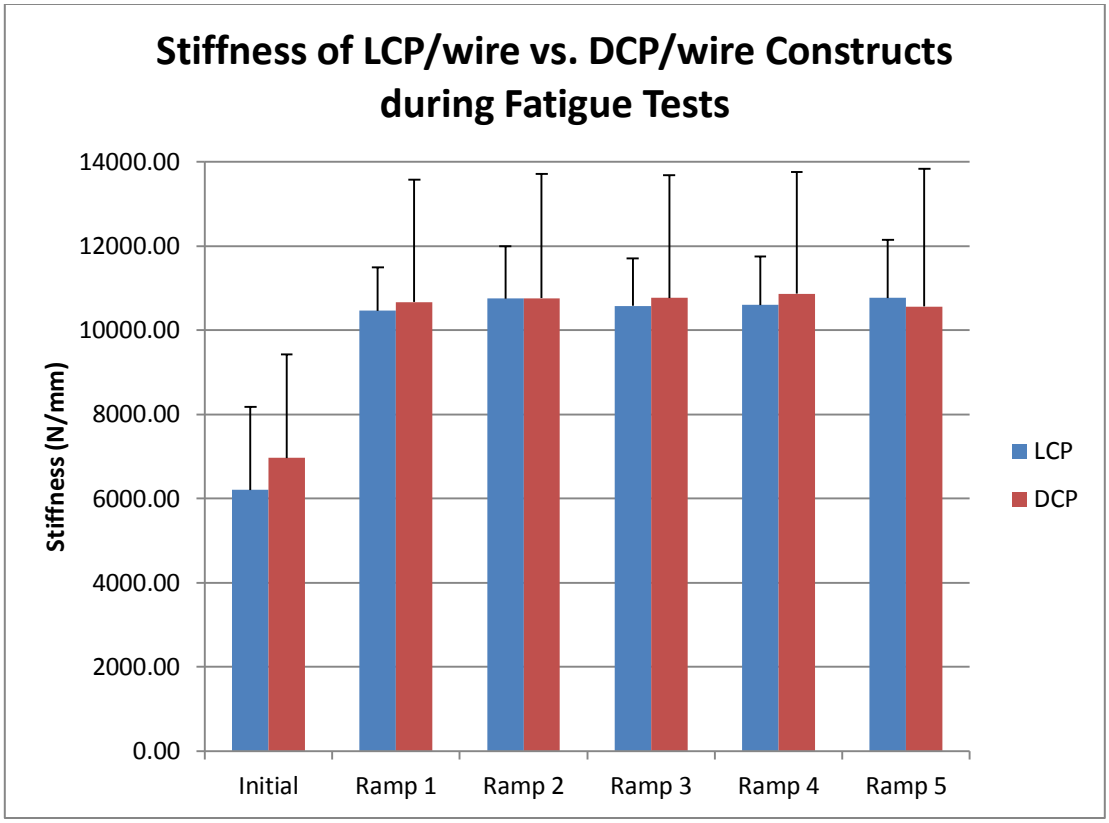

Figure 25. The bar graph above shows how the LCP/wire and DCP/wire constructs compared from the initial to final ramp stage. There was during no ramp stage a statistically significant difference in stiffness between the two constructs, as is seen in Table 4.

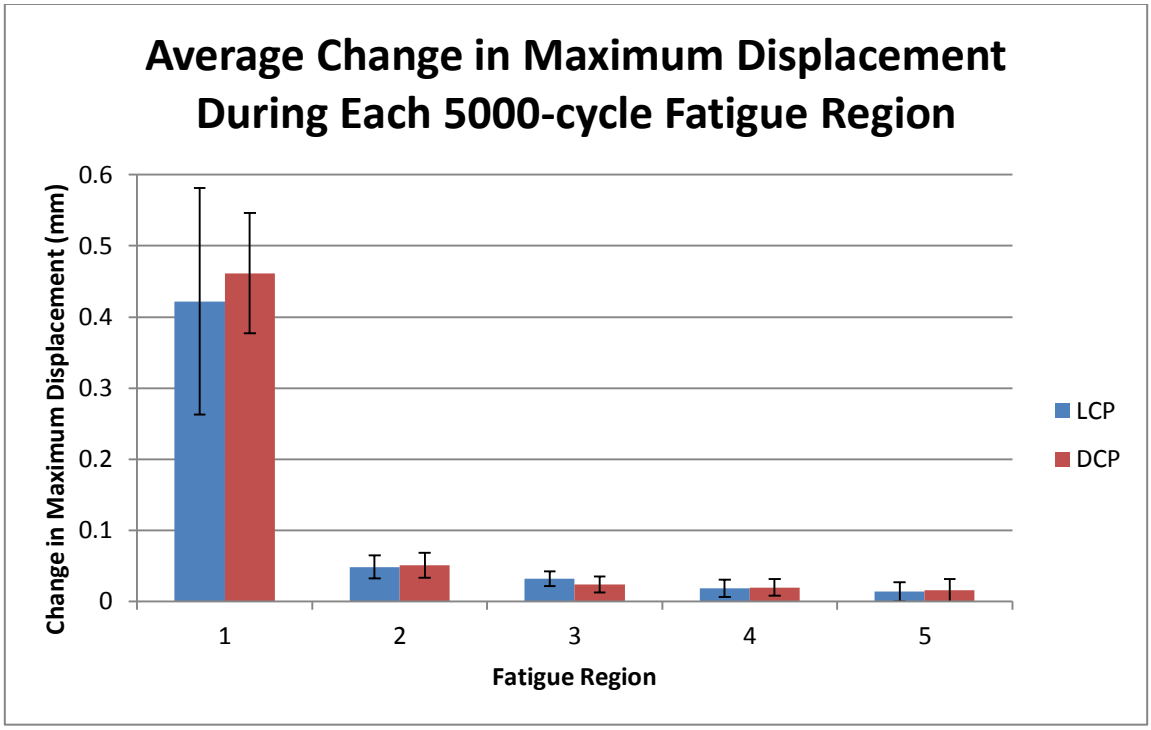

Figure 26. The bar graph above shows the average change in maximum displacement during each fatigue cycle. The first fatigue cycle shows the most significant change in displacement with each successive fatigue cycle decreasing in axial displacement per cycle.

Table 4. Shown below are the stiffness results for each LCP/wire and DCP/wire specimen for the ramp stages in the fatigue tests. Each ramp is intended to measure the stiffness of the specimen prior and after a cycling regimen of 5000 cycles at 2Hz from 0-7500N compressive load. All stiffness values are in N/mm.

LCP/wire and DCP/wire Fatigue Test Stiffness Results												
Stiffness [N/mm]	**Initial**		**Ramp 1**		**Ramp 2**		**Ramp 3**		**Ramp 4**		**Ramp 5**	
Sample	LCP/wire	DCP/wire	LCP/wire	DCP/wire	LCP/wire	DCP/wire	LCP/wire	DCP/wire	LCP/wire	DCP/wire	LCP/wire	DCP/wire
1	5017.97	7302.97	10339.52	11880.07	10309.59	12047.17	10166.78	12081.22	10075.40	12139.07		
3	8314.92	10818.22	10926.76	14727.72	11978.41	14945.76	11308.10	14890.04	11473.49	14960.93	11715.98	15043.81
4	8387.83	6700.76	11076.45	10835.24	11250.29	10813.61	11227.48	10814.56	11193.83	10848.20	11127.55	10814.50
5	4412.68	5836.62	11235.89	8626.57	11413.40	8393.86	11405.61	8371.57	11435.32	8734.63	11502.39	8830.50
6	4893.40	4168.07	8741.71	7276.75	8817.86	7592.31	8790.23	7685.81	8799.81	7642.06	8721.53	7558.70
Mean	6205.36	6965.33	10464.06	10669.27	10753.91	10758.54	10579.64	10768.64	10595.57	10864.98	10766.86	10561.88
SD	1972.20	2455.98	1020.64	2900.27	1237.58	2950.13	1118.59	2913.79	1154.25	2886.44	1385.08	3274.57
P-Value	0.42		0.86		1.00		0.88		0.82		0.88	

Table 5. Shown below are the percent change in stiffness's results for each LCP/wire and DCP/wire specimen for the ramp stages in the fatigue tests. Each ramp is intended to measure the stiffness of the specimen prior and after a cycling regimen of 5000 cycles at 2Hz from 0-7500N compressive load. The initial columns for LCP/wire and DCP/wire are stiffness values in N/mm, while all remaining columns represent percent change from the initial stiffness.

LCP/wire and DCP/wire Percent Change in Stiffness from Initial Ramp												
	Initial Stiffness [N/mm]		**Ramp 1**		**Ramp 2**		**Ramp 3**		**Ramp 4**		**Ramp 5**	
Sample	LCP/wire	DCP/wire	LCP/wire	DCP/wire	LCP/wire	DCP/wire	LCP/wire	DCP/wire	LCP/wire	DCP/wire	LCP/wire	DCP/wire
1	5017.97	7302.97	106.05%	62.67%	105.45%	64.96%	102.61%	65.43%	100.79%	66.22%		
3	8314.92	10818.22	31.41%	36.14%	44.06%	38.15%	36.00%	37.64%	37.99%	38.29%	40.90%	39.06%
4	8387.83	6700.76	32.05%	61.70%	34.13%	61.38%	33.85%	61.39%	33.45%	61.90%	32.66%	61.39%
5	4412.68	5836.62	154.63%	47.80%	158.65%	43.81%	158.47%	43.43%	159.15%	49.65%	160.67%	51.29%
6	4893.40	4168.07	78.64%	74.58%	80.20%	82.15%	79.63%	84.40%	79.83%	83.35%	78.23%	81.35%
Mean	*6205.36*	*6965.33*	*80.56%*	*56.58%*	*84.50%*	*58.09%*	*82.11%*	*58.46%*	*82.24%*	*59.88%*	*78.12%*	*58.27%*
SD	*1972.20*	*2455.98*	*0.52*	*0.15*	*0.50*	*0.18*	*0.52*	*0.19*	*0.51*	*0.17*	*0.58*	*0.18*
P-Value	0.42		0.37		0.34		0.40		0.40		0.56	

Table 6. Shown below are the percent change in stiffness's between each ramp stage for each LCP/wire and DCP/wire specimen for the ramp stages in the fatigue tests. Each ramp is intended to measure the stiffness of the specimen prior and after a cycling regimen of 5000 cycles at 2Hz from 0-7500N compressive load. The initial columns for LCP/wire and DCP/wire are stiffness values in N/mm, while all remaining columns represent percent change from the prior ramp stages stiffness.

LCP/wire and DCP/wire Percent Change in Stiffness from Preceding Ramp Stage												
	Initial Stiffness [N/mm]		**Ramp 1**		**Ramp 2**		**Ramp 3**		**Ramp 4**		**Ramp 5**	
Sample	LCP/wire	DCP/wire	LCP/wire	DCP/wire	LCP/wire	DCP/wire	LCP/wire	DCP/wire	LCP/wire	DCP/wire	LCP/wire	DCP/wire
1	5017.97	7302.97	106.05%	62.67%	-0.29%	1.41%	-1.39%	0.28%	-0.90%	0.48%		
3	8314.92	10818.22	31.41%	36.14%	9.62%	1.48%	-5.60%	-0.37%	1.46%	0.48%	2.11%	0.55%
4	8387.83	6700.76	32.05%	61.70%	1.57%	-0.20%	-0.20%	0.01%	-0.30%	0.31%	-0.59%	-0.31%
5	4412.68	5836.62	154.63%	47.80%	1.58%	-2.70%	-0.07%	-0.27%	0.26%	4.34%	0.59%	1.10%
6	4893.40	4168.07	78.64%	74.58%	0.87%	4.34%	-0.31%	1.23%	0.11%	-0.57%	-0.89%	-1.09%
Mean	*6205.36*	*6965.33*	*80.56%*	*56.58%*	4.01%	4.05%	*-1.51%*	*0.18%*	*0.13%*	*1.01%*	*0.30%*	*0.06%*
SD	*1972.20*	*2455.98*	*52.22%*	*14.85%*	*3.96%*	*2.58%*	*2.34%*	*0.64%*	*0.87%*	*1.91%*	*1.36%*	*0.96%*
P-Value	0.42		0.37		0.43		0.15		0.39		0.64	

Table 7. The table below shows the change in displacement during each fatigue cycle for each specimen, as well as the average, standard deviation, and statistical significance of a paired students t-test for construct groups. The only stage that shows any statistical difference is stage three, but stages 1-2 and 4-5 show no statistical difference.

Change in Displacement during Fatigue Stages (mm)										
	Fatigue Cycle 1		Fatigue Cycle 2		Fatigue Cycle 3		Fatigue Cycle 4		Fatigue Cycle 5	
Sample	LCP	DCP	LCP	DCP	LCP	DCP	LCP	DCP	LCP	DCP
1	0.180	0.509	0.056	0.047	0.031	0.022	0.022	0.019	0.021	0.014
3	0.480	0.330	0.025	0.032	0.014	0.006	-0.002	0.004	-0.007	-0.003
4	0.351	0.552	0.042	0.040	0.040	0.028	0.017	0.021	0.008	0.010
5	0.513	0.438	0.049	0.077	0.037	0.037	0.030	0.037	0.018	0.041
6	0.585	0.479	0.068	0.058	0.037	0.028	0.023	0.018	0.028	0.015
Mean	0.422	0.461	0.048	0.051	0.032	0.024	0.018	0.020	0.013	0.015
SD	0.159	0.085	0.016	0.018	0.010	0.011	0.012	0.012	0.014	0.016
P-value	0.699		0.741		0.018		0.609		0.770	

Table 8. The table below shows the percent change in each test specimens maximum displacement from the initial ramp stages maximum displacement. This table shows how much each specimen changed from the initial ramps maximum axial compression length, as well as mean, standard deviation, and statistical significance for each construct group. Fatigue cycle 2 and 3 show a statistical difference in the percent change from initial displacement, but fatigue cycles 1, 4, and 5 do not show a statistical difference.

Change in Displacement during Fatigue Stages (% of Initial Displacement)										
	Fatigue Cycle 1		Fatigue Cycle 2		Fatigue Cycle 3		Fatigue Cycle 4		Fatigue Cycle 5	
Sample	LCP	DCP	LCP	DCP	LCP	DCP	LCP	DCP	LCP	DCP
1	15.784	45.364	5.779	6.703	3.297	1.879	1.373	1.378	1.177	0.750
3	41.963	29.396	2.617	4.483	1.455	0.530	-0.147	0.282	-0.415	-0.193
4	30.703	49.189	4.331	5.643	4.155	2.391	1.036	1.519	0.426	0.535
5	44.895	39.007	5.009	10.946	3.830	3.117	1.844	2.756	0.986	2.289
6	51.203	42.698	7.020	8.132	3.904	2.366	1.428	1.297	1.564	0.838
Mean	36.910	41.131	4.951	7.181	3.328	2.057	1.107	1.446	0.748	0.844
SD	13.950	7.542	1.643	2.498	1.093	0.961	0.757	0.881	0.768	0.904
P-value	0.640		0.077		0.003		0.141		0.796	

10.2 Single Ramp to Failure Data

The results of the fatigue test for phase one LCP/wire and DCP/wire constructs can be found in Table 9, Figure 27, and Figure 28. There was no statistically significant difference between the two constructs when evaluated as a stiffness comprised of the aggregate data for each specimen. However, when the mean load and stroke are taken the two constructs show statistically significant stiffness's after 3.5mm of axial deformation. A paired student's t-test details that the aggregate load changes from not statistically significant to statistically significant at 3.5mm of axial deformation. Below 3.5mm the mean construct stiffness of the LCP/wire (5390.62+/-860.20 N/mm) is not statistically different from the DCP/wire (3824.12+/-751.84 N/mm)(P=0.12). Above 3.5mm of axial deformation the mean construct stiffness of the LCP/wire (4907.37+/-655.12 N/mm) is not statistically different from the DCP/wire (3009.7+/-718.25 N/mm)(P=0.038). This result is likely due to the small sample size and variations between each constructs performance based on bone strength. The mean load at failure for the LCP/wire (25,663.72+/-5,174.71 N) was higher but not statistically different from the DCP/wire (19,780.44+/-2,812.88 N) (P=0.08). The mean axial compression at failure for the LCP/wire (7.88+/-2.95 mm) was lower but not statistically different from the DCP/wire (10.44+/-2.21 mm) (P=2.78).

Table 9. Shown below are the results of the LCP/wire and DCP/wire single ramp to failure results. The two constructs are by the mean stiffness of each construct statistically different above or below 2.5mm. The 2.5mm stroke value comes from the aggregate stiffness average detailing a point where the difference between construct stiffness becomes statistically significant.

Single Ramp to Failure Test Results LCP/wire and DCP/wire					
	LCP		**DCP**		
	Mean	Stdev	Mean	Stdev	P-Value
Construct Mean Stiffness under 3.5mm [N/mm]	5390.62	860.20	3824.12	751.84	0.12
Construct Mean Stiffness over 3.5mm [N/mm]	4907.37	655.11	3009.65	718.25	0.04
Mean Failure Load [N]	25663.72	5174.71	19780.44	2812.88	0.08
Mean Failure Stroke [mm]	7.88	2.95	10.44	2.21	2.78
Max Load at Failure [N]	30528.48		23811.44		
Min Load at Failure [N]	20846.25		17442.72		
Max Stroke at Failure [mm]	11.50		13.50		
Min Stroke at Failure [mm]	5.00		8.25		

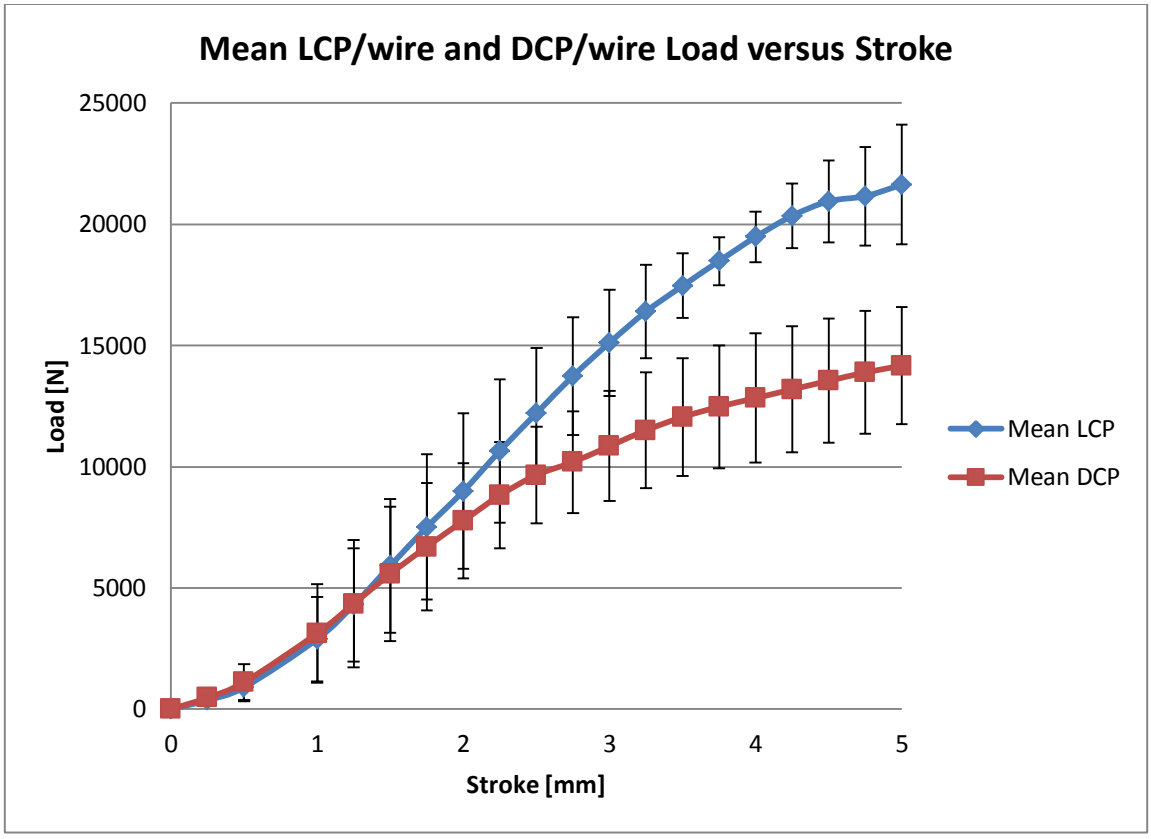

Figure 27. The plot above shows the mean and standard deviation results for the LCP/wire and DCP/wire single ramp to failure test results. The load [N] versus stroke [mm] is averaged for each construct from each specimens test data. This plot shows stroke data from 0-5mm, as the first construct to fail occurred at 5mm.

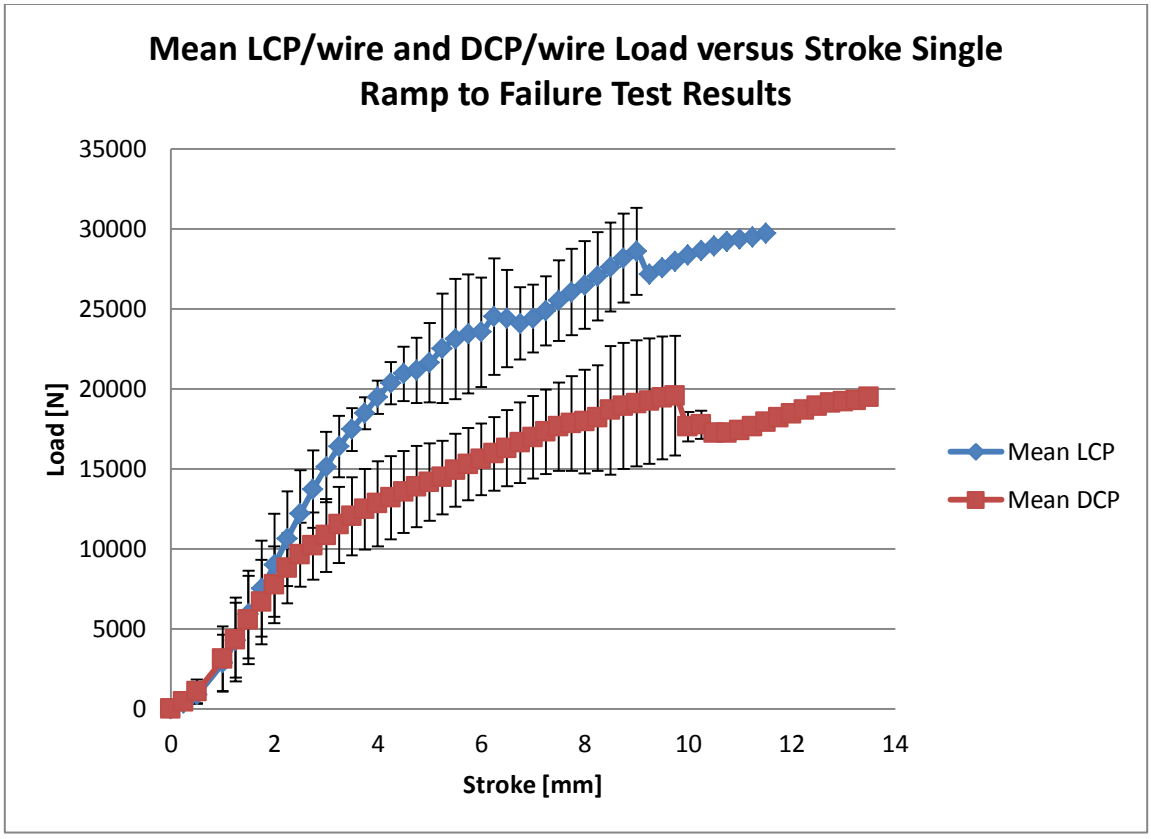

Figure 28. The plot above shows the mean and standard deviation results for the LCP/wire and DCP/wire single ramp to failure test results. The load [N] versus stroke [mm] is averaged for each construct from each specimens test data. This plot shows stroke data from for the full range of each construct, as the test specimen with the longest stroke length was a DCP/wire at 13.5mm.The point where there are no standard deviation bars shows only a single test specimen, the strongest for that construct.

11. EQUINE DISCUSSION AND SUMMARY

11.1 Fatigue Results Discussion

The fatigue tests in this study were meant to simulate a compliant horse with normal everyday loads bearing on the implants. In cyclic fatigue testing, under axial compression, the loading rates are chosen to represent loads on MC3 during walking (7.52kN for a weight range of 450-550kg) (56). When both walking and shifting of weight are included the activity of the forelimb in a 24-hour period is 190±184steps/h. (56) In vivo forces exerted in a longitudinal direction along the radius and metacarpus places the majority of load in axial compression limiting the importance of testing constructs in torsion or bending. Construct stiffness was be defined as the slope of load versus displacement curve, with displacement measured by the Test Resources 830 machine.

Previous studies have demonstrated the success of the LCP/cable in fetlock arthrodesis (23). It was hypothesized that the success of the LCP/cable would be comparable to the LCP/wire in the fatigue studies, with the LCP/cable having a higher stiffness but both constructs would prove to be acceptable construct for fetlock arthrodesis. Carpernter evaluated the LCP/cable for fetlock arthrodesis in six thoroughbred racehorses and found that four out of six horses with suspensory apparatus disruption were sound for breeding one year later. Another study reported 34 of 52 horses with fetlock arthrodesis went on to unrestricted exercise leading to an approximate success rate of 66% between the two studies. (23) (44) These success rates

are low due to the many complications that can arise with fetlock arthrodesis implants. The majority of fractures for horses occur in the distal aspect of the limbs where soft tissue coverage is poor, and the addition of an internal fixation method can easily obstruct local vascularity. Infection and cast sores are common issues associated with the distal limbs of horses after surgery, but in the Carpenter case the 2 out of 6 horses that were euthanized for pastern joint luxation. The dislocation of the pastern joint, which is the joint more distal from the fetlock, was hypothesized to have resulted from sesamoidean ligament and damage from comminuted fracture of the sesamoid bone. Upon inspection of the fetlock arthrodesis technique it was observed to be intact and stable. This study shows that the all LCP/wire test specimens survived the fatigue tests without fracture, and would be acceptable for a compliant specimens fetlock arthrodesis. From the Carpenter study, the LCP/cable is a successful means of fetlock arthrodesis but that careful attention must be paid to damage of the surrounding tissue. With the close proximity of joints and soft tissues the prognosis for arthrodesis has better results when the treatment is used to treat degenerative disease versus disruption of the suspensory apparatus (45). Assuming disruption of the suspensory apparatus by injury would lead one to rationalize that the LCP/wire or LCP/cable would serve as suitable equine fetlock arthrodesis constructs provided the surgeon was well aware of the surrounding tissue damage. For degenerative disease such as arthritis the LCP/wire or LCP/cable will provide adequate stabilization for a compliant horse.

A well-established technique for MCP arthrodesis by Bramlage is one of the most commonly utilized and successful MCP arthrodesis techniques. (51) (46) (32) This

procedure uses a 14-16 holes DCP on the dorsal face of the third metacarpal and proximal phalanx to maintain limb stability, and a tension band wire on the palmar surface to mitigate some of the cyclic loads. The limb is placed in 10 degrees of extension with a contoured bend in the DCP. This technique suffers from contralateral limb laminitis, infection, implant failure, and cast sores that develop during healing. (32) (51) (38) Despite successful implantations, 19 out of 43 horses were euthanatized due to implant complications. (51) Again as with the LCP/cable study, the success rates are in the 66% range due to the many complications that can arise during fetlock arthrodesis. Surgeons often try to mitigate the effects of cyclic loading on the implant and reduce the risk of implant failure by changing the configuration of the DCP and MCP joint to closer to a linear arthrodesis with the negative result of a slightly longer limb. (32) (34) While horses can adapt to the longer limb length the result is often overloading of the contralateral limb, which can result in degenerative joint disease and pastern joint subluxation. (46) The tension band is used to mitigate the effects of cyclic loading, allowing surgeons to place the MCP joint at an angle that allows for better anatomical length with the contralateral limb, and prevent failure of the DCP. (41) (54)

This study demonstrates that with a compliant subject the LCP/wire and DCP/wire both suffer from initial axial compression and interfragmentary motion that results in an increase in construct stiffness. This result is predictable as the large weight of the horse pressing down on the repaired limb for the first time will result in some interfragmentary motion from the constructs. The veterinarian has to surgically implant this device while there is no load on the limb, thus upon initial standing and everyday

use of the limb by the equine it can be expected that the large weight of the horse will compress a construct that was implanted with no weight applied to the limb or construct during surgery. Both constructs showed significant changes in stiffness after the first fatigue cycle stage, and decreasing amounts of axial compression and change in stiffness from the first fatigue cycle to the last. This demonstrates that the constructs compress over time, settling into a more permanent position that is suitable for bearing the repeated everyday loads of the equines body weight. The method of interfragmentary motion between constructs should differ, as each plate is mechanically fixed to the bone by different methods. The transarticular screws, tension band, and plate will all have different influences upon the constructs axial deformation and increased stiffness. In this fatigue study, there was no failure of any specimen or construct, where failure of a sharp decrease in load and the inability to bear stress with increasing strain. Interfragmentary motion could occur in several places. First, the DCP/wire would experience motion of the plate relative to the screws, as the plate is not securely attached to the screws as in the LCP. Motion could also come from motion of the screws relative to the bone and plate, as the axial loading for a DCP can result in motion of the plate about the screw fixed to the bone or motion of the screw and the plate relative to the bone as the bone deforms under the shear forces.

From a clinical standpoint, the difference between what a horse applies at a trot is higher than what a horse applies to a limb at a walk, or when confined to a stall. Based on in vivo strain and load measurements taken, a horse applies approximately -7500N at a walk, and a normal horse has 4,560 forelimb loading activities per day. From the

results in this study, and based on the forelimb loading activities of a normal horse, after three days of normal activity the limbs will have compressed by interfragmentary motion to the point where axial deformation is less than 2%. Assuming that axial compression is related to the motion between the MC3 and P1 bones, then both constructs are suitable for primary bone healing and can serve as fetlock arthrodesis constructs for a compliant horse sustaining only walking loads. (55) (56)

11.2 Single Ramp to Failure Discussion

The single ramp to failure tests in this study were meant to simulate the situation in which a horse is non-compliant and places above everyday use loads on the implants. Construct stiffness was be defined as the slope of load versus displacement curve, with displacement measured by the MTS 810 22kip capacity machine. The number of contralateral specimens dropped from 5 to 4 for the single ramp to failure study due to the failure of the test rig created for the loading to failure study. The aluminum housing created used a threaded pin attachment designed to interface with existing MTS components. Due to the off axis loading created by the angle at the MCP joint, the threaded attachment bent during testing, and it could not be determined if the loads recorded were from the bone or metal attachment deforming.

While the fatigue study showed no statistical difference between the constructs, in the single ramp to failure study the LCP/wire was consistently stiffer than the DCP/wire. This can be attributed to the locking screws and bone cortical screws used on the LCP specifically designed to create a fixed angle construct that functions as a single

beam device. It was hypothesized that the LCP/wire device would be stiffer, and the results verify this. Figure 27 shows clearly the statistically significant difference that occurs between construct groups above 3.5mm of axial deformation. The reason Figure 27 only reaches 5mm is because the first construct failed at 5mm of axial compression. Above this point contralateral comparisons are not possible. The stiffness values seen in Table 9 are contralateral stiffness comparisons. Above 5mm the contralateral comparison would need to drop to three specimens per construct group and is not included here due to the changing stiffness values that would be generated.

Table 9 also shows the maximum and minimum load and axial compression at failure. The LCP/wire has higher maximum and minimum load at failure values than the DCP/wire, as well as shorter axial compression values for both maximum and minimum axial compression at failure. This supports the conclusion that the LCP/wire is the stiffer construct.

Failure mode for the LCP/wire and DCP/wire had some similarities that can be reported. During the early stage of the single ramp to failure tests, loads under 10,000N, both devices could visibly be seen compressing under the loads. The third metacarpal and proximal phalanx could be seen pressing into one another, shrinking the visible gap on the dorsal and palmar aspect of the MCP joint. After this phase the two constructs deformed differently. The only motion detectable from the LCP/wire was a small increase in the angle at the MCP joint by observing the LCP at the joint. The angle generated on the ventral aspect of the MCP joint by the LCP would slowly shrink, until a loud audible cracking noise would sound out. Visible inspection of the LCP/wire

constructs would reveal no bone failure or implant failure, but the MTS readouts confirmed a significant vertical drop in load and the inability of the construct to continue bearing load. Upon removal of LabStone potting material from the bone via cracking the LabStone in a vice, a crack along the center of the most distal end of the proximal phalanx was visible. The DCP/wire constructs failed by deforming at the MCP joint as well as bone failure at the distal end of the proximal phalanx. The visible deformation of the DCP plate, necking of the wire tension band, and permanent angular deformation at the MCP joint suggest that this construct was significantly weaker. The deformation could be seen at the MCP joint caused significant bending in the third metacarpal bone. As the MTS 810 machine loaded the DCP/wire constructs, and the MCP joint deformed, the forces in the construct resulted in a transaxial motion of the MCP joint. The MCP could be seen moving in the palmar direction, and flexion of the third metacarpal could be seen.

From a clinical standpoint, the single ramp to failure test is designed to measure the constructs response to a non-compliant horse that loads the forelimb outside of normal walking loads. A horse at a trot applies approximately -13kN. The largest load recorded during that study was immediately following anesthetic, where the horse stomps its numbed limb at loads near -20kN. An adjusted single ramp to failure plot has been included here with additional information to demonstrate the significance of these loads, and can be seen in Figure 29. From this plot it is evident that under 5mm of axial compression, the LCP/wire is the only construct that is capable of bearing 20kN loads. While the fatigue study demonstrated that the walking loads did not affect either

construct in a statistically significant way, the single ramp to failure study demonstrates that if a horse were to apply a load beyond normal walking then the DCP/wire construct is not suitable. (55)

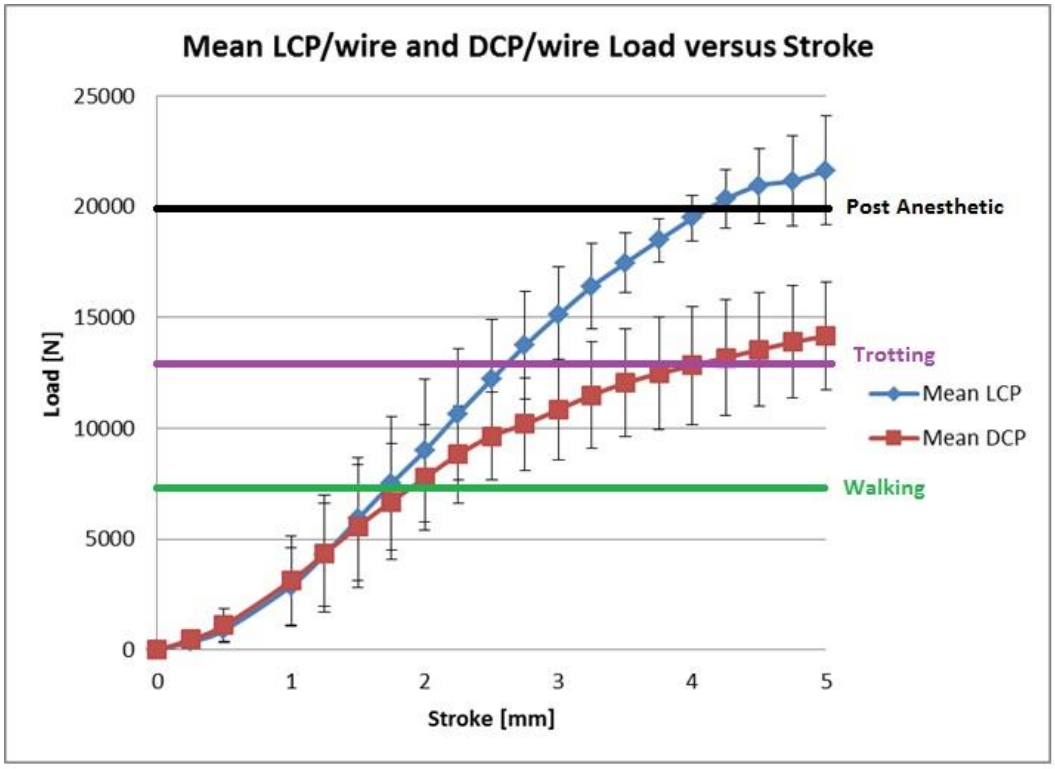

Figure 29. This is an adjusted mean load and stroke for the single ramp to failure tests. Included are the walking (-7500N), trotting (-13kN), and post anesthetic stomp (-20kN) loads.

11.5 Study and Device Strengths and Limitations

In vitro biomechanical testing of orthopedic constructs does not completely replicate loading of the equine limb. This study is designed to replicate the loading of the equine limb postoperatively following fetlock arthrodesis, without soft tissue involvement. The maximum bending moment may exceed physiological bending

moment placed on the equine MC3 during walking (11.8 Nm for a weight range of 450-500k) (55). The cyclic rate of 6Hz is considerably greater that the mean rate of walking and weight shifting within a box stall (190±184steps/h) (56). Non-physiologic cycling rates may result in differences in absorption and dissipation of loading energy. Increased loading rates can also result in bone sustaining increased loads before failure and failure bending moments (56) (59). As time progresses in the patient and bone healing ensues, the distribution of load in the construct shifts from primarily loading the implants to gradually increasing load the implants to gradually increasing load by arthrodesis and decreasing the load of the implants.

This study will use a novel design to determine the biomechanical behavior of 2 different techniques for fetlock arthrodesis will be investigated. One study compared the biomechanical properties of an intramedullary pin-plate implant with a DCP system however; comparisons of current clinically employed fetlock arthrodesis techniques have not been published (35). To date, previous biomechanical studies have tested bone plate constructs over a straight plane (43) (57) (58) (60). A ten to twelve degree angle is used to re-establish the natural angle of the fetlock in standing extension. Using this model will provide additional information on bone plate stiffness over a fixed angle. In addition, biomechanical studies in studies investigating the tension band constructs are limited. This study will evaluate the potential benefits of using stainless steel cable compared to wire for maintaining palmar support to the fetlock region. CT documentation of bone density prior to mechanical testing and quantitative description of mode of failure has not been published.

11.6 Potential Improvements

Several improvements could be made to this study that would allow for a better overall evaluation of these techniques for equine MCP arthrodesis. Frist, the biomechanical testing conducted in this study may not replicate in vivo loading of the equine limb. Soft tissues help support joints, and in this study the tendons that would normally be present were removed. It is unknown how the muscle and tendons surrounding the MCP joint would affect the mechanical performance of constructs and affect arthrodesis. Also, the test specimen provided was disarticulated at the proximal metacarpus and the distal proximal phalanx limiting the evaluation of the test specimen to the MCP, P1, and MC3 of the equine. It is unknown how joints or soft tissues more proximal than the MC3 or more distal than the P1 would respond to these tests conditions. Along with the removal of soft tissues and the disarticulation of the surrounding anatomy, the testing conditions in this study are reversed from the actual loading conditions experienced by a horse. The Carpenter study reported that the highest loads experienced by the MC3 are immediately following anesthetic, followed by normal walking conditions. This study simulated walking first followed by a ramp to failure. This was done to preserve the integrity of the test specimens for the single ramp to failure study as it was unknown if the constructs would survive a ramp to 20kN before a cycling test. Based on the single ramp to failure tests the DCP would not have survived the ramp to 20kN test, and the study would have been in jeopardy due to the limited number of contralateral pairs for the cyclic study. (23)

Over the course of a single day a normal horse following surgery will sustain approximately 4600 forelimb loadings as established by Carpenter. (23) Our study simulated 25000 cycles in just under 4 hours. It is unknown how swelling, healing over the course of 5 days, and the rate of loading affects interfragmentary motion. It is possible that the interfragmentary settling seen in this study is unrealistic due to the accelerated rate of loading.

Finally it is unknown how much displacement actually occurred between the MC3 and P1 bones at the MCP joint. This is important to know to evaluate the ability of each construct to provide an adequate environment for primary bone healing. The displacement of the MC3 relative to the P1 must be less than 2% in order for arthrodesis to occur. This study only utilized axial displacement of the crosshead during the fatigue study as an evaluation of motion within the construct. It can be rationalized that because axial displacement was less than 2% that the displacement between the MC3 and P1 was less than 2%, but there is not means of verifying this rationale.

12. SUMMARY

12.1 Canine Summary

In summary, there were no significant differences in the torsional rigidity of these systems below 10degrees of torsion. However, above 4.92Nm of torsion, LC-DCP/rod constructs display significantly higher torsional rigidity, whereas CRIF/rod constructs are not as rigid at higher torsional loads and exhibit significantly higher permanent angular deformation. In clinical relevance, both constructs sufficiently achieve everyday bending and torsion loads with minimal strain and deformation and are suitable for fracture fixation use on compliant canines in highly comminuted diaphyseal femur fractures based on this study. However, as canines cannot be guaranteed to be compliant in minimizing the loads placed on the bone after fracture, the LC-DCP/rod construct will sustain higher loads in torsion than the CRIF/rod. Additional cyclical studies are necessary to determine the response of the CRIF/rod system to repetitive physiologic loads.

12.2 Equine Summary

In summary, there were no significant differences in the mean stiffness of the LCP/wire and DCP/wire constructs during the fatigue tests. Both constructs showed significant increases in stiffness as well as significant reduction in axial deformation after the first fatigue cycle. The fatigue cycles were designed around loads that simulate everyday body weight loading of the MCP joint. No construct failed during the fatigue

study, suggesting that both constructs are suitable for equine arthrodesis. However, arthrodesis is accomplished by primary bone healing and requires strains of less than 2% to achieve arthrodesis. It is likely that the large reduction in axial compression and large increase in stiffness is attributable to interfragmentary motion, but whether or not the strains at the joint are below 2% has yet to be determined. Should the strain at the joint be less than 2%, both constructs would be suitable for MCP arthrodesis for a compliant horse. As with human treatments, patient compliance with a healing regimen is not always 100%, and the single ramp to failure tests were designed to determine which construct would fare better for a noncompliant horse. The LCP/wire showed higher mean stiffness above and below 3.5mm axial compression, but was only statistically significant above 3.5mm. The LCP/wire also showed higher average failure load, lower average failure stroke, higher maximum/minimum failure load, and lower maximum/minimum failure stroke. The fatigue results show that the two construct are comparable when loading is within everyday loading limits. However, for extreme loading scenarios the LCP/wire construct is superior to the DCP/wire.

REFERENCES

1. *Mechanical Properties of 18 Different AO Bone Plates and the Clamp-Rod Internal Fixation System Tested on a Gap Model Construct.* **Zahn, K et al.** 2008, Vet Comp Orthop Traumatol, pp. 21: 185-194.

2. *The Clamp Rod Internal Fixator: Application and Results of 120 Small Animal Fracture Patients.* **Zahn, K and Matis, U.** 2004, Vet Comp Ortho Traumatol, pp. 3: 110-120.

3. *Stress Fields in the Unplated and Plated Canine Femur Calculated from In Vivo Strain Measurements.* **Carter, DR, et al., et al.** 14: 63-70, s.l. : J Biomechanics, 1981.

4. *Some Remarks on the Treatment of Fractures.* **Lane, WA.** 1895, BMJ, pp. 1: 861-3.

5. *Internal Plate Fixation of Fractures: Short History and Recent Developments.* **Uhthoff, Hans K, Poitras, Philippe and Backman, David S.** 2006, J Orthop Sci, pp. 11: 118-126.

6. *Early Temporary Porosis of Bone Induced by Internal Fixation Implants.* **Cordey, J, Perren, SM and Rahn BA et al .** 1988, ClinOrthopedRel, pp. 232: 139-151.

7. *The Evolution of Modern Plate Osteosynthesis.* **Miclau, T and Martin, R.E.** A3-A6, s.l. : Injury, 1997, Vol. 28.

8. *Early Temporary Porosis of Bone Induced by Internal Fixation Implants: A Reaction to Necrosis, not to Stress Protection?* **Perren, SM, et al., et al.** 1988, Clin Orthop , pp. 232:139-51.

9. *Reduction in Plate Strain by Addition of an Intramedullary Pin* . **Hulse, Don, et al., et al.** 1997, Veterinary Surgery, pp. 26: 451-459.

10. *The Concept of Biological Plating using the Limited Contact Dynamic Compression Plate (LC-DCP). Scientific Background, Design, and Application.* **Perren SM.** 1991, Injury, pp. 22: 1-41.

11. *Biologic Strategies and a Balanced Concept for Repair of Highly Comminuted Long Bone Fractures.* **Aron , DN, Palmer , RH and Johnson , AL.** 1995, Comp Cont Ed Pract Vet, pp. 17: 35-38.

12. *Less Rigid Internal Fixation Plates: Historical Perspectives and New Concepts.* **Woo, SLY, Lothringer, KS and Akeson, WH et al .** 1984, J Orthop Res, pp. 1: 431-435.

13. *A Biomechanical Assessment of Plate Fixation, with Insufficient Bony Support.* **Beaupre , GS, et al., et al.** 1988, J Orthop Res, pp. 6: 721-729.

14. *Effect of Intramedullary Pin Size on Reducing Bone Plate Strain.* **Hulse, D, et al., et al.** 2000, Vet Comp Orthop Traumatol , pp. 13: 185-190.

15. *The Role of Interfragmentary Strain in Fracture Healing: Ovine Model of a Healing Osteotomy.* **Cheal, EI, et al., et al.** 1991, J Orthrop Res, Vol. 9, pp. 131-142.

16. *Influence of Plate Design on Cortical Bone Perfusion and Fracture Healing in Canine Segmental Tibial Fractures* . **Hupel TM et al.** 1999, J Orthop Trauma, pp. 13: 178-186.

17. *The Limited Contact Dynamic Compression Plate (LC-DCP).* **Perren, S M, et al., et al.** 1990, Arch Orthop Trauma Surg , pp. 109:304-310.

18. *Comparison of Double Dynamic Compression Plating Versus Two Configurations of an Internal Veterinary Fixation Device: Results of In Vitro Testing Using a Bone Substitute.* **Linke B et al .** 2002, Vet Surg, pp. 31: 582-588.

19. *Der Clamp Rod Internal Fixator zur Behandlung von Pseudarthrosen beim Kleintier.* **Zahn, K and Matis, U.** 2004, OP-Journal, pp. 20: 128-132.

20. *Use of the VetFix for the Treatment of Fractures in Dogs.* **Kerwin, S, Hulse, D and Mertens , W.** Denver, Colorado : s.n., October 2004. Proceedings of the 14th annual SCVS Symposium.

21. **Johnson , AL, Houlton, JEF and Vannini, R.** *AO Principles of Fracture Management in the Dog and Cat.* Davos, Switzerland : AO Publishing, 2005.

22. *Stress and Strain Distribution in the Intact Canine Femur: Finite Element Analysis.* **Shahar, R, Banks-Sills, L and Eliasy, R.** 25: 387-395, s.l. : Med Eng & Phys, 2003.

23. *Clinical Evaluation of the Locking Compression Plate for Fetlock Arthrodesis in Six Thoroughbred Racehorses.* **Carpenter, R.S. and et al .** 2008, Veterinary Surgery , pp. 37: 263-268.

24. *Causes of Death in Racehorses over a 2 year period.* **B.J., Johnson, et al., et al.** 26:327-330, s.l. : Equine Vet Journal, 1994.

25. *Functional Anatomy of Equine Locomotor Organs.* **Kainer, R.A.** pp 1-72, Philadelphia, PA : Lippincott Williams and Wilkins, 2002.

26. **Sisson, S and Grossman, J.** *The Anatomy of the Domestic Animals.* Philadelphis, PA : W.B. Saunders Co., 1953.

27. *An Initial Report on a Surgical Technique for Arthrodesis of the Metacarpophalangeal Joint in the Horse.* **Bramlage, L.R.** 257-261, s.l. : Proc Am Assoc Equine Practn, 1982, Vol. 27.

28. *Prevalence of, and Factors Associated with, Musculoskeletal Racing Injuries of Thoroughbreds.* **Peloso, J.G., Mundy, G.D. and Cohen, N.D.** 620-626, s.l. : Journal of hte American Veterinary Medical Association, 1994, Vol. 204.

29. *A Modified Cloward's Technique for Arthrodesis of the Normal Metacarpophalangeal Joint in the Horse.* **Crawley, G.R., et al., et al.** 117-127, s.l. : Veterinary Surgery, 1988, Vol. 17.

30. *Diaphyseal Structural Properties of Equine Long Bones.* **Hanson, P.D., Markel, M.D. and Vanderby, R.** 233-240, s.l. : American Journal of Veterinary Research, 1995, Vol. 56.

31. **Ozkaya, N and Nordin, M.** *Fundamentals of Biomechanics, Equilibrium, Motion, and Deformation.* New York, NY : Van Nostrant Reinhold, 1991. pp 277-278.

32. *Stress Protection Afforded by a Cast on Plate Fixation of Distal Forelimb in the Horse In Vitro.* **Parente, E.J. and Nunamaker, D.M.** 49-54, s.l. : Veterinary Surgery, 1995, Vol. 24.

33. *Complications During Treatment of Traumatic Disruption of the Suspensory Apparatus in Thoroughbred Horses.* **Bowman, K.F., et al., et al.** 706-715, s.l. : Journal of Veterinary Medicine, 1984, Vol. 184.

34. *Arthrodesis Techniques.* **Auer, J.A.** 1073-1086, Philadelphia, PA : Saunders, 2006, Vol. 3.

35. *An In Vitro Biomechanical Comparison of a Prototype Intramedullary Pin-Plate with a Dynamic Compression Plate for Equine Metacarpophalangeal Arthrodesis* . **Sod, G.A. and Martin, G.S.** 2004, Verterinary Surgery , pp. 33: 83-91.

36. *Locking Compression Plate(LCP): An Osteosynthesis Plate Based on the Dynamic Compression Plate and the Point Contact Fixators (PC-Fix).* **Frigg, R.** 63-B66, s.l. : Injury, 2001, Vol. 32.

37. **Auer, J.A.** Principles of Fracture Treatment. [book auth.] J.A. Stick. *Equine Surgery.* Philadelphia : Saunders, 2006.

38. **Lischer, C and Auer , J.** Arthrodesis Techniques, in Equine Surgery. St. Louis, MO : Elsevier, 2012, pp. 1137-1139.

39. **Bramlage, L.R.** Fetlock Arthrodesis. [book auth.] A.J. Nixon and W.B. Saunders. *Equine Fracture Repair.* Philadelphia : s.n., 1996, pp. 172-178.

40. *Arthrodesis Techniques in Horses.* **Subrod , C.J. and Schneider, R.K.** s.l. : Elxevier Saunders, 2005, Veterinary Clinics of North America , Vols. 691-711, pp. 691-711.

41. *Arthrodesis of the Metacarpal/Metatarsal Phalangeal Joint in the Horse.* **Bramlage, L.R.** s.l. : AAEP Proceedings , 2009.

42. *Development of the Locking Compression Plate* . **Figg, R.** 2003, Injury, pp. 34: S-B6-S-B10.

43. *Assessment of Stiffness and Strength of 4 Different Implants Avaliable for Equine Fracture Treatment: A Study on a 20° Oblique Long-Bone Fracture Model Using a Bone Substitute.* **Florin , M and et al .** 2005, Veterinary Surgery, pp. 34: 231-238.

44. *Arthrodesis of the Metacarpophalangeal Joint: Results in 52 Horses.* **Bramlage, LR.** 45, s.l. : Vet Surg, 1985, Vol. 14.

45. **Nixon, AJ.** *Equine Fracture Repair.* Philadelphia, PA : Saunders, 1996. pp 172-178.

46. *Biomechanics of Locked Plates and Screws.* **Koval KJ, Egol KA, Kubiak EN, et al.** 488-493, s.l. : J Orthop Trauma, 2004, Vol. 18.

47. **Fackelman, GE, Auer, JA and Nunamaker, DM.** *AO Principles of Equine Osteosynthesis.* Stuttgart, Germany : Thieme, 2000.

48. *Biomechanics of Locked Plates and Screws.* **Egol, Kenneth A, et al., et al.** 488-493, s.l. : J Orthop Trauma, 2004, Vol. 18.

49. *Point Contact Fixator: Part 1. Scientific Background, Design, and Application.* **Perren, S.** 1-10, s.l. : Injury, 1995, Vol. 22.

50. *Strain Distribution in Plated and Unplated Sheep Tibia: An In Vivo Experiment.* **Gautier, E, Perren, SM and Cordey, J.** C37-C44, s.l. : Injury, 2000, Vol. 31.

51. *First Clinical Results of the Locking Compression Plate (LCP).* **Sommer, C, et al., et al.** B43-B54, s.l. : Injury, 2003, Vol. 34.

52. *General Principles for the Clinical use of the LCP.* **Wagner, M.** B31-B42, s.l. : Injury, 2003, Vol. 34.

53. *Stabilization of Proximal Tibial Fractures with the LIS-System: Early Experience in Berlin.* **Schutz, M, Kaab, MJ and Haas, N.** A30-A35, s.l. : Injury, 2003, Vol. 34.

54. *Accurate Measurement of Bone Mineral Density using Clinical CT Imaging with Single Energy Beam Spectral Intensity Correction.* **Zhang, J and et al .** 2010, IEEE Transactions on Medical Imaging , pp. 29: 1382-1389.

55. *In Vivo and Analtical Studies of Forces and Moments in Equine Long Bones.* **Rybicki, E.F. and et al .** 1977, Journal of Biomechanics , pp. 10(11-12): 701-705.

56. *Limb Loading Activity of Adult Horses Confined to Box Stalls in an Equine Hospital Barn.* **McDuffee, L.A., Stover, S.M. and Coleman, K.** 2000, American Journal of Veterinary Research , pp. 61: 234-237.

57. *In Vitro Biomechanical Comparison of Locking Compression Plate Fixation and Limited-Contact Dynamic Compression Plate Fixation of Osteomized Equine Third Metacarpal Bones.* **Sod, G.A. and et al.** 2008, Veterinary Surgery , pp. 37: 283-288.

58. *Arthrodesis of the Equine Proximal Interphalangeal Joint: A Biomechanical Comparison of 3-Hole 4.5mm Locking Compression Plate and 3-Hole 4.5mm Narrow Dynamic Compression Plate, with Two Transarticular 5.5mm Cortex Screws.* **Zoppa, A.L.V. and et al.** 2011, Veterinary Surgery , pp. 40: 253-259.

59. *An In Vitro Biomechanical Investigation of the Mechanical Properties of Dynamic Compression Plated Osteomized Adult Equine Tibiae.* **McDuffee, L.A., Stover, S.M. and Kenneth, T.T.** 1997, Veterinary Surgery , pp. 26: 126-136.

60. *A Mechanical Comparison of Equine Metacarpophalangeal Joint Arthrodesis Techniques: An Axial Compression Plate and Two Abaxial Transarticular Cortical Screws versus an Axial Dynamic Compression Plate and Two Abaxial Transarticular Cortical Screws .* **Sod , G.A. and et al.** 2011, Veterinary Surgery , pp. 40: 571-578.

61. *Complications During Treatment of Traumatic Disruption of the Suspensory Apparatus in Thoroughbred Horses.* **Bowman, K, Leitch, M and Nunamaker , D.** 1984, Journal of American Veterinary Medical Association , pp. 184: 706-715.

62. *The Concept of Biological Plating using the Limited Contact Dynamic Compression Plate (LC-DCP) - Scientific Background, Design, and Application.* **Perren , SM.** 1991, Injury, pp. 22: 1-41.

APPENDIX A

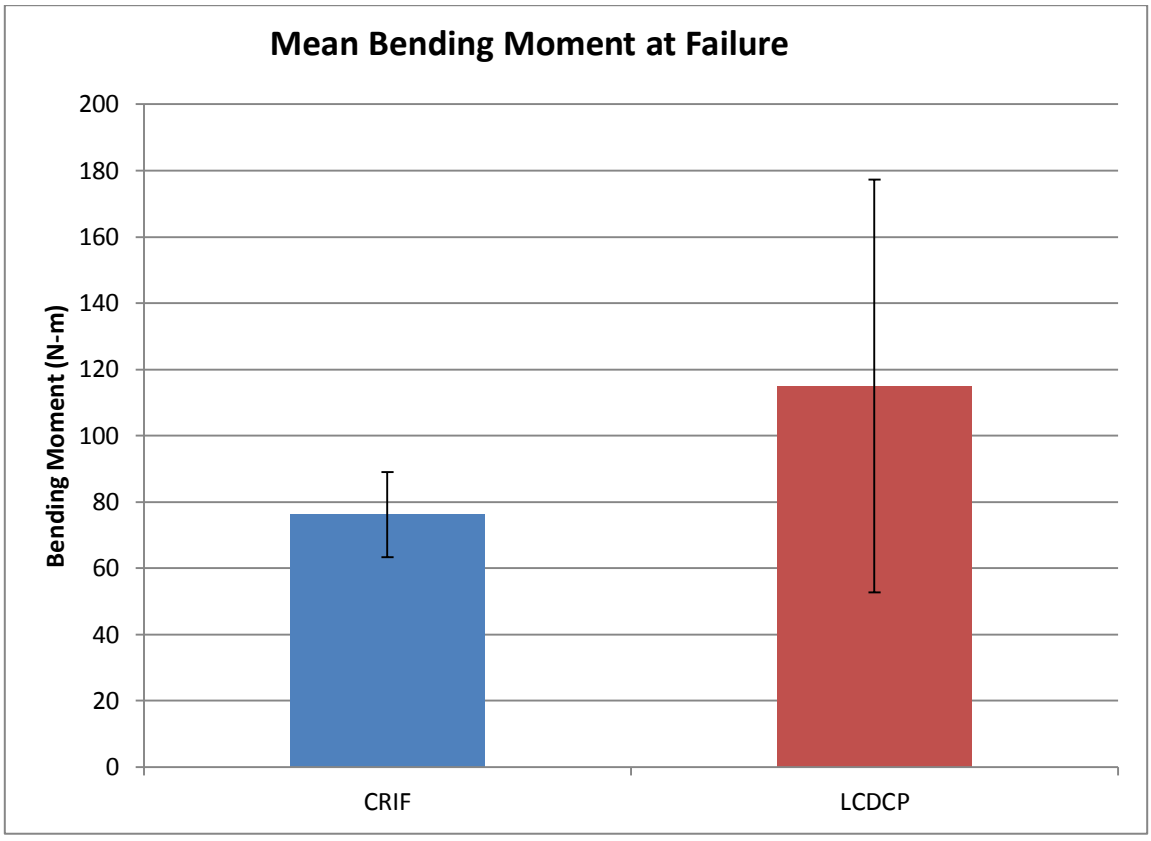

Figure 30. Shown are the mean bending moments at failure for the four point bending experiments on the CRIF/rod and LC-DCP/rod constructs.

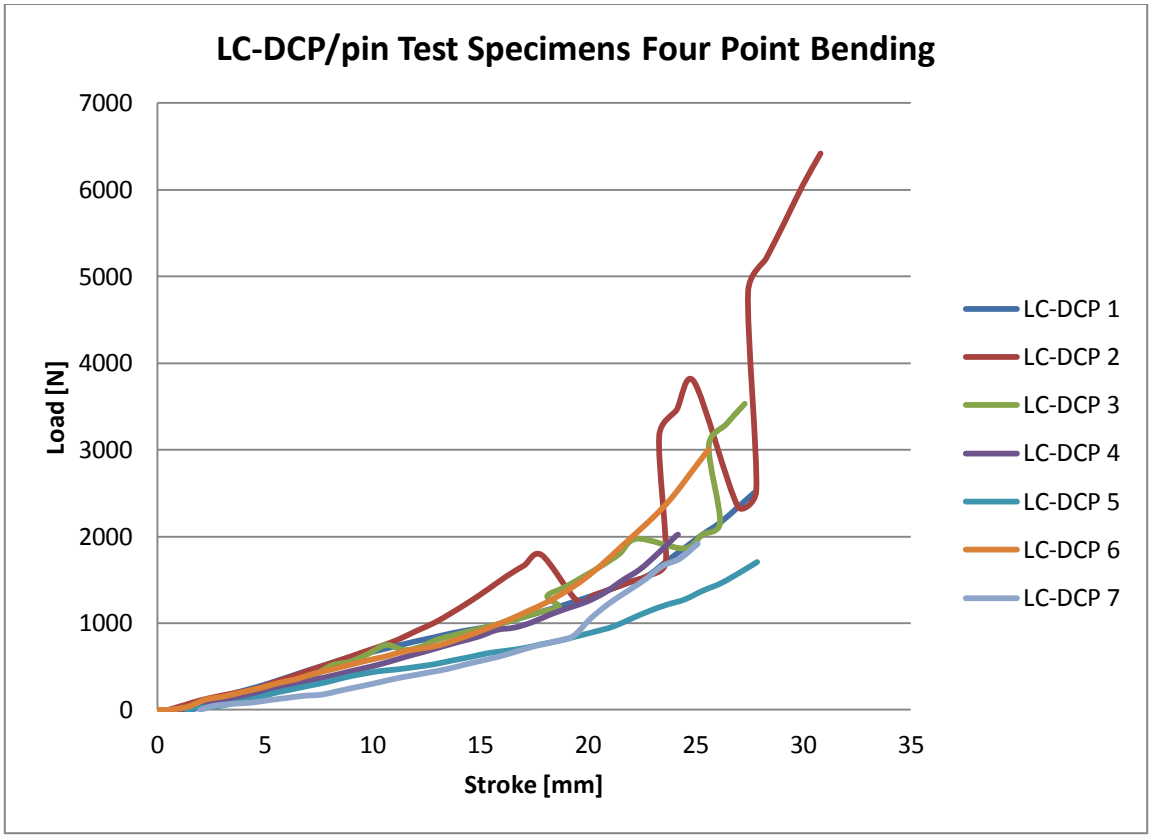

Figure 31. This plot shows all seven LC-DCP/rod constructs in load [N] versus axial displacement [mm] of the Test Resources 830 axial system. This plot is included to detail the multiple yield points of several test specimens. Ultimately, failure was determined to be fracture or bone pullout from the epoxy, all subsequent yield points were undetectable by visual and audible inspection during the experiment and could not be determined at the time to be a viable construct failure.

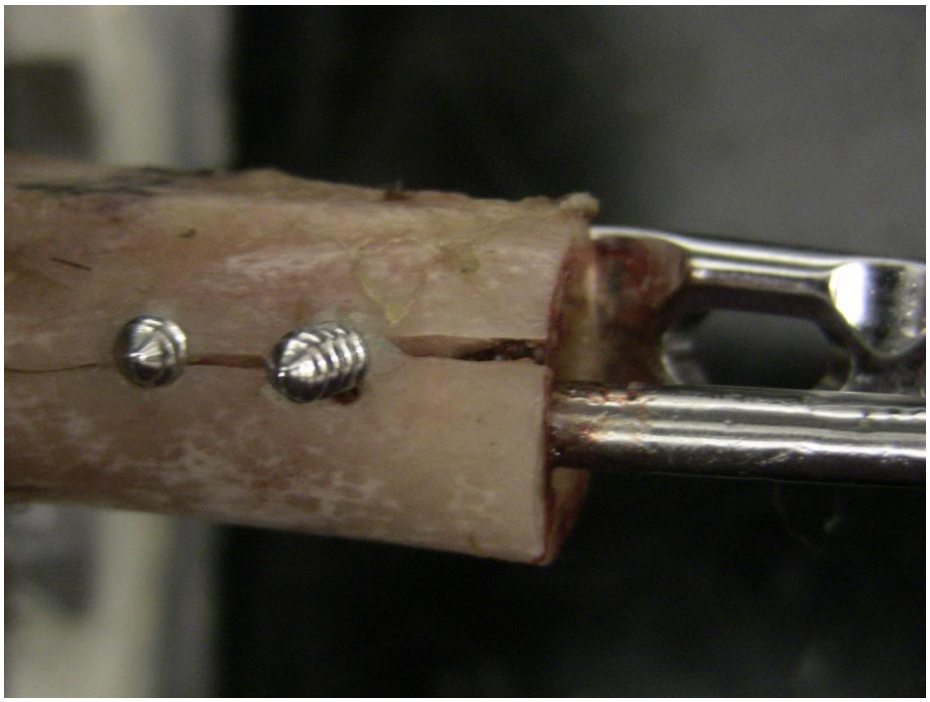

Figure 32. Fracture of LC-DCP #1 from four point bending experiment.

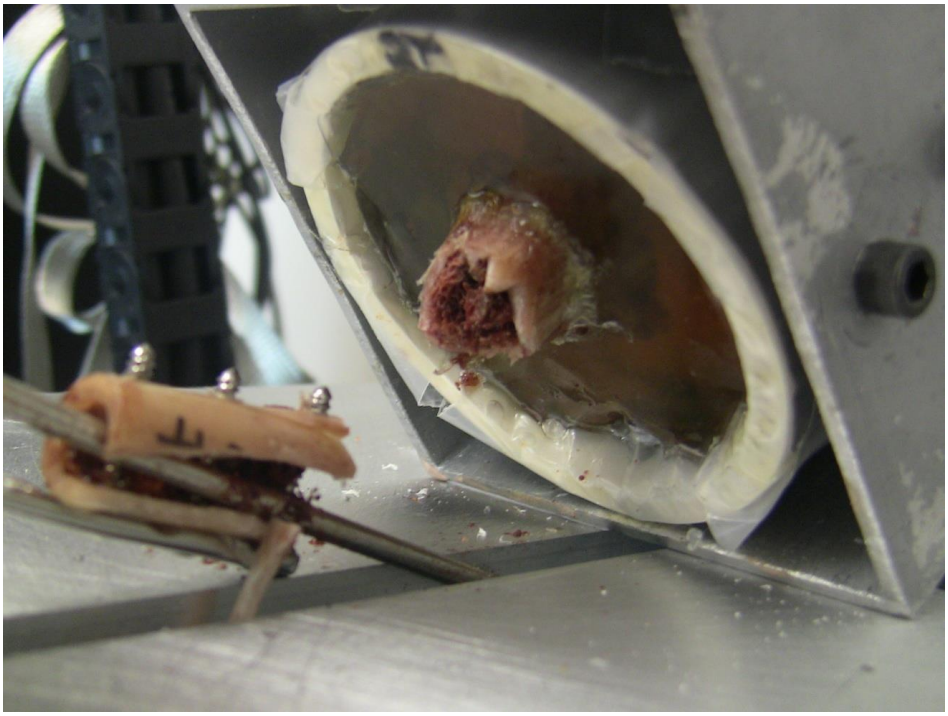

Figure 33. Explosive fracture of LC-DCP #2 from four point bending.

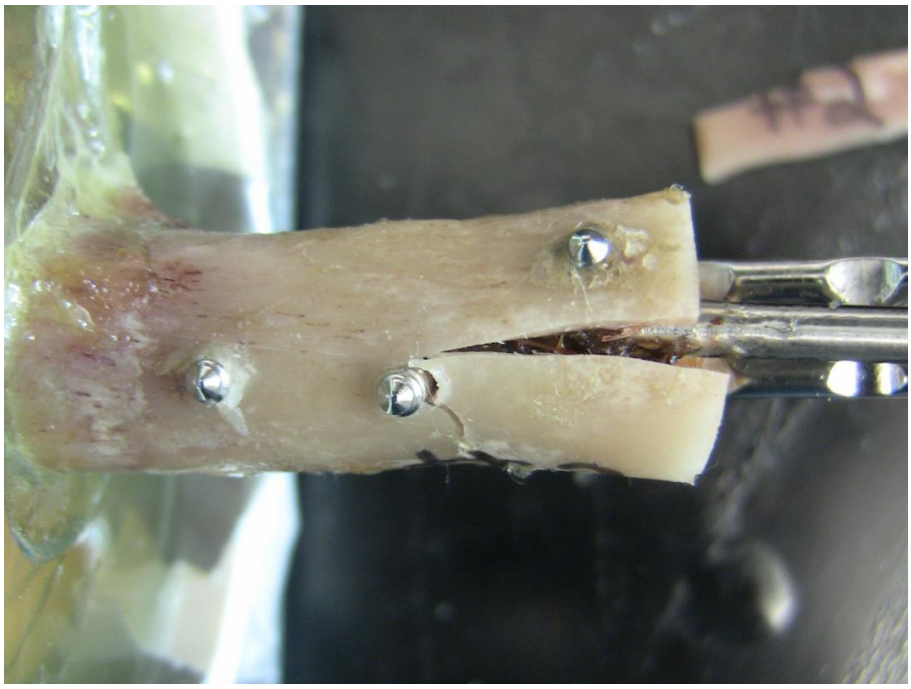

Figure 34. Secondary fracture on LC-DCP #2.

Figure 35. Fracture of LC-DCP #3.

Figure 36. Fracture of LC-DCP #3 from transcortex view. Crack propagates along bone screw – bone interface.

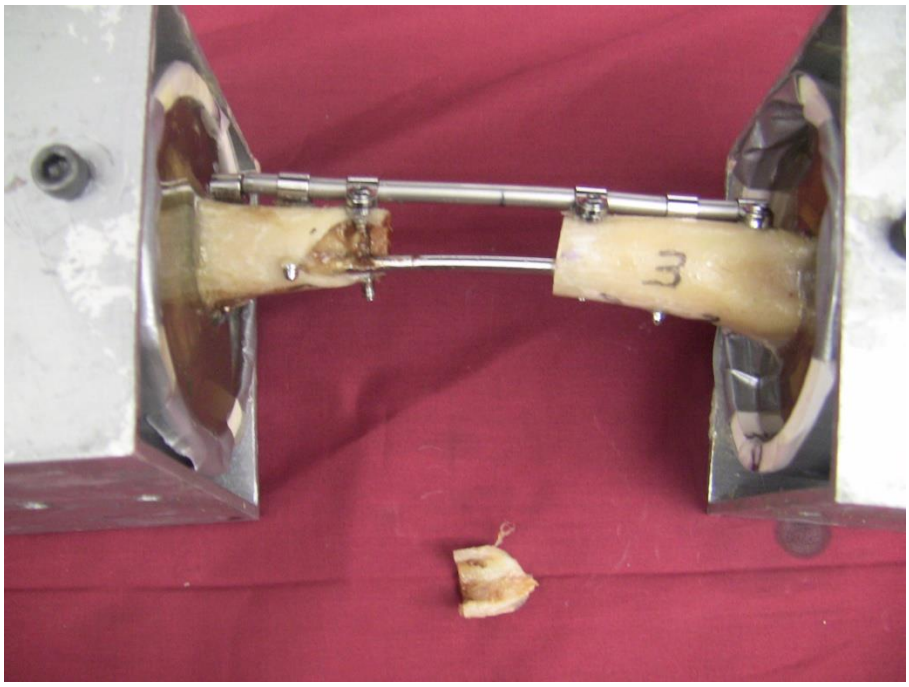

Figure 37. Fracture of CRIF #3.

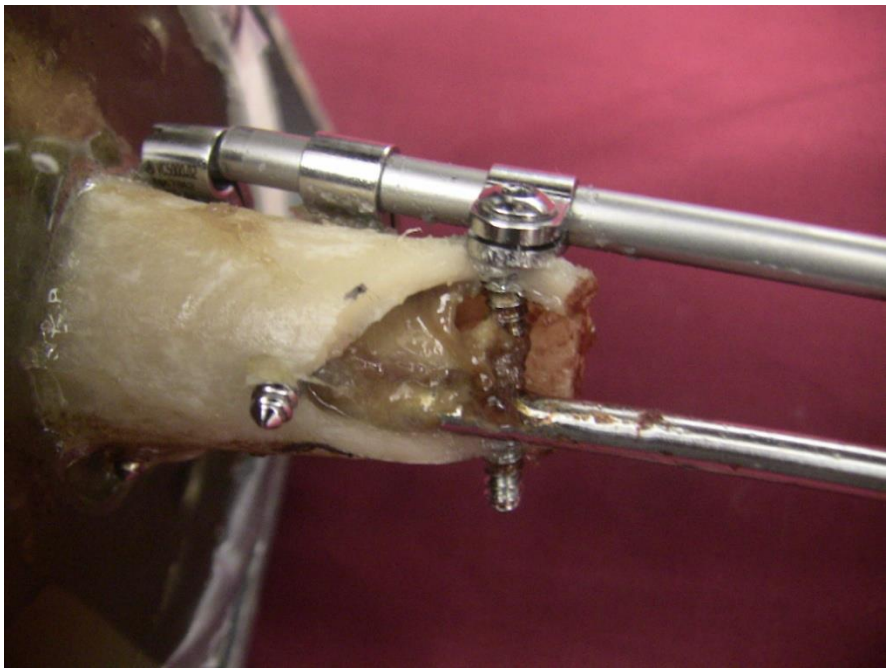

Figure 38. Closer inspection of CRIF #3 fracture site. Fracture formed around interface between bone screw and bone.

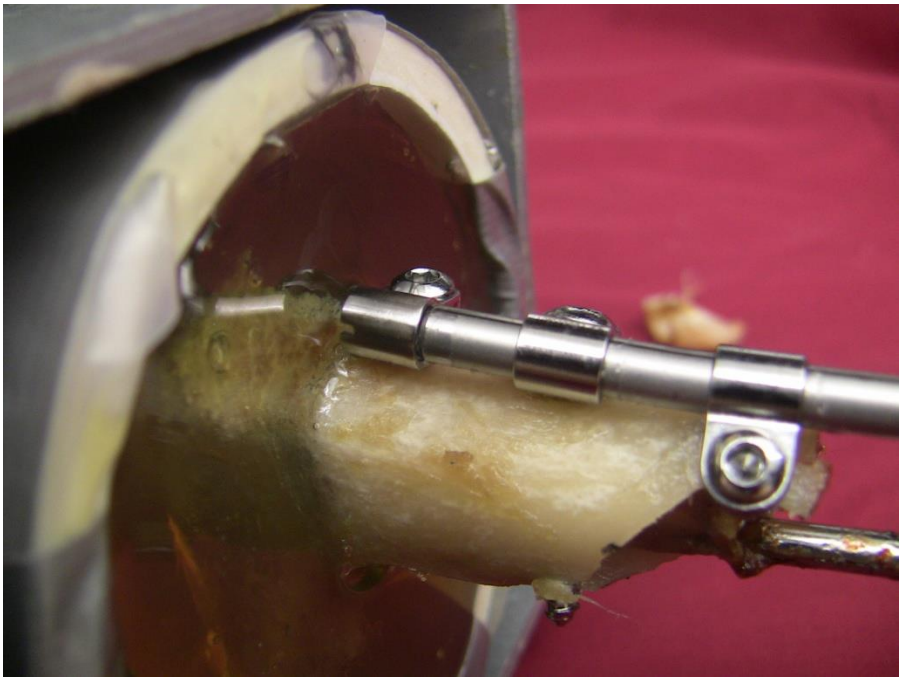

Figure 39. CRIF rod pullout from anchor clamp on CRIF #3.

Figure 40. Fracture of LC-DCP #4 where crack initiates at gap and moves to second bone screw hole on transcortex.

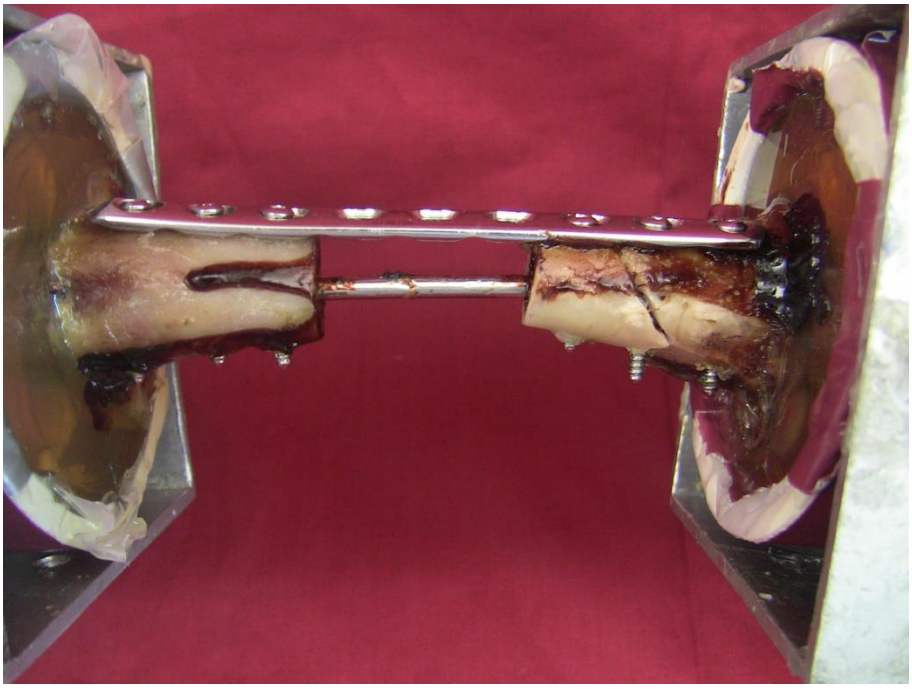

Figure 41. Secondary view of fracture for LC-DCP #4.

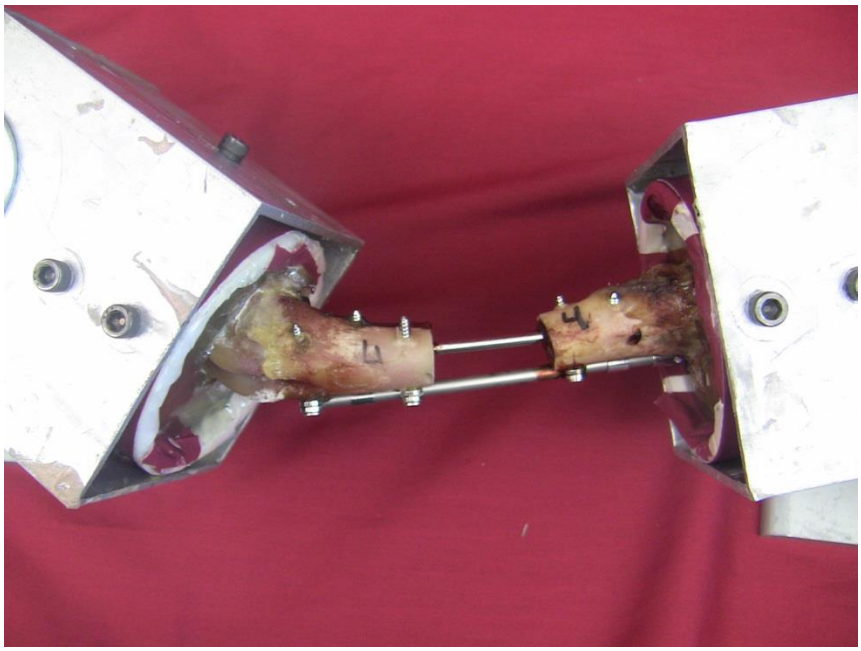

Figure 42. Image showing bone pullout from epoxy potting material for CRIF #4.

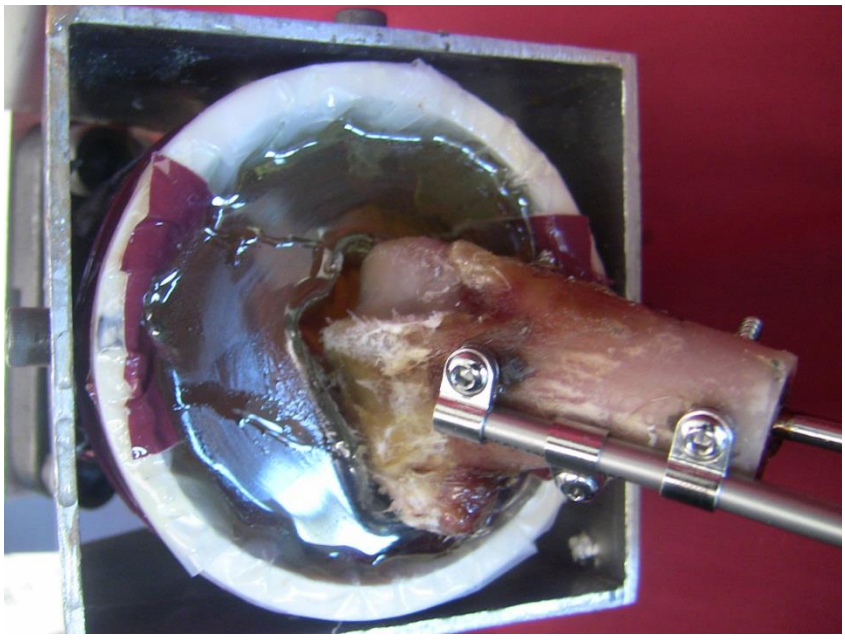

Figure 43. Secondary view of CRIF #4 bone pullout.

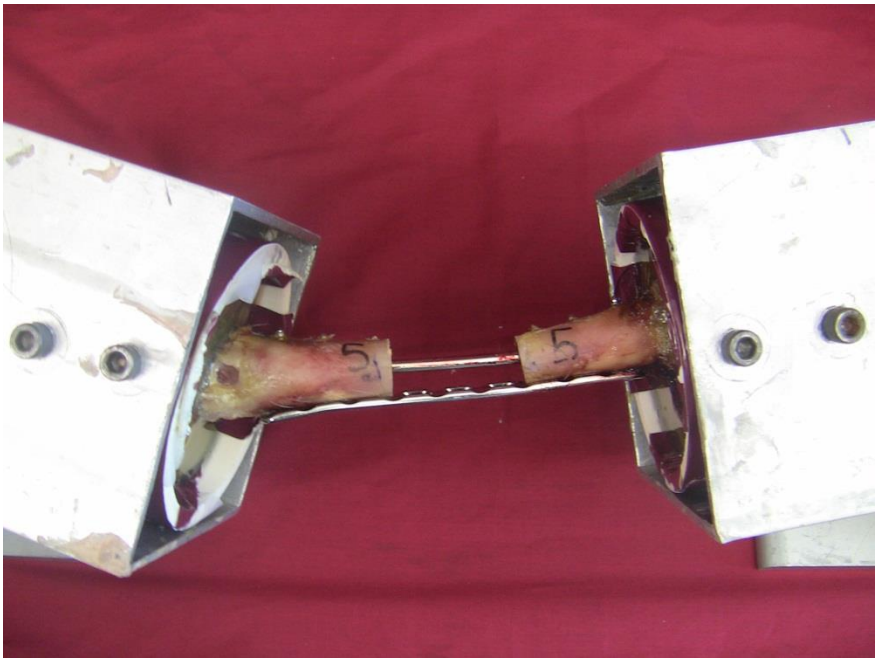

Figure 44. After four point bending test static position of LC-DCP #5.

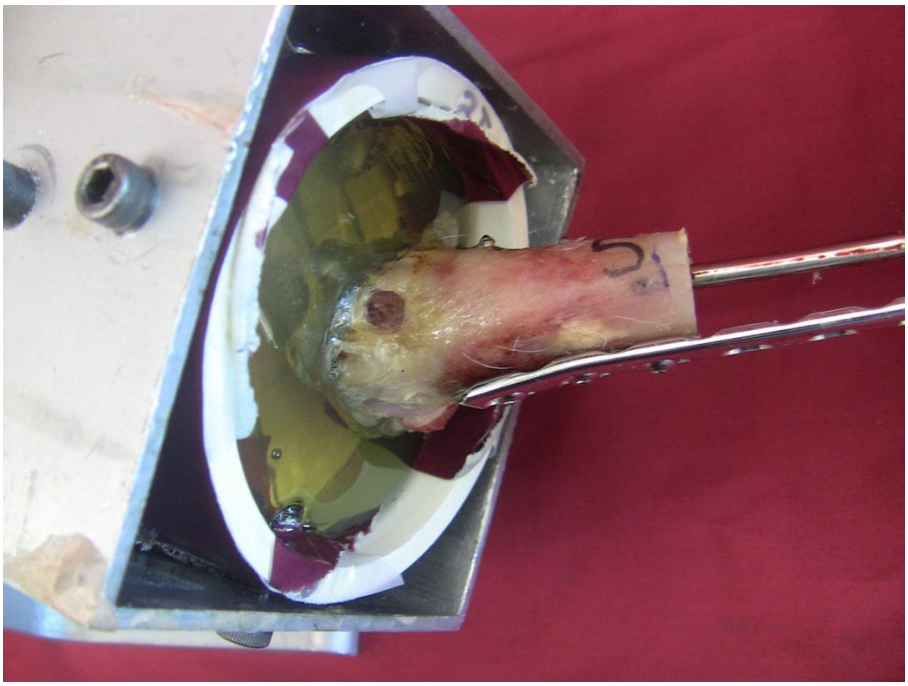

Figure 45. Closer inspection of the bone pullout for LC-DCP#5.

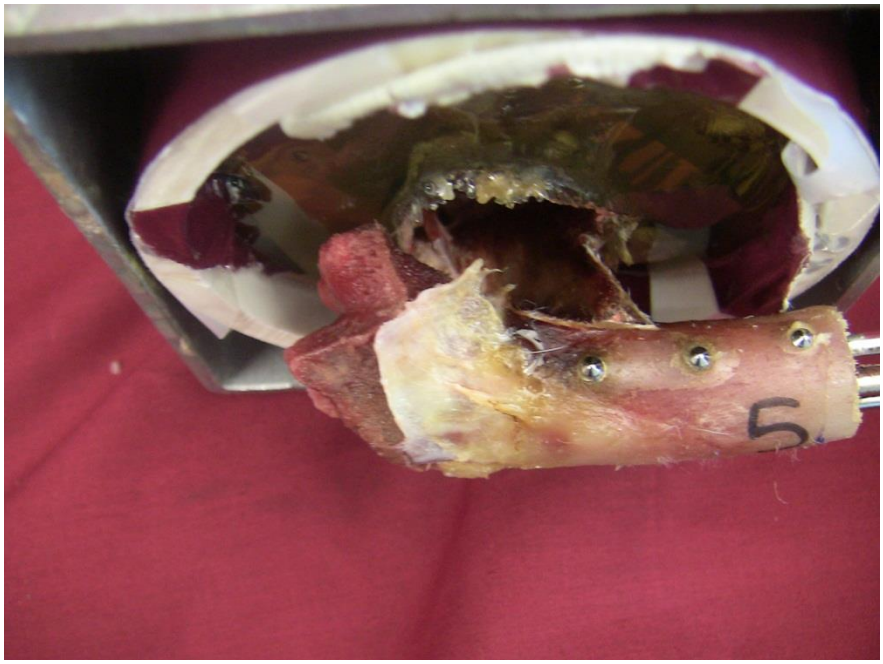

Figure 46. After four point bending test during inspection of LC-DCP #5 the bone separated into two distinct pieces, the portion connected to the plate and the portion attached to the epoxy.

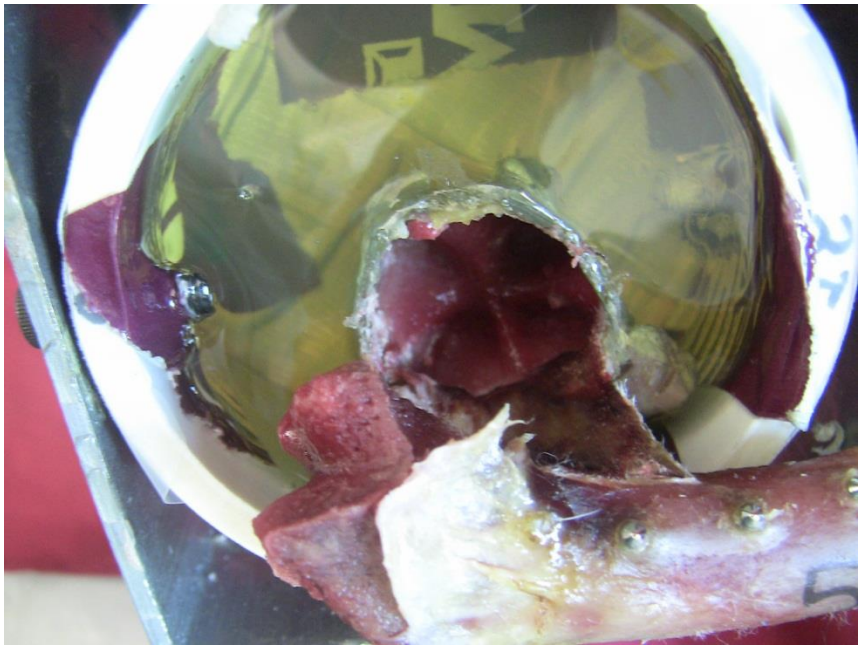

Figure 47. View of LC-DCP #5 failure inside of potting epoxy.

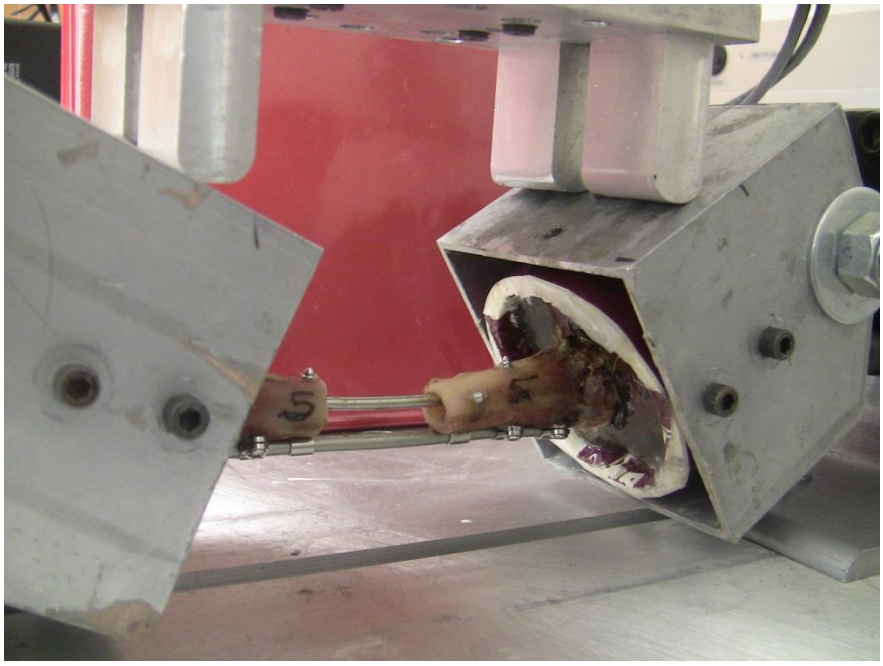

Figure 48. Image showing the position of CRIF #5 at the end of four point bending test.

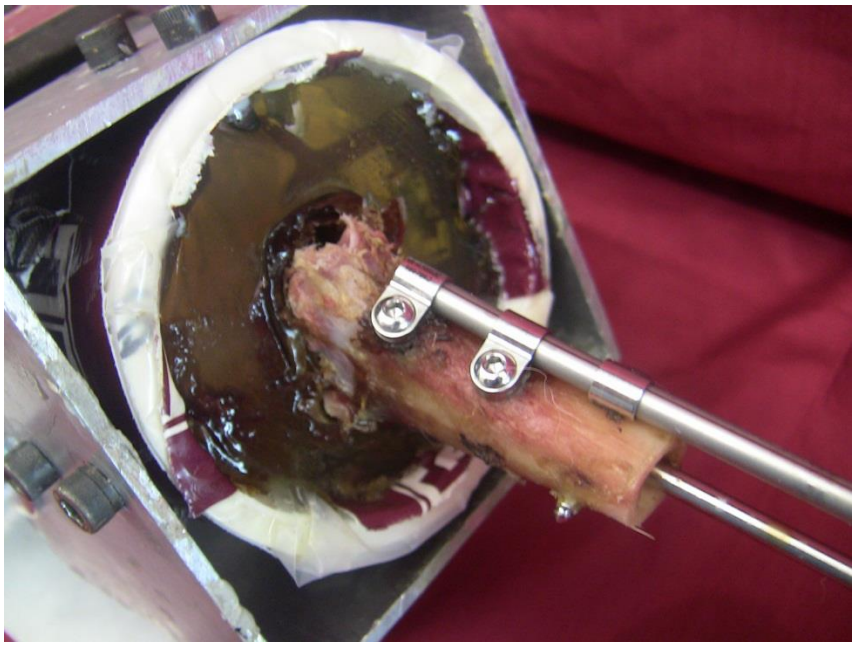

Figure 49. Fracture of CRIF #5 inside of epoxy potting material.

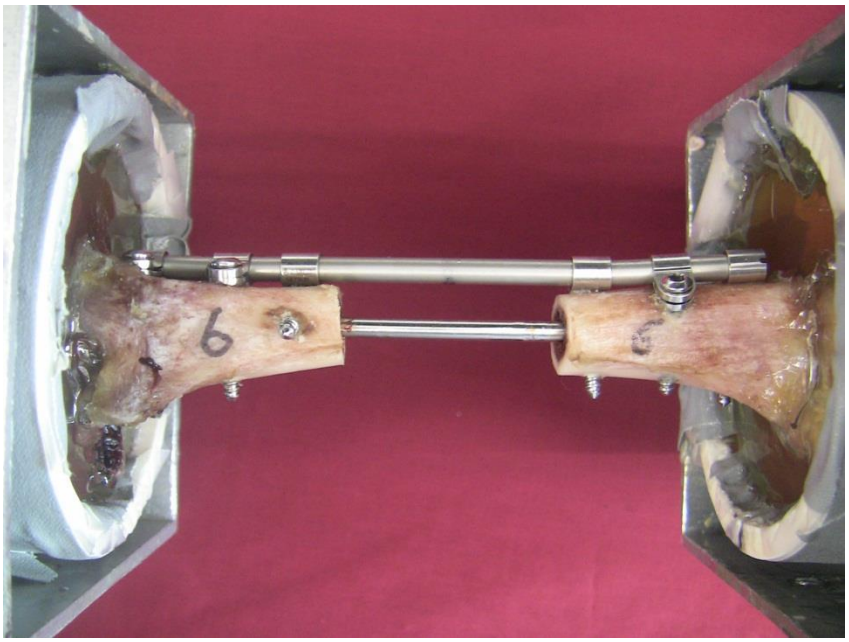

Figure 50. CRIF #6 before four point bending experiment.

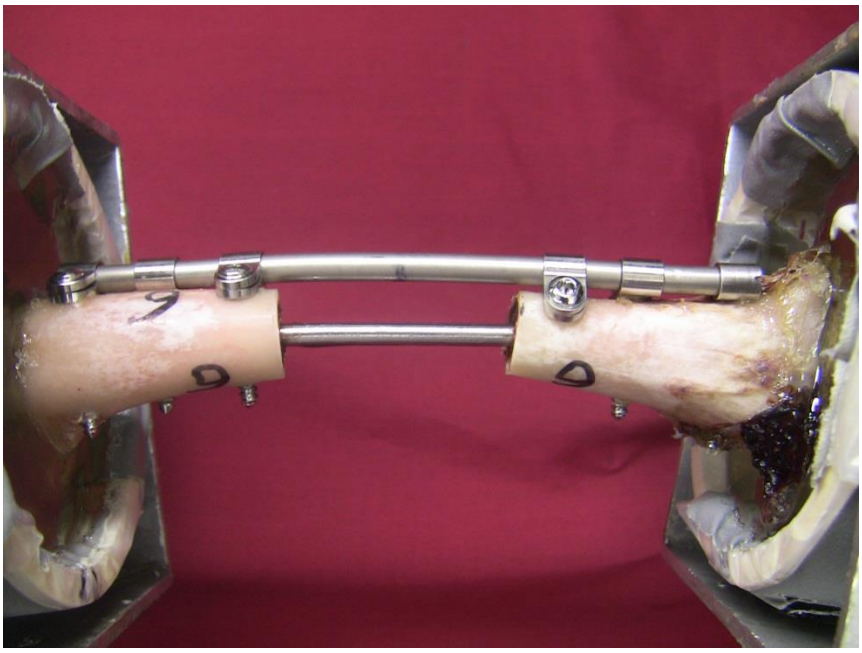

Figure 51. CRIF #6 after four point bending experiment.

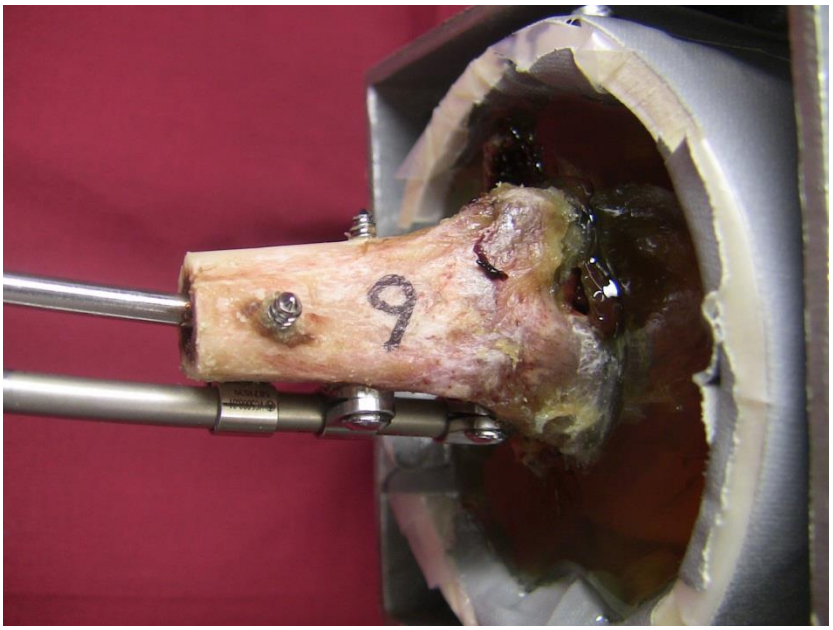

Figure 52. Image showing CRIF #6 bone pullout from epoxy potting material. Failure of bone inside of epoxy.

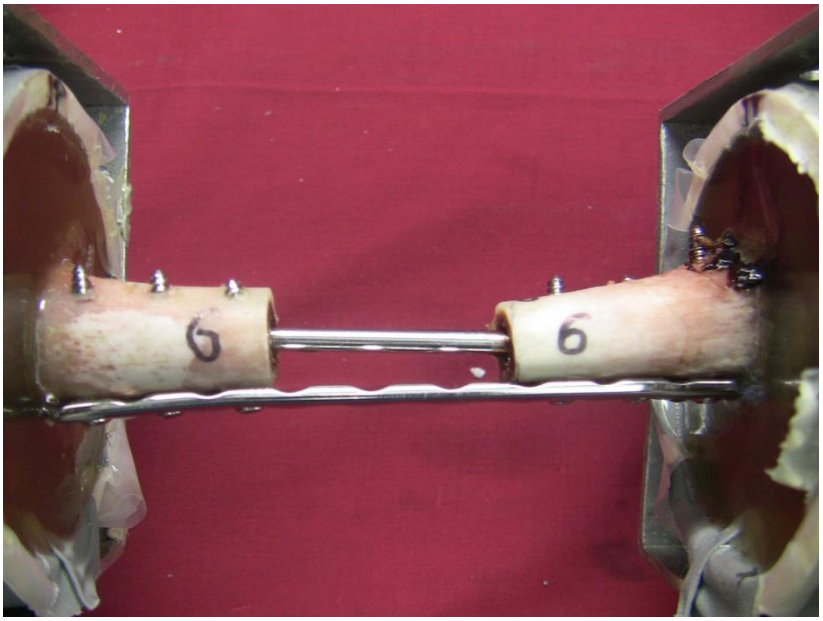

Figure 53. Image of LC-DCP #6 before four point bending experiment.

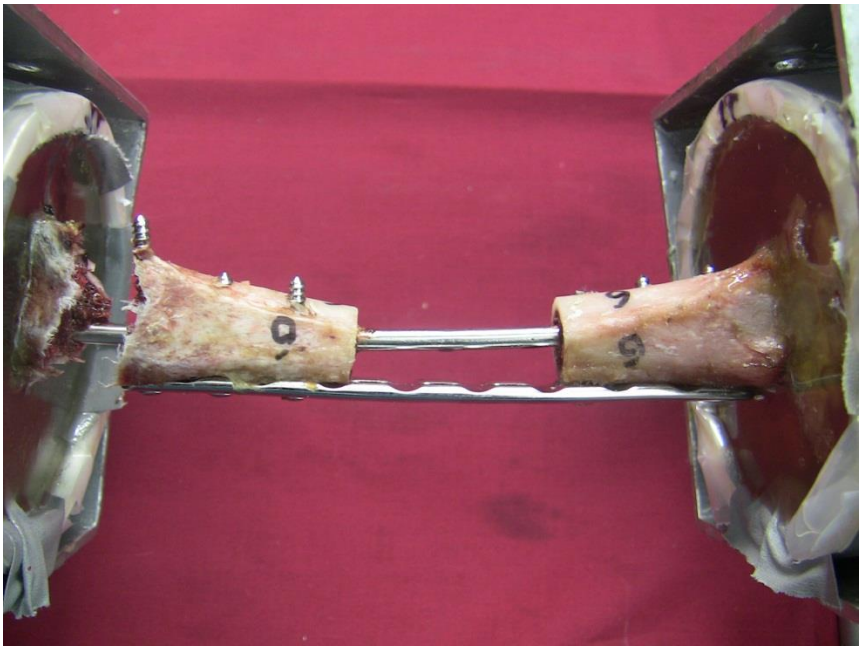

Figure 54. Explosive fracture of LC-DCP #6.

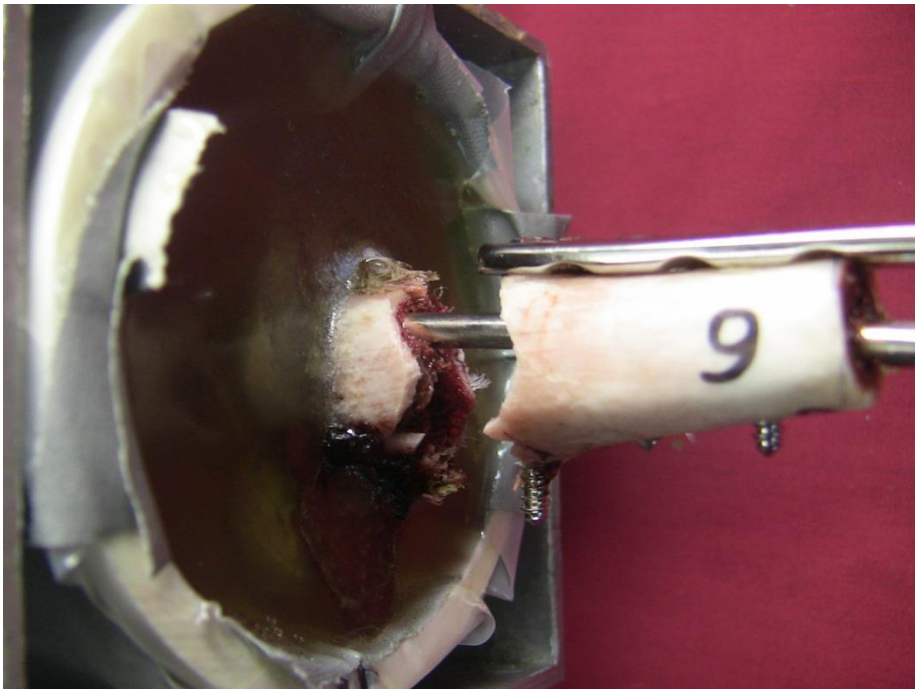

Figure 55. Closer inspection of fracture gap of LC-DCP #6.

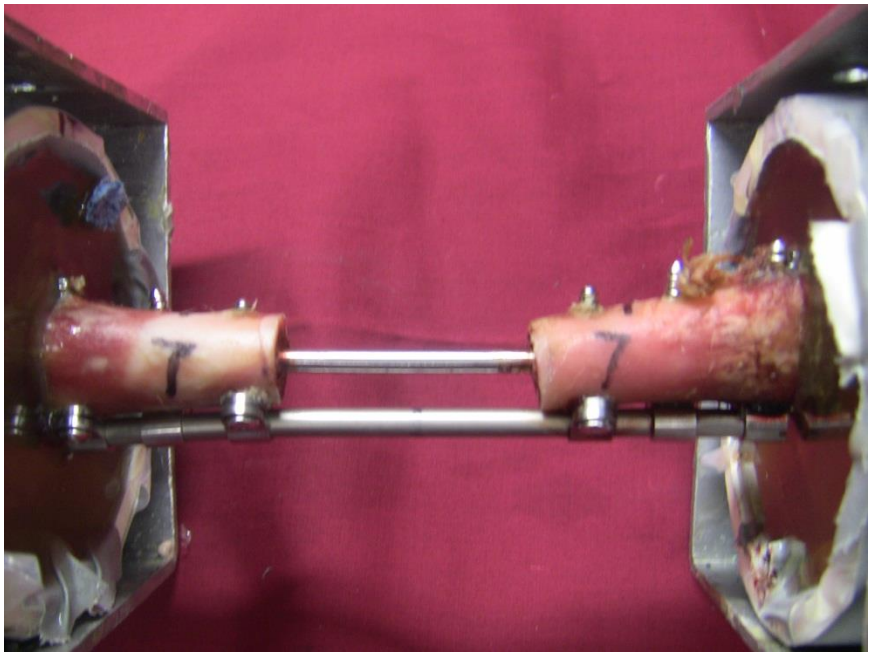

Figure 56. CRIF #7 before four point bending experiment.

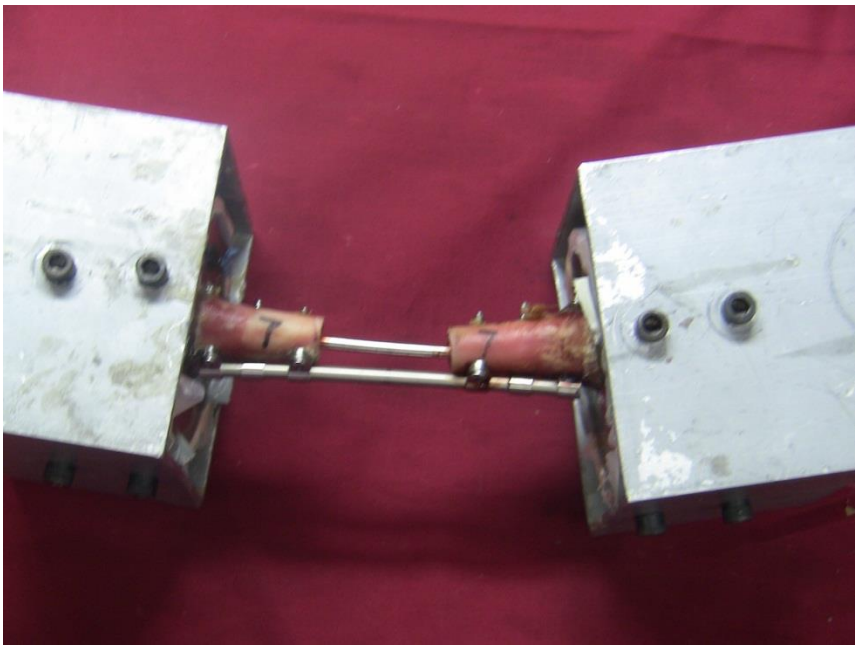

Figure 57. CRIF #7 after four point bending experiment. From orientation of the aluminum housings and test specimen the failure of the bone resulted from a bone failure inside the epoxy.

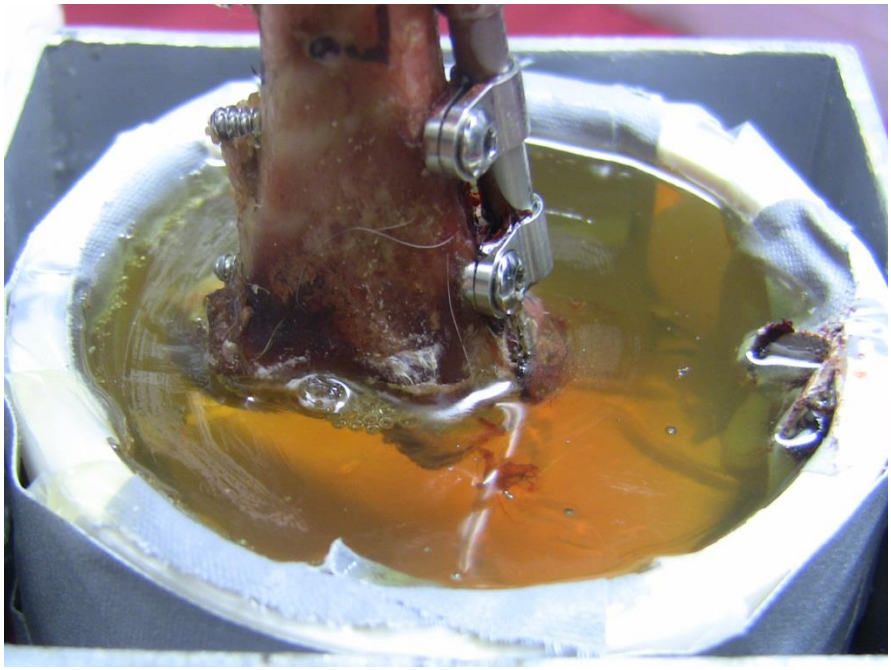

Figure 58. Closer inspection of CRIF #7 failure of the bone inside of the epoxy.

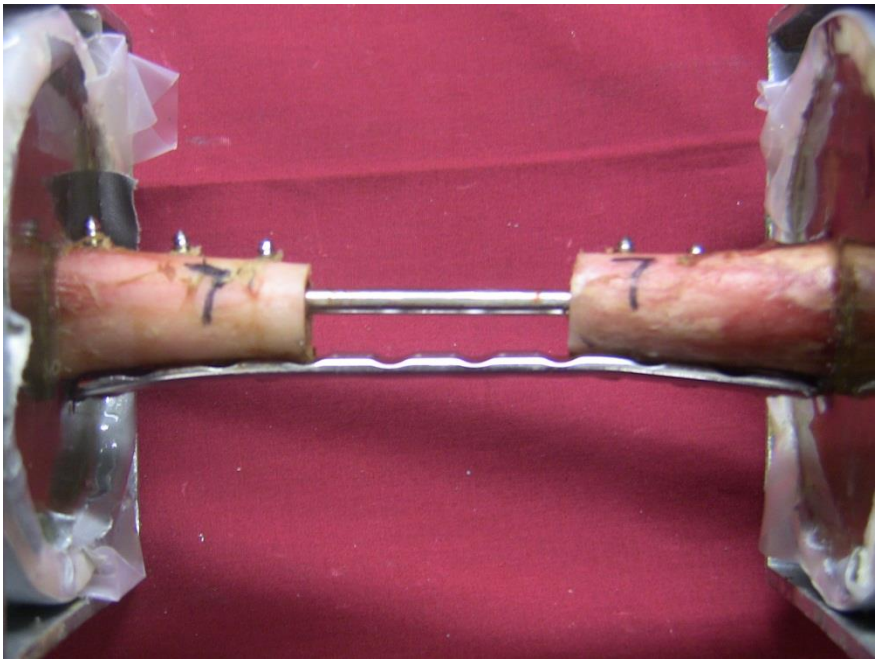

Figure 59. LC-DCP #7 before four point bending experiment.

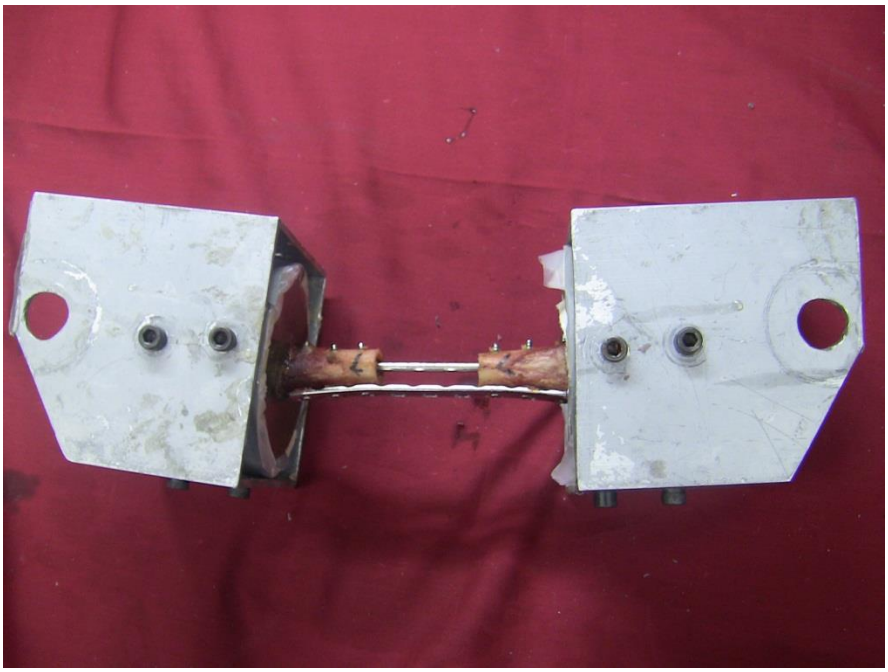

Figure 60. LC-DCP #7 after four point bending experiment. Failure of bone occurred inside of potting material as indicated by orientation of bone and aluminum housing.

APPENDIX B

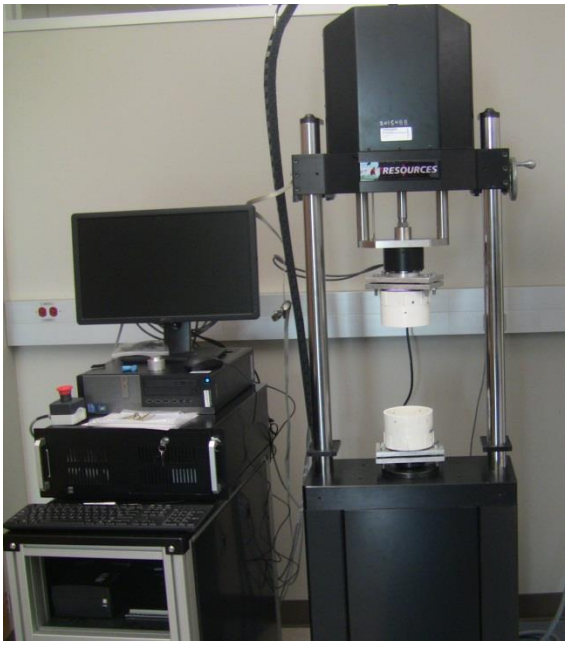

Figure 61. Test Resources 830 Biaxial machine with aluminum interface plates and PVC housings for torsion tests.

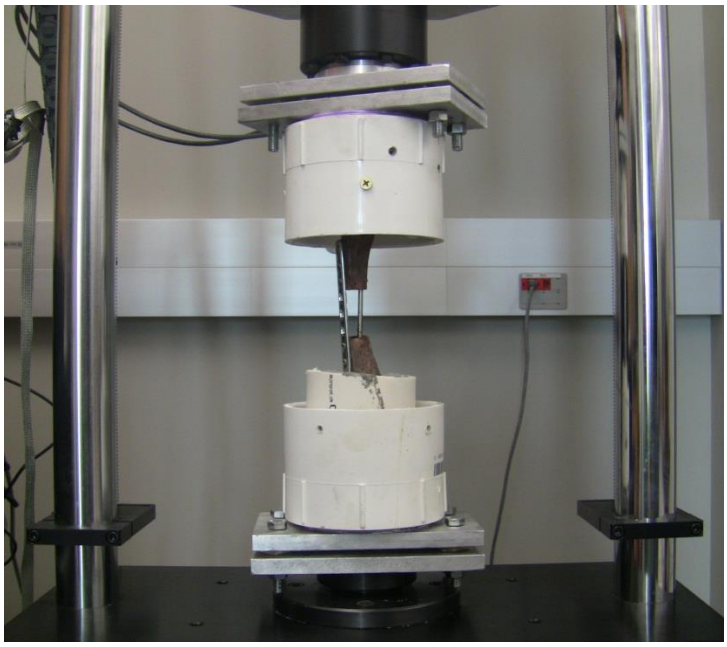

Figure 62. Image of LC-DCP specimen potted and attached to PVC housings.

APPENDIX C

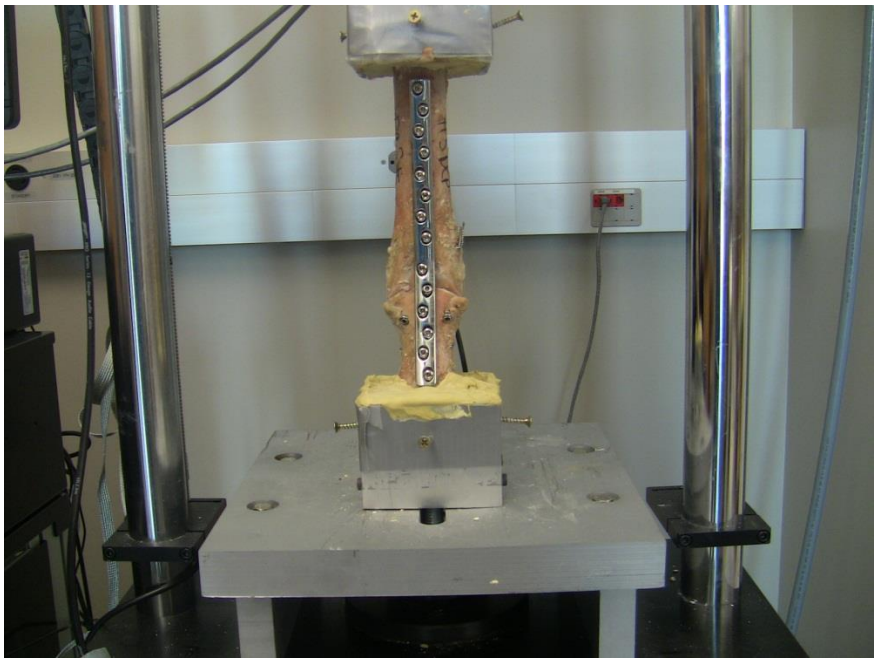

Figure 63. Image of DCP #5 before fatigue testing.

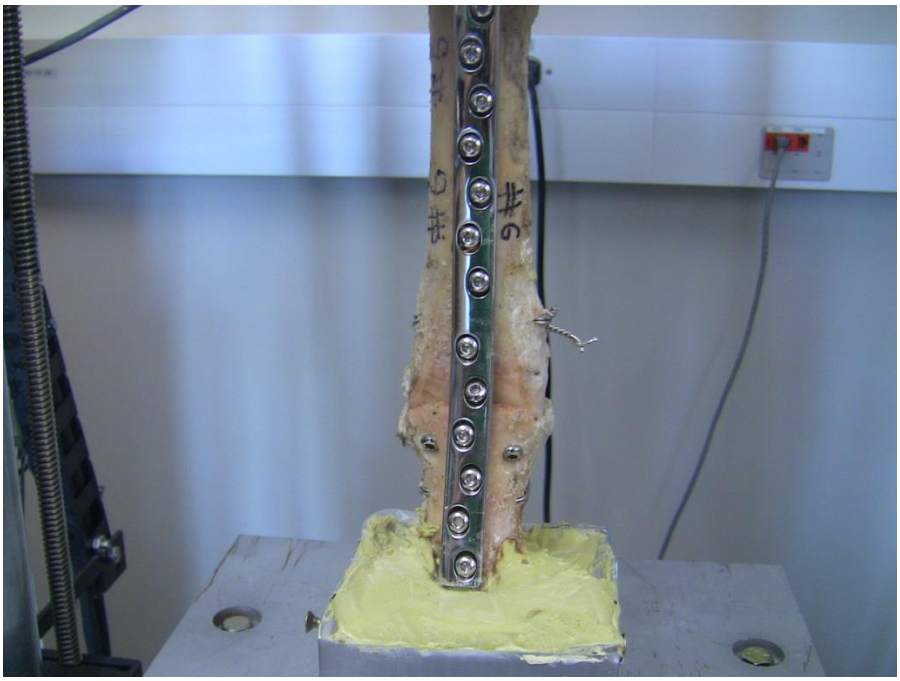

Figure 64. DCP #6 before fatigue test.

Figure 65. Image showing integrity and buildup of LabStone potting material around base of DCP #6.

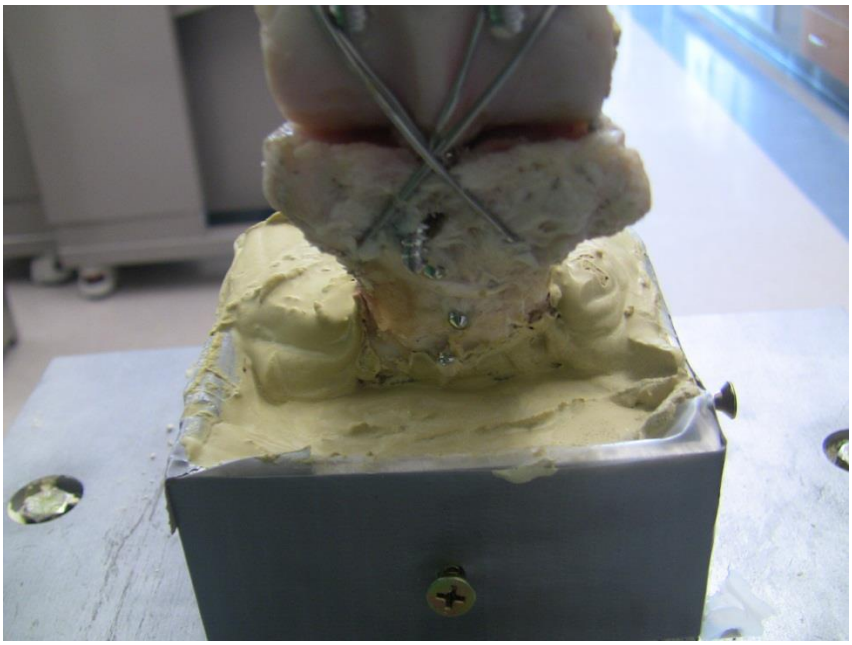

Figure 66. Image showing cavity of LabStone potting material at ventral aspect of base on DCP #6.

APPENDIX D

Figure 67. DCP #1 mounted to the MTS 810. Image is used to detail angle in plate before single ramp to failure test.

Figure 68. DCP #1 after single ramp to failure test. This image shows the change in angle of the bone plate construct that results from ramp to failure testing.

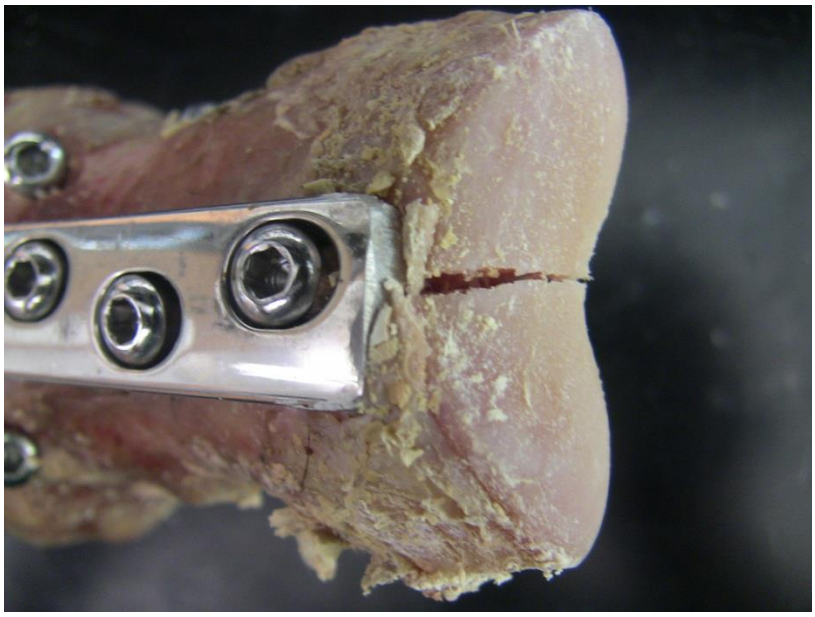

Figure 69. DCP #3 after single ramp to failure test. This image shows the bone fracture at the distal end of the proximal phalanx bone.

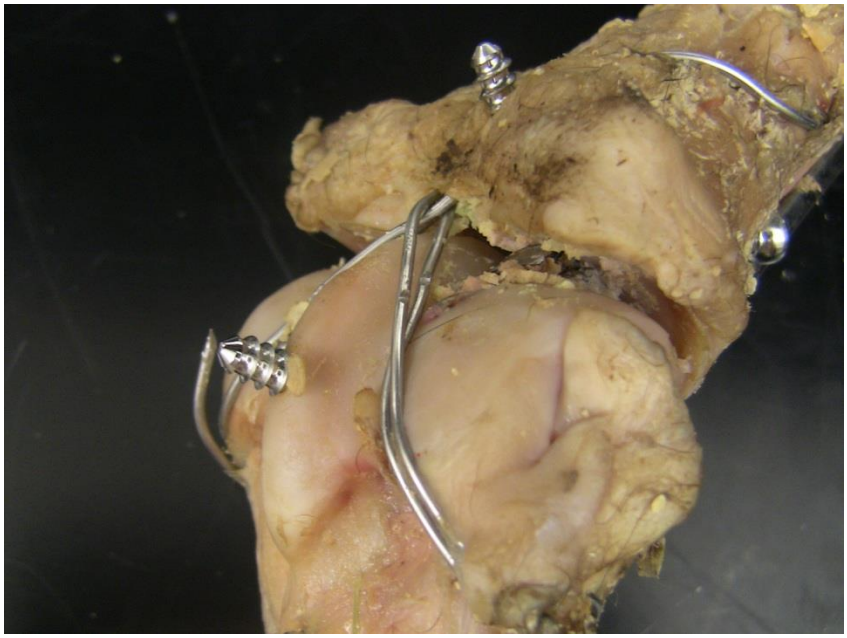

Figure 70. DCP #4 after single ramp to failure experiment. This image shows the failure of the tension band as well as two necking regions. DCP #4 failed by snapping of the tension band as well as pullout of the transarticular screws.

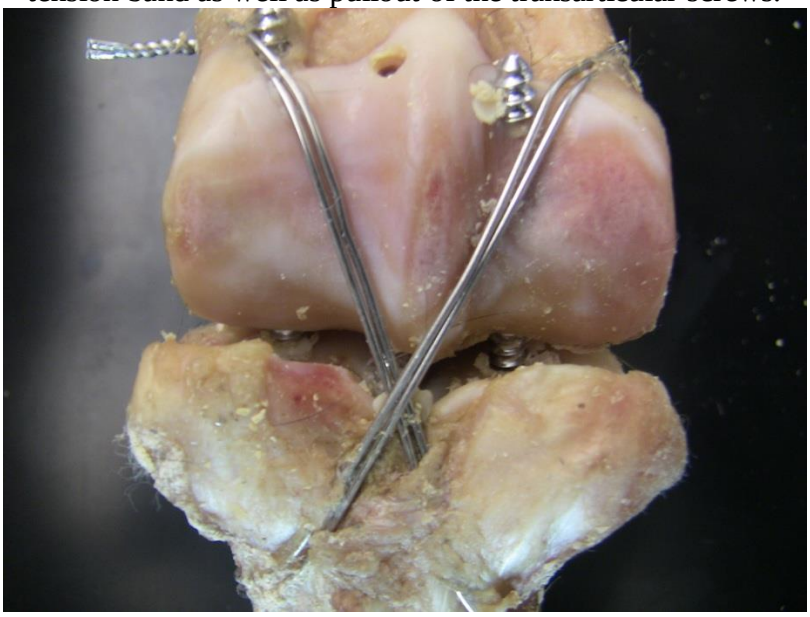

Figure 71. DCP #5 after single ramp to failure experiment. The gap shown was a permanent result without failure of the tension band. The transarticular screws likely suffered from pullout during loading, resulting in the permanent gap upon removal of applied load.

Figure 72. DCP #6 after single ramp to failure experiment. Consistent with the other DCP test specimens, the bone screws and transarticular screws suffered from bone pullout. It is possible that there was bone failure around a cortical bone screw right at the MCP joint, but this will have to be determined by radiograph.

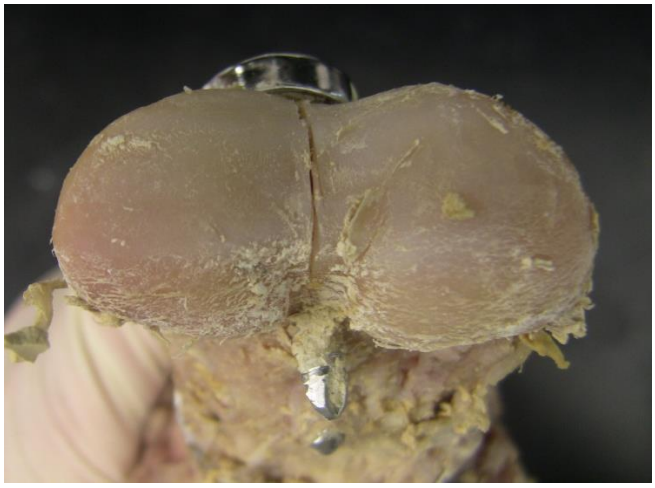

Figure 73. LCP #1 after single ramp to failure experiment. The bone/plate construct failed about the most distal face on the proximal phalanx bone along the holes created by the locking screws and cortical bone screws.

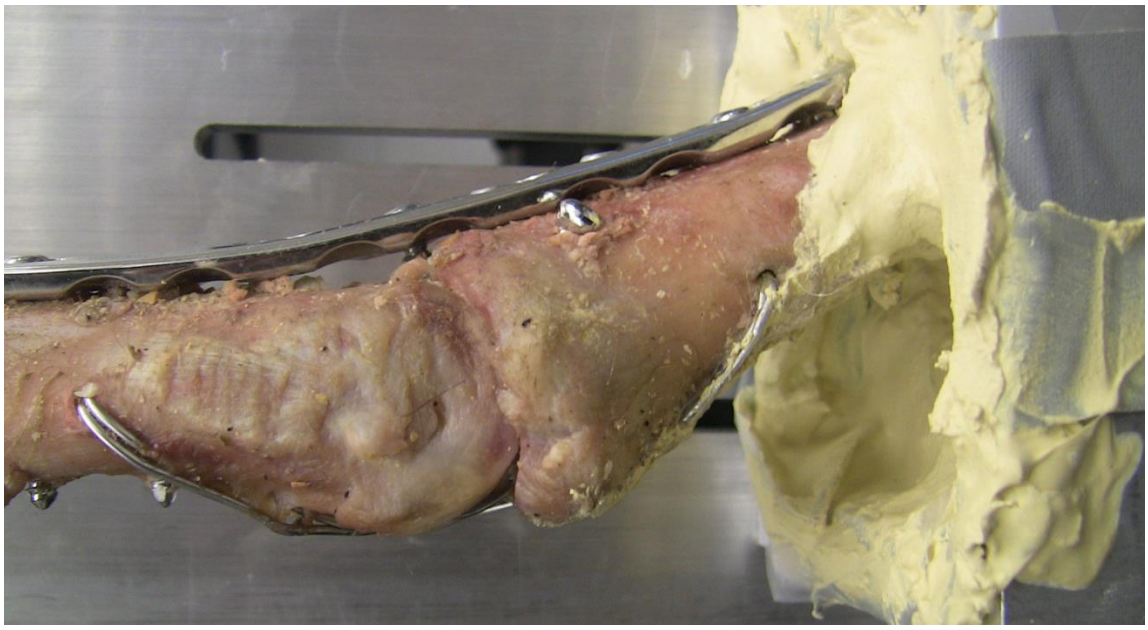

Figure 74. LCP #2 before the single ramp to failure run. This image partnered with Figure 75 helps to show how the LCP constructs suffered from significantly less permanent deformation of the plate by observing the limited change in angle of the plate.

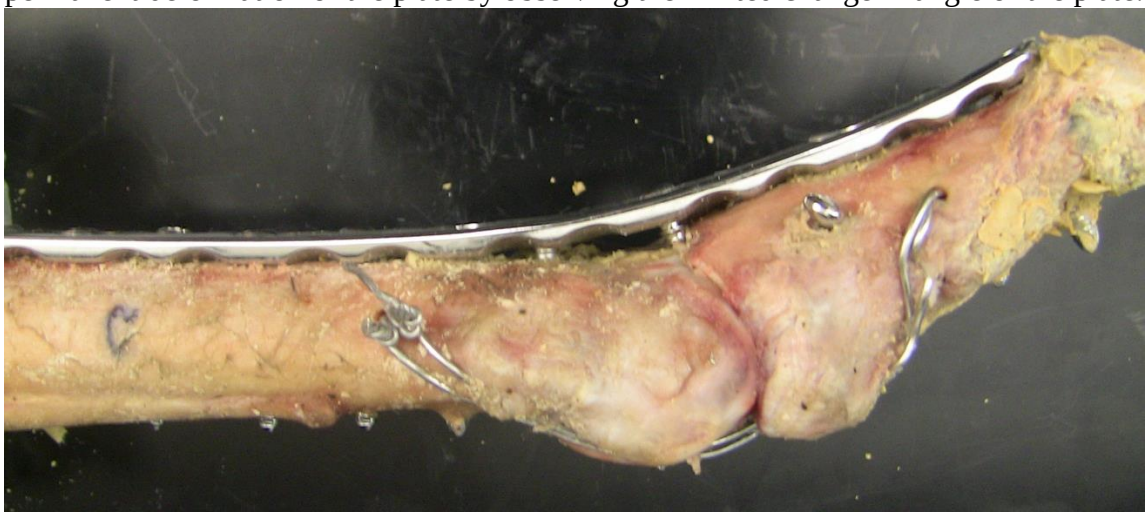

Figure 75. LCP #2 after the single ramp to failure test. This image partnered with Figure 75shows how the before and after angle of the LCP plate are very similar. Visibly the LCP/wire constructs did not show nearly as much angular deformation at the MCP joint, and fracture of the bone was the failure mode.

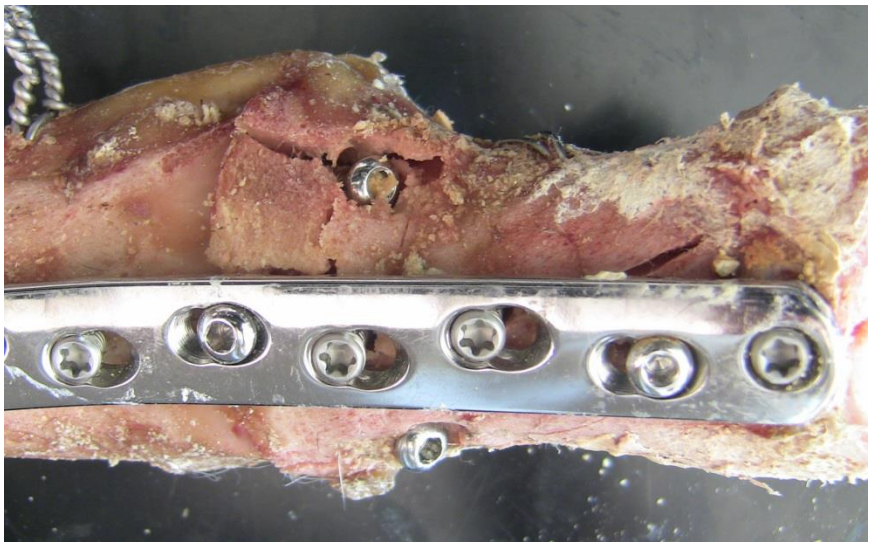

Figure 76. LCP #3 after single ramp to failure experiment. This bone fractured in multiple places, but most likely fracture propagated from the distal end of the proximal phalanx bone up through the screw holes along the plate and finally propagating to the transarticular screw holes.

Figure 77. LCP #3 after the single ramp to failure test. This image shows the distal end of the proximal phalanx bone where fracture occurred. The fracture, similar to the other LCP/wire constructs, bisects the bone connecting the locking bone screw holes.

Figure 78. LCP #4 before the single ramp to failure test.